MEASUREMENT OF SELECTED THERMAL AND PHYSICAL PROPERTIES OF ORGANIC SOIL BY DIRECT AND INDIRECT METHODS

by

Neil Goeller
B.A., McMaster University, 1999

THESIS SUBMITTED IN PARTIAL FULFILLMENT OF
THE REQUIREMENTS FOR THE DEGREE OF

MASTER OF SCIENCE

In the
Department
of
Geography

© Neil Goeller 2005

SIMON FRASER UNIVERSITY

Summer 2005

All rights reserved. This work may not be
reproduced in whole or in part, by photocopy
or other means, without permission of the author.

APPROVAL

Name: **Neil Thomas Goeller**

Degree: **Master of Science**

Title of Thesis: Measurement of Selected Thermal and Physical Properties of Organic Soil by Direct and Indirect Methods

Examining Committee:

Chair: **Dr. E.J. Hickin**
Professor

Dr. W.L. Quinton, Assistant Professor
Senior Supervisor
Department of Geography, SFU

Dr. L. Lesack, Associate Professor
Committee Member
Department of Geography, SFU

Dr. M. Hayashi, Associate Professor
Committee Member
Department of Geology and Geophysics,
University of Calgary

Dr. D. Allen, Associate Professor
External Examiner
Department of Earth Sciences, SFU

Date Approved: July 19, 2005

SIMON FRASER UNIVERSITY

PARTIAL COPYRIGHT LICENCE

The author, whose copyright is declared on the title page of this work, has granted to Simon Fraser University the right to lend this thesis, project or extended essay to users of the Simon Fraser University Library, and to make partial or single copies only for such users or in response to a request from the library of any other university, or other educational institution, on its own behalf or for one of its users.

The author has further granted permission to Simon Fraser University to keep or make a digital copy for use in its circulating collection.

The author has further agreed that permission for multiple copying of this work for scholarly purposes may be granted by either the author or the Dean of Graduate Studies.

It is understood that copying or publication of this work for financial gain shall not be allowed without the author's written permission.

Permission for public performance, or limited permission for private scholarly use, of any multimedia materials forming part of this work, may have been granted by the author. This information may be found on the separately catalogued multimedia material and in the signed Partial Copyright Licence.

The original Partial Copyright Licence attesting to these terms, and signed by this author, may be found in the original bound copy of this work, retained in the Simon Fraser University Archive.

W. A. C. Bennett Library
Simon Fraser University
Burnaby, BC, Canada

ABSTRACT

Results suggest that a linear relation between cumulative ground heat flux and cumulative skin temperature provides a reasonable representation of soil thaw and is relatively consistent between the two sub-arctic permafrost sites. However, a power equation showed better potential for thaw depth prediction and a better compatibility between sites. The partitioning of the ground heat flux at the two study sites was significantly different due to variations in soil moisture. At the wetter site, a larger fraction of the ground heat flux is partitioned to melt ground ice and warm the soil; whereas the dryer site experienced larger fluxes to the permafrost. Comparison of image analysis and pressure plate extractor test data suggests that 2D images of soil are a reasonable analogue for the 3D structure of soil, and that this method provides a fairly accurate approximation for use in characterizing soil and pore structure.

I would like to dedicate this piece of work

and all the effort that went into creating it

to my family: Mom, Dad and Lars

and my girlfriend Bronwyn

For all their support

and the occasional kick in the pants

ACKNOWLEDGEMENTS

This thesis was not possible without the support and contributions of many people over these years. I have tried to remember you all, I hope I have.

I would like to thank my senior supervisor, Bill Quinton for his support both intellectually and financially in the many stages of this work and Masaki Hayashi for valuable advice and guidance at some critical points in the research. I would also like to thank Taskin, Kim and Nicole for moral and editorial support in the hydrology lab, Tom Brown for playing the host in Saskatoon and Steve and Chris for an entertaining, if cold and lonely, field season. I would also like to recognize the contributions of Dr. Sean Carey in various capacities in the field and Marcia, Diane and the many others in the geography office. As well, thanks to all those instructors that I TA'd for over the years.

I would like to extend a special thanks again to my family, Mom, Dad and Lars for supporting me, especially the financial support of my parents who believed that this was actually possible. To my girlfriend Bronwyn for her endless support and faith in my abilities. To my band The Impossible Machine, Darel, Ross, Scott and Mike for keeping the dream alive. Finally I would like to thank all my friends in both Vancouver and Toronto that helped alleviate the frustrations of grad school by offering welcome distractions and being totally non-academic.

TABLE OF CONTENTS

LIST OF FIGURES

LIST OF TABLES

CHAPTER 1 INTRODUCTION

"The significance of a concept ought to be measured not by the frequency with which it is invoked but by the insights to which it leads and its effectiveness in solving problems" (Ingram, 1983)

1.1 PERMAFROST TERRAINS

Permafrost is defined as "a condition existing below the ground surface, irrespective of its texture, water content, or geological character, in which the temperature in the material has remained below 0°C continuously for more than two years and, if pore water is present in the material, a sufficiently high percentage is frozen to 'cement' the mineral and organic particles" (Whittow, 1984). The top of this layer, called the permafrost table is "the more or less irregular surface which marks the upper limit of permafrost and separates it from the overlying active layer in the soil" (Whittow, 1984). The active layer is a surface layer of ground, above the permafrost that is frozen in the winter and thawed in the summer (Jackson and Bates, 1984). In this zone, the boundary between saturated frozen soil below and thawed soil above is called the frost table (Figure 1-1). Spring thaw results in the downward progression of the frost table.

The location of the frost table can be defined by either the thawing front or the cyrofront. The thawing front is defined as "the boundary between frozen and unfrozen soil" and can be measured by probing with a metal rod to the resistant layer if the soil below the frost table is saturated and frozen. The cryofront is the thermal definition of

frost table depth determined by the position of the zero degree isotherm (French, 1996). In this study, the cryofront is used to indicate the position of the boundary between frozen and unfrozen soil, and it is assumed that the soil below is frozen and saturated (relatively impermeable) and the water table is perched on this boundary.

1.2 ACTIVE LAYER HYDROLOGY

Permafrost plays an important role in the northern hydrological cycle because it restricts moisture exchanges between surface water and deep ground water (Prowse, 1990) and also has notable influences on catchment hydrology and streamflow generation (Woo and Carey, 1998). Runoff processes in organic-covered permafrost terrains are distinct from those of other permafrost terrains in that the dominant runoff mechanism is subsurface flow through the seasonally thawed organic layer (Quinton and Marsh, 1999).

In dry northern climates there is little precipitation through the summer, and almost all winter precipitation falls as snow. Thus, the snowmelt season in spring is the single most important hydrologic event of the year (Woo, 1986; Carey and Woo, 1999; Bolton et al., 2000; Woo et al., 2000). The rate of movement of this meltwater over and through the soil is controlled by the thermal and hydraulic properties of the thawing soils in the active layer.

Seasonal ice in the active layer limits the vertical and horizontal movement of subsurface water. As a result, lateral drainage occurs in a saturated zone perched on the frozen-saturated soil (Figure 1-1) (Woo, 1986; Quinton and Gray, 2001). As thawing progresses the frost table and the thawed saturated zone above it descend through the soil profile (Woo, 1986). In order to estimate the rate of subsurface flow in organic-covered

terrains underlain by permafrost, it is imperative to know the elevation of the saturated layer and the corresponding hydraulic conductivity of the soil at that depth (Quinton and Gray, 2001). Since flow through the active layer and the surface energy balance are linked by the thawing of impermeable frozen soil, their close coupling requires an understanding of the soil thaw rate in order to properly and completely represent soil water flows during spring thaw in hydrologic models (Woo, 1983; Woo and Steer, 1983; Woo, 1986; Halliwell and Rouse, 1987; Carey and Woo, 1998; Bolton et al., 2000). The transferability of this understanding between basins is also an important issue due to the paucity of gauging stations and lack of available data in these less hospitable climates.

Quinton et al. (2000) identified the non-homogenous nature of northern peat profiles. In particular, they determined that changes in soil physical properties through the profile led to a corresponding exponential decrease in hydraulic conductivity with depth (Quinton and Gray, 2001). They proposed a two-layer model of peat that consists of a highly porous and hydraulically conductive upper horizon composed of living organics and a lower less conductive layer of decomposing and compacted peat. Rather than a distinct boundary separating these two layers, a transition zone exists in which there is a continuous change in hydraulic properties (Quinton and Gray, 2001). In this transition zone, the hydraulic and physical properties of the soil change from a very open and connected structure to one that is closed and disconnected with increasing depth (Quinton et al., In press).

The dependence of hydraulic and thermal properties on soil physical properties has been noted in several studies (Farouki, 1981; Ahuja et al., 1989; Schaap and Lebron, 2001; Kluitenberg, 2003). Many mathematical expressions make use of pore geometry

which is often a difficult parameter to quantify and measure. Image analysis of soil blocks or thin sections is an underexploited source of such data. However, the degree to which the two-dimensional data obtained from the image analysis represents the actual three-dimensional structure of soil has not been well established.

1.3 OBJECTIVES

The overall objective of this study is to improve the model representation of the thermal and hydraulic processes controlling runoff through the active layer during thaw at two representative permafrost sites with organic soils. The two sites including, Granger Basin: sub-arctic tundra and Scotty Creek: a high boreal wetland, were selected as representing widely occurring biophysical land cover types of cold regions (Quinton and Gray, 2001). Because of the depth dependency of mass flow properties and because the frost table is relatively impermeable and descends with time during soil thawing, the soil thaw and water flux processes are closely coupled. Therefore the specific objectives of this research are to examine and assess:

1) the energy flow and storage processes that result in seasonal active layer development and to develop a soil thaw algorithm to estimate frost table and saturated layer position;

2) the viability of two-dimensional image analysis of resin impregnated peat soil blocks to characterize pore structure for use in equations for calculating functional soil properties.

1.4 SCOPE OF WORK

The objectives of this project as outlined above are addressed in two separate studies. The first is a thermal study examining soil thaw and the primary factors affecting its rate and magnitude and the second is a hydraulic study which addresses the measurement of pore structure, a key physical property controlling the flow of fluids in porous media. Data for both these studies have been drawn from two contrasting sub-arctic sites, each selected because it represents a widely occurring permafrost terrain type with a mantle of organic soil. The two sites are; Granger Basin, a sub-arctic alpine tundra site, and Scotty Creek, a high boreal wetland.

In the thermal study the magnitude of ground heat flux and its components at two sub-arctic sites are calculated. A relationship between the cumulative ground heat flux and cumulative Infra-Red surface temperature is presented using both a linear and power equation as a method of predicting the magnitude of the ground heat flux.

The hydraulic study examines the physical properties of the soil by comparing two methods of quantifying soil pore structure. An image analysis approach to directly measuring pore size is compared with pressure plate extractor tests by plotting both data sets as cumulative pore size distributions and water retention characteristic curves. These data sets are compared to determine if the image analysis approach is a viable method of soil pore measurement.

1.5 FIGURES

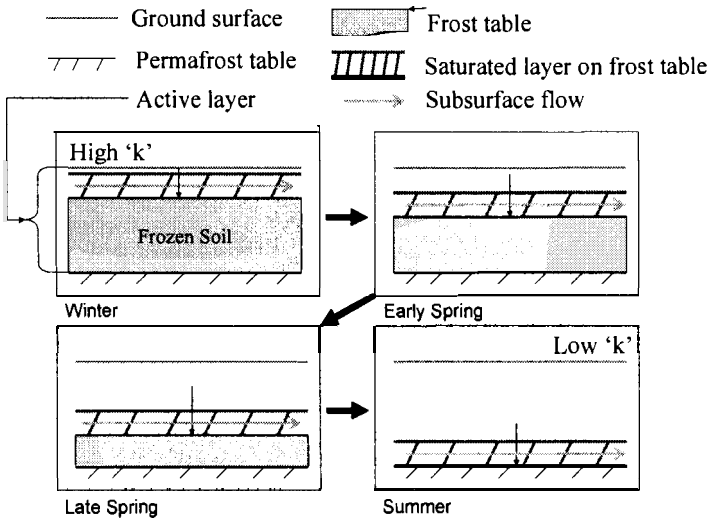

Figure 1-1. Hydrologic and thermal development of the active layer as soil thaw causes the frost table to descend through the peat profile, lowering the water table. Deeper soils, having a lower saturated hydraulic conductivity convey subsurface flow more slowly.

CHAPTER 2 THE RELATIONSHIP BETWEEN CUMULATIVE SURFACE TEMPERATURE AND CUMULATIVE GROUND HEAT FLUX

2.1 INTRODUCTION

The seasonal ice in the active layer limits the vertical movement of water through the soil profile. As a result, the thawed saturated zone, through which subsurface flow is conducted, is perched on top of the relatively impermeable frost table (the frozen-saturated soil) (see Figure 1-1) (Woo, 1986; Quinton and Gray, 2001). As thawing progresses, the frost table and its perched saturated zone descend through the soil profile, thereby increasing the soil available for storage and conduction of subsurface flow (Woo, 1983; Woo, 1986). Therefore, knowledge of the frost table depth is crucial for modeling snowmelt runoff. The index approach is a common approach used in calculating thaw depth (Abbey et al., 1978; Woo, 1986; Quinton et al., 2000). An index relationship assumes a simple interaction between two variables making use of a surrogate measurement to estimate the quantity of the variable in question and using some coefficient or exponent to relate the two.

Index relationships offer a reasonable estimate of thaw depth but can be difficult to transfer to other sites (Abbey et al., 1978; Woo, 1986). An early index approach approximated thaw using an association between percent bare ground and average frost table depth (Wright, 1981). However, this association neglects important factors such as ice content, soil moisture and porosity. Also, Carey and Woo (2000) reported finding no relation between exposure and frost table position.

Another available equation used to approximate thaw depth is a modification of the Neumann equation by Carslaw and Jaeger (1959) (Nixon, 1973).

$$ThawDepth = K\sqrt{t} \qquad [2\text{-}1]$$

where K is a constant and t is time. Application of this equation requires parameterization of the coefficient K and, as a result, is highly site and seasonally specific (Haag and Bliss, 1974; McRoberts, 1975; Woo, 1983). Such relations can be improved by relating soil thaw to a more transferable term, which accounts for some or all of the different storages and fluxes of energy that occur in the active layer.

Thawing of the active layer occurs as a result of heat flux into the soil. The position of the frost table has been linked to the ground heat flux density (Qg), which is "the amount of energy transported through a unit area of soil per unit time ($MJm^{-2}s^{-1}$ or Wm^{-2})" (Kluitenberg, 2003). Qg is a portion of net solar radiation (Q*) transferred to the ground for thawing and heating of the soil (Figure 2-1). It is typically 10-15% of Q* in northern regions and is the primary factor for use in the estimation of soil thaw (Haag and Bliss, 1974; Carey and Woo, 1998; Lynch et al., 1999; Woo and Carey).

The most commonly used methods for calculating Qg are the gradient, force-restore, combination or null alignment and thermo-calorimetric methods (Karam, 2003; Kluitenberg, 2003). The gradient method is a simple association using the temperature profile and thermal conductivity of the soil to calculate heat flow. In permafrost environments this method is unsuitable as it is not able to account for the latent heat involved in phase changes. The force-restore method uses forcing and restoring functions to estimate ground surface temperatures but until recently has not been

applicable to subsurface temperatures. However, a recent extension of the model has shown promise in modeling frozen soils and possibly permafrost (Hirota et al., 2003). The null alignment method was developed to use only a few (2-3) near surface soil temperature measurements. It is a combination of the thermo-calorimetric approach and the gradient method (Horton and Wierenga, 1983). However, it is restricted to relatively homogenous soils and uses only mean soil properties. The null alignment method is not easily applied in permafrost environments as it relies on the existence of points of zero temperature change within the soil at fixed depths and similarities from day to day in the soil temperature profile. The long term variability of the active layer temperature profile prevents the persistence of such static points (De Vries and Philip, 1986). This study makes use of the thermo-calorimetric method because it has been frequently and successfully applied to active layer thaw (Woo and Xia, 1996; Carey and Woo, 1998; Quinton and Gray, 2001).

The thermo calorimetric method (Lettau and Davidson, 1957) measures changes in heat storage for discrete layers (Horton and Wierenga, 1983) and is frequently used to validate other heat budget calculations (Fuchs, 1986; Kluitenberg, 2003). The drawback of this method is the requirement to estimate soil thermal properties, which are difficult to accurately measure (Kluitenberg, 2003). For this purpose, the thermal conductivity and heat capacity are often calculated using the relatively reliable and widely used equations of DeVries (1963) (Kluitenberg, 2003). However, this research replaces the calculation of thermal conductivity with the methods of Mickley (1951) and Farouki (1981), which have also been used successfully in Qg calculations in an organic

permafrost environment (Farouki, 1981; Woo and Xia, 1996). The thermo-calorimetric method accounts for Qg by calculating it as three components as described below.

The flow of energy into the active layer is partitioned to three purposes: warming the thawed portion of the active layer (Qs), melting the ice (i.e. lowering the frost table) (Qi) and warming the permafrost (Qp). The sum of these parts is the total ground heat flux (Qg) (Figure 2-1). Differences in soil properties and moisture contents affect the magnitude of each component.

Rouse (1984) established that Qs only accounts for about 10% of Qg (Roulet and Woo, 1986). Larger values of Qs occur at sites with deeper thaw and wetter conditions because of their higher heat capacity which require more energy per unit temperature change (Carey and Woo, 2000). The importance of Qs decreases as soil ice increases, as more energy is consumed to melt the ice (Qi) and conducted to the permafrost (Qp)(Roulet and Woo, 1986; Rouse et al., 2003). Qi is commonly the largest partition of Qg (Woo, 1983; Roulet and Woo, 1986; Halliwell and Rouse, 1987), on average, accounting for about 60-80% of total ground heat flux (Vasilenko and Zhuravin, 1997; Carey and Woo, 2000). However, Carey and Woo (1998) have reported a value as low as 27%. Thaw depth is strongly linked to soil ice content (Woo, 1986; Woo and Xia, 1996; Carey and Woo, 1998) and high porosity organic soils can contain large amounts of ice per unit volume of soil. This can lead to larger Qp values due to the higher conductivity of ice and reduced thaw rates, causing stronger subsurface temperature gradients (Carey and Woo, 1998; Carey and Woo, 2000). Qp also acts as a heat sink, maintaining lower soil temperatures (Kane et al., 1990). The importance of Qp increases as thaw progresses

and stronger thermal gradients are established deeper in the active layer (Halliwell and Rouse, 1987).

Water content is a major variable determining the thermal properties of porous soils (Wolfe, 1963; Nixon, 1973; Haag and Bliss, 1974; Price, 1983; Pare, 1984; Hinzman et al., 1991; Woo and Xia, 1996; Carey and Woo, 1998; Bolton et al., 2000; Woo et al., 2000). High porosity results in a strong dependence of thermal properties on soil water content (Wright, 1981; Pare, 1984) and thaw depth has been closely linked, but is not entirely dependent on, trends in soil moisture (Hinzman et al., 1991; Carey and Woo, 2000). The other important factor is the state of the soil water content, as ice has a thermal conductivity nearly four times that of water (Farouki, 1981). Initially, thaw is usually rapid due to the low heat capacity and high thermal conductivity of frozen peat and ice. As water replaces the ice, heat capacity increases, reducing the rate of heating and cooling (Haag and Bliss, 1974; Price, 1983; Woo and Steer, 1983; Carey and Woo, 1998). The presence of water at the soil surface attenuates heat maintaining warmer surface temperatures and stronger thermal gradients (Woo and Xia, 1996). As a result, wetter sites with higher heat conduction experience deeper thaw, while dry sites have shallower thaw depths (Carey and Woo, 1998). A greater thaw rate combined with the large amount of ice present in organic soils results in higher values of Qi because ice requires a large amount of energy to melt (Woo and Steer, 1983; Pare, 1984). However, in the case of thick dry organic soils, lower soil moisture results in decreased heat conduction and increased insulation, with less heat conducted to the deeper soils (Haag and Bliss, 1974; Smith, 1975; Price, 1983; Pare, 1984; Hinzman et al., 1991; Hinzman et al., 1993).

The thermal properties of the soil are also influenced by topography, since on sloping terrain, the drainage of water causes a decrease in the soil moisture content. Carey and Woo (2000) found that the initial ground heat flux at several different sites was similar due to similar soil ice content. However, as thaw progressed and lateral drainage occurred, wetter sites had larger Qg values due to increased thermal conductivity. Qg was greatest following snowmelt when thermal conductivity and surface temperature gradients were high, and energy was easily transferred to the soil (Woo and Xia, 1996).

Calculating frost table position requires an estimation of Qg and the relative magnitudes of its components. However, the calculation of Qg is computationally and data intensive; therefore, it is advantageous to be able to estimate it from a more readily measurable property of the soil or atmosphere. Various attempts have been made to relate Qg to meteorological and surface variables, such as net radiation, air and skin temperature; where skin temperature is the Infra-Red temperature of the surface soil layer. It is known that net radiation (Q*) dominates the energy supply for periods longer than one day; however, Qg is not a fixed percentage of Q* (Abbey et al., 1978). Abbey and Gray (1974) suggested, instead, that cumulative values provide a more accurate index for estimation of energy fluxes. They developed two relationships relating cumulative Qg to each of cumulative values of Q* and air temperature (Ta). Using measured Q* required two regressions, one for dry and one for rainy periods. The second association between Qg and Ta, was improved as the temperature of rain was closely approximated by that of air, but the results were of limited transferability to other sites. However, in a

later study, Walker and Jia (2003) found little correspondence between Ta and frost table position.

Quinton and Gray (2001) proposed that cumulative skin temperature ($\sum$Ts) is more transportable between different sites. They found that for a high arctic wetland site, the relationship between $\sum$Ts and cumulative Qg ($\sum$Qg) worked relatively well in predicting frost table position. They also suggest that the applicability of the $\sum$Ts-$\sum$Qg relationship over large areas offers potential widespread application through the use of remotely sensed thermal data for measurements of Ts in order to estimate Qg (Quinton and Gray, 2001). As yet, the transferability of this relationship to other sites is still undetermined.

2.2 OBJECTIVES

The first objective is to determine how Qg is partitioned into its three major components (Qp, Qs and Qi) for two representative cold regions sites. The second objective is to define a relationship between $\sum$Ts and $\sum$Qg for each site. The third objective is to compare the partitioning of energy and the $\sum$Ts-$\sum$Qg relationship between the two sites.

2.2.1 Rationale

The two sites selected for this study are considered to be representative of widely occurring biophysical land cover types in sub-arctic Canada (Quinton and Gray, 2001). However there are distinct differences which make their selection ideal for this study. Scotty Creek is a flat wetland environment where lack of slope and poor drainage result in the soils remaining at saturation for most of the thaw period. Granger Basin, on the

other hand, is located on a slope where lateral drainage results in relatively dry surface soils. These contrasting environments will provide insight into the influence of soil moisture on the rate and depth of thaw. Results will indicate the portability of the $\sum Ts$-$\sum Qg$ and energy partitioning relationships between the two contrasting sites. A method that makes use of Ts could reduce the need to instrument basins using soil pits or extensive field measurements, instead making use of infra red sensors. Further research may also allow the calculation of Qg and soil thaw depth from remotely sensed infra-red images to estimate skin temperature, thus reducing the demand for intensive field instrumentation.

2.3 STUDY SITE

In this chapter, the climate, soils and vegetation of the two northern sites selected for this study are described. All sites have a continuous organic cover and are underlain by permafrost.

2.3.1 The Granger Subcatchment

The Granger subcatchment, located at latitude: 60°30'N, longitude: 135°11'W, is a headwaters basin in the Wolf Creek watershed. The watershed is located 15 km south of Whitehorse, Yukon (Figure 2-2 and 2-3) in the boreal Cordillera ecozone straddling the Southern Yukon Lakes and the Yukon-Stikine Highlands ecoregions (Granger, 1999; Janowicz, 1999). Elevations range from 800 to 2250 m. The treeline is located at roughly 1300 m (Granger, 1999). The Granger subcatchment has an average elevation of 1250 m and lies within the discontinuous permafrost zone, where permafrost underlies north facing slopes and higher elevations (Carey and Woo, 1998; Granger, 1999).

2.3.1.1 Climate

The basin has a sub-arctic continental climate characterized by a large annual variation in temperature, low relative humidity, and relatively low precipitation. Mean annual temperature over the period of 1971-2000 is -3° C, with average temperatures of 5° C to 15°C in summer, and -10° to -20° C in winter (MSC, 2005). Average annual precipitation is between 300 to 400 mm and approximately 40% falls as snow (MSC, 2005).

2.3.1.2 The North-Facing Slope

Data for this study was collected on the north facing slope of Granger basin. The soil cores (in Ch. 3) were extracted near the soil pit which is located about midway to the top of the slope (Figure 2-3). The north-facing slope has an average gradient of 17.5° (Pomeroy et al., 2003). It is located above tree line, but supports patches of dwarf willow (*Salix sp.*), dwarf birch (*Betula sp.*) and alder (*Alnus sp.*) shrubs ranging in height from 0.5 to 1.5 m (Janowicz, 1999; Jones and Pomeroy, 1999). The north facing slope is underlain by permafrost and by late summer the active layer thaws to an average depth of 0.4 m (Quinton and Gray, 2001). Peak river flows are due to snowmelt, intense summer storms, or rain on snow events (Janowicz, 1999).

2.3.1.3 Soils

Soils on the north facing slope consist of a nearly continuous organic cover with an average thickness of 0.4 m; broken by sporadic patches of the underlying mineral soil and the occasional large boulder (Quinton et al., 2000). The upper layer of organic soil consists of living vegetation mixed with lightly decomposed peat. The degree of

decomposition, bulk density, porosity, and small, closed and dead-end pores increases proportionally with depth (Quinton and Gray, 2001).

2.3.2 Scotty Creek

The Scotty Creek drainage basin (61°18'N; 121°18'W) is a 152 km^2 peatland complex of bogs, fens and peat plateaus in the Lower Liard River Valley, 55 km south of Fort Simpson, Northwest Territories (Quinton et al., 2003) (Figure 2-2). Scotty Creek lies in the continental high boreal wetland region of Canada (NWWG, 1998), and is in the zone of discontinuous permafrost. Only the peat plateaus overlie permafrost, while bogs and fens experience seasonal freeze-thaw (Robinson and Moore, 1999)

2.3.2.1 Climate

Mean annual air temperature and precipitation are –3.2° C and 369 mm, respectively, with 46% of annual precipitation falling as snow (MSC, 2005). Snowmelt usually begins in late March and continues through most of April, with small amounts of snow remaining into May.

2.3.2.2 Peat Plateaus

Soil cores were extracted and a soil pit was installed on a peat plateau to collect data for both studies (Figure 2-2). The plateaus are elevated 1 to 2 m above the surface of the surrounding fens and bogs. By late summer, the average frost table depth at the site is approximately 0.6 m (Quinton et al., 2000), though some researchers have reported frost depths as great as 1 m at similar locations (Quinton et al., 2003). The soil stratigraphy consists of a continuous organic layer of varying thickness, 0-8 m, overlying

a silt-sand layer, below which lies a thick clay to silt-clay deposit of low permeability (Pietroniro et al., 1996; Quinton et al., 2003).

Mature plateaus support shrubs and black spruce (*Picea mariana*) with a ground cover composed of lichens and mosses overlying sylvic peat containing dark, woody material and the remains of lichen, rootlets and needles (Robinson and Moore, 1999; Quinton et al., 2003). The underlying permafrost forms an impermeable layer above which water is conducted laterally to the adjacent bogs and fens.

2.4 METHODOLOGY

Ground heat flux was calculated using the method of Woo and Xia (1996). Soil temperature data and moisture content data in the soil profile were collected using the instrumented soil pits excavated to a depth of 0.4 m at Granger Basin and 0.7 m at Scotty creek in the summer of 2001. Pits were then backfilled once the sensors were installed. Other data for this study was collected from field observations at Granger Basin in 2002 as described below and soil pit data loggers collected climate data at Granger Basin and Scotty Creek during the spring and summer of 2002 and 2003.

2.4.1 Water Table and Frost Table

Daily water table and frost table measurements were taken at fixed points along a transect line from the base of the snow drift upslope to the stream bank down slope. Measurement points were established at 6 m intervals for a total of 20 points. To avoid measurements affected by the impact of frequent walking along the survey line, the actual measurements were taken at fixed points established a distance of 2 – 3 m to one side of the marked transect. These points were marked to ensure the same point was measured

each day. The frost table depth was measured by walking out to the measurement point and inserting a length of rebar into the ground until sufficient resistance was encountered. A precaution was taken to ensure that roots were not impeding the rebar from reaching the frost table. This was accomplished by striking the rebar with a hammer to determine if the obstruction was the frost table or a root; if the rebar was resting on a root it would bounce. Thickness of the saturated layer was determined by visual inspection and minor excavation. By simply pulling apart the organic soil layers, the water table could be directly observed and measured using a ruler with the frost table as the datum. Measurements along this transect began as the area below the drift became snow free, so some points were available for a longer record than others.

2.4.2 Soil Pit

Temperature and moisture probes were installed horizontally into the walls of the pit prior to backfilling. Soil temperature was measured using Campbell scientific 107B thermistors paired at most depths with Campbell Scientific CS615 (water content reflectometer) probes. Snow depth was measured using a Campbell scientific SR50 sonic ranging sensor at about 1.5 m above the pit. The SR50 has a 22° viewing angle and an error of 0.4% or 1cm. An Apogee IRTS-P infrared (IR) sensor located at 1.5m above the pit measures skin temperature. The IR sensor has a 3:1 field of view (FOV), with 80-90% of the reading from within the FOV and an error of 0.1-0.3° C. The IR reading is an areal average of the soil surface temperature within this area, and reports above zero temperatures once enough unfrozen soil is exposed.

Locations of temperature probes and soil moisture sensors are given in Table 2-1. All sensors were connected to CR10X data loggers, measurements were taken every 60

seconds and averaged half-hourly. Quinton et al. (in press) discuss the shortcomings of using the Campbell CS615 water content reflectometer in these environments; the data acquired were adjusted according their calibration.

2.4.3 Meteorological Data

Granger basin is instrumented with several meteorological towers, one on each slope and one at the bottom of the valley. These have been instrumented to measure snow depth, net radiation, wind, precipitation, and air temperature across the basin. The towers used in this study are referred to as GB2 and GB4. GB2 is located in the valley bottom and GB4 is located on the north facing slope at the down slope edge of the snowdrift. Meteorological data from these towers are used to run the soil thaw model.

2.5 ANALYTICAL METHODS

2.5.1 Calculation of Total Ground Heat Flux

Stratified temperature and moisture data provided by the sensors in the soil pit were used to calculate total ground heat flux (Qg) using the thermo-calorimetric method outlined by Woo and Xia (1996). Qg is the sum of three soil responses to energy input during thawing of the active layer: Qp, Qi and Qs (Woo and Xia, 1996). Each component is calculated separately in units of W/m^2 then converted to units of $MJ/m^2 \cdot day$ to allow daily summation of Qg.

2.5.2 Data Requirements

The thermo-calorimetric method requires data on the rate of decline of the cryofront, average daily soil temperature, soil moisture and layer thickness, in addition, thermal conductivity and specific heat of the soil constituents (soil, ice and air) are used

to calculate heat capacity and thermal conductivity of the soil-ice-air mixture. Because temperature and moisture sensors are located at prescribed depths, the soil profile was divided into discrete layers around these sensors in order to calculate the change in heat storage throughout the profile and accommodate for the depth dependency of porosity.

Sensor and layer divisions of the soil pits at Scotty and Granger are shown in Table 2-2. Qs was calculated individually for each layer, Qp was calculated at the bottom of each soil pit where heat is transferred to the permafrost, and Qi is calculated for the layer containing the cryofront. Bulk density and porosity data were obtained by Quinton (2001) from analysis of soil samples and cores taken from the face of the soil pits at 0.05 m intervals to a depth of 0.4 m at Granger, and a depth of 0.5 m at Scotty using standard methods (Table 2-3).

2.5.3 The Thermo-Calorimetric Method

Bulk heat capacity (C) was calculated for each day using Woo and Xia (1996).

$$C = \sum_j C_j f_j \qquad [2\text{-}2]$$

Where C_j is the volumetric heat capacity of constituent j (soil, ice, air or water), values for all constituents were taken from Quinton and Gray (2001) (Table 2-3), and f_j is the volume fraction of j. The soil fraction was always considered as $f_{soil}=1-\phi$, where ϕ is porosity. Although the majority of the moisture in frozen soils exists as ice, a certain fraction remains unfrozen. In some cases this unfrozen water content can influence the thermal properties of frozen soils by providing pathways for heat transfer (Romanovsky and Osterkamp, 2000). For this study, in the frozen state, the pore ice fraction was approximated by ϕ minus the unfrozen water content indicated by the Campbell CS615

water content reflectometer in the soil pits. This value was on average 18% in all layers prior to thaw. This approach is assumed to provide a reasonable estimate and agreed with values from the literature (Quinton and Hayashi, 2005) which indicated an average of 18% volumetric water content when the soil is frozen. Although there is likely air present in the frozen soils, the actual air content is not known. As a result, this study does not include the air content for the frozen soil calculation and, instead, considers the remaining pore space filled with ice. In the unfrozen-unsaturated state, water and air fractions were taken from the CS615 data, similar to the method above by replacing ice with air.

Bulk thermal conductivity was calculated for each day based on combinations of: frozen – unfrozen and saturated – unsaturated soil conditions. For all conditions, thermal conductivity was calculated using DeVries (1963) equation [2-3] from Farouki (1981):

$$k = \frac{x_w k_w + F_a x_a k_a + F_s x_s k_s}{x_w + F_a x_a + F_s x_s} \qquad [2\text{-}3]$$

where;

$$F_s = \frac{1}{3}\left[\frac{2}{1+\left(\frac{k_s}{k_w}-1\right)0.125} + \frac{1}{1+\left(\frac{k_s}{k_w}-1\right)0.75}\right] \qquad [2\text{-}4]$$

$$F_a = \frac{1}{3}\left[\frac{2}{1+\left(\frac{k_a}{k_w}-1\right)g_a} + \frac{1}{1+\left(\frac{k_a}{k_w}-1\right)g_c}\right] \quad [2\text{-}5]$$

$$g_a = 0.333 - \frac{x_a}{[n(0.333-0.035)]} \quad [2\text{-}6]$$

([5-6] if for $0<x_w<n$)

$$g_a = 0.013 + 0.944x_w \quad [2\text{-}7]$$

([5-7] is for $0<x_w<0.09$)

$$g_c = 1 - 2g_a \quad [2\text{-}8]$$

Where k is the thermal conductivity and x is the volume fraction of the constituents, air (a), water (w) and soil (s) (Table 2-3); for the frozen case air was replaced by ice. For this study, equation [2-3] is assumed to be representative of organic soils. Although there is no direct research addressing the reliability of applying these equations to organic soils, they reported to be relatively reliable when applied to frozen coarse soils (Farouki, 1981), and have also been used previously for heat budget calculations on similar organic soils (Woo and Xia, 1996; Quinton and Gray, 2001). In this study, the calculation of thermal conductivity is presumed to be less reliable than that of heat capacity, with errors in the range of 10%-25% and about 1%, respectively, based on values from the literature (Hillel, 1998; Bristow, 2002; Kluitenberg, 2003).

Q_s was calculated for each layer using equation [2-9]

$$Q_s = C\left(\frac{dT}{dt}\right)z \qquad [2\text{-}9]$$

where z is the thickness of the soil layer, C is the heat capacity and dT/dt is the change in daily average temperature, calculated as the difference between the previous day and the current day. Heat capacity is calculated using the current day's soil moisture. Qs for each layer is added together to obtain total Qs for the thickness of the organic layer for each day and cumulative Qs for the thaw period.

Q_p was calculated using equation [2-10]

$$Q_p = k\left(\frac{dT}{dz}\right)_{bottom} \qquad [2\text{-}10]$$

where, k is the thermal conductivity at the base of the soil pit and dT/dz is the temperature gradient between the last two sensors at the bottom of the soil pit. At Granger these are the sensors at 30 cm and 40 cm, while at Scotty, the sensors at 50 and 70 cm were used for 2003 and the sensors at 40 and 60 cm were used for 2002. The inconsistencies between the two years at Scotty were required due to malfunctions in the deeper sensors. The temperature gradient at the bottom of the soil pit is assumed to be indicative of the energy being conducted to the mineral soil below the organic soil.

Q_i is calculated using equation [2-11],

$$Q_i = \rho_i \lambda f_{ice}\left(\frac{dh}{dt}\right) \qquad [2\text{-}11]$$

where ρ_{ice} is the density of ice, λ is the latent heat of fusion, f_{ice} is the fractional ice content, and (dh/dt) is the rate of decline of the frost table (in m/day). The f_{ice} was set

equal to the porosity minus the unfrozen water content of the layer containing the zero degree isotherm (Roulet and Woo, 1986) with porosity values determined from soil pit samples. As outlined above, the CS615 data were used to estimate unfrozen water content. The air content of the frozen soils is not included in this calculation as this data was not available. To calculate the rate of frost table decline, the position of the cryofront was estimated from soil pit temperature measurements (Hinkel and Nicholas, 1995; Carey and Woo, 1998; Hinkel et al., 2001). The cryofront coincides with the depth at which the average temperature equalled or exceeded zero degrees. All intermediate points were calculated by linear interpolation.

The thermo-calorimetric method requires information regarding the saturation and temperature of each soil layer. Thermal conductivity and heat capacity change as the soil changes from frozen to thawed, and from saturated to unsaturated. Combinations of data sets were utilized to approximate the state of each soil layer. Water level recorders in wells, pressure transducers and the soil moisture measurements were combined to estimate saturated layer position. In all cases, the first approximation of saturation was taken from the soil moisture measurements. All soil moisture data show an initial peak shortly after the passing of the zero degree isotherm, and then a decline (Figure 2-4). In some cases the moisture declines substantially after the peak; in other cases only a slight decline in soil moisture was observed. Layers with a substantial decrease in soil moisture are considered to become unsaturated, while in the other case the layer is considered to remain saturated until a significant decline in soil moisture is observed. Each layer is saturated with a combination of unfrozen water and ice until the zero degree isotherm has passed. This method poses some problems when the calculation is switched from frozen

to unfrozen and the constituent formerly considered ice is now air. In reality, this transition would be a gradual one of ice melting, water draining and air infiltrating, but the limitations of this method result in the ice content declining as volumetric water content increases until the cryofront has passed and the ice is considered to be completely replaced by air. At Scotty Creek where soil moisture increases quite significantly, this transition is relatively smooth, while at Granger, the soil moisture does not increase as greatly and the change is much more abrupt (Figure 2-6 and 2-5).

2.5.4 ΣQg and ΣTs

Summation of Qg began on the first day that daily average skin temperature (Ts) rose above 0°C, the day prior has cumulative Qg = 0. This point was chosen as it coincides within a few days of the disappearance of snow cover according to digital photographs, field observations, SR50 data and the literature (Woo and Steer, 1983; Roulet and Woo, 1986; Woo, 1986). Plots of snow depth, Ts and soil temperature from Scotty Creek in 2002 (Figure 2-5a) indicate that Ts rose above zero with an areal average snow depth of 0.2 m; while in 2003 (Figure 2-3b) snow depth declines to zero prior to Ts and soil temperatures rising above zero. Soil temperature measurements and snow depth observations at Granger Basin in 2002 showed that soil thaw began as soon as the snowcover above the soilpit was patchy, even though the areal average snow depth was still greater than zero. In all cases, data and observations support the assumption that snow cover is at most thin and patchy at the point when skin temperature increases above zero.

Cumulative skin temperatures (ΣTs) at the soil pits were corrected for sensor error, and daily averages were summed. Cumulative Qg (ΣQg) was calculated using

daily sums in units of $MJ/m^2 \cdot day$. These were plotted against each other to determine a ΣQg-ΣTs relationship. Following the work of Quinton et al. (2001), and in order to run the Cold Regions Hydrological Model (CRHM), a linear regression was fit to the plot of ΣQg - ΣTs. The regression was plotted through the origin, as the application of this equation in CRHM requires the initial energy to be zero. The intention is to start the soil thaw algorithm on the first day the ground becomes snow free. Regression lines and associated equations and R^2 values were calculated using Microsoft Excel's trendline function. Cumulative plots were also fit with a derivation of the one dimensional heat transport equation [2-12] from Fourriers' equation suggested by Hayashi (personal communication)

$$\Sigma Qg = k\sqrt{\Sigma Ts} \qquad [2\text{-}12]$$

where k is an empirical fitting parameter to compare a non-linear model against the current representation of soil thaw in CRHM.

2.5.5 The Cold Regions Hydrologic Model (CRHM)

CRHM is an analytical tool used to simulate soil thaw and slope runoff. Slope units are represented as a stack of discrete layers where soil properties such as porosity, initial temperature and soil type are user defined. These properties were set equal to those used in the thermo-calorimetric calculations. The model is driven by the use of time series measurements of ground skin temperature (Ts), rainfall and air temperature. The data required to run the model were taken from IR temperature measurements over the soil pit (Ts), and air temperature and precipitation measurements from the nearby met towers. The current representation of soil thaw in CRHM uses a linear relationship to

calculate Qg from Ts with the constant of proportionality from the linear regressions, soil thermal and physical properties input by the user. Soil layers are successively thawed using Qg to first warm the soil layers to zero degrees and then melt the ice. Model runs were performed using a single hillslope unit to simulate soil thaw for each pit. The linear regression coefficients derived from the ΣQg-ΣTs relationship were used for their corresponding site and year and an average coefficient of all sites and years was also tested.

2.6 RESULTS AND DISCUSSION

The following section discusses the magnitude of Qg, its components, their dependence on soil moisture and the ΣQg-ΣTs relationship for Granger Basin and Scotty Creek.

2.6.1 Thermal Conductivity, Heat Capacity and Soil Moisture

The high porosity of organic soils means that changes in heat capacity and thermal conductivity are closely linked to the soil moisture content (Wolfe, 1963; Nixon, 1973; Hinzman et al., 1991; Woo and Xia, 1996; Carey and Woo, 1998; Quinton and Gray, 2001). As moisture in the soil changes state, from ice to water, and then drains to allow air into the pores, the thermal conductivity decreases (Figure 2-6). Conversely, heat capacity increases as water replaces ice, but then decreases, below that of the initial frozen state, as water drains and air infiltrates the pores (Figure 2-7). However, in this study, the gradual transition from frozen to unfrozen, as water replaces ice, appears as an abrupt change to the unsaturated state because the volumetric water content (from CS615

data) does not increase to the point where it entirely replaces the ice content (fully thawed-saturated state).

2.6.2 Thaw Rate and Frost Table Position

The location of the frost table was assumed to be equal to the depth of the cryofront, estimated using soil pit temperature readings and compared with field measurements of thawed layer thickness (Figure 2-8 to 2-9). The cryofront has been shown to agree to within 0.02 to 0.03 m of field measurements (Carey and Woo, 1998; Hinkel et al., 2001) and data from the Granger site in 2002 suggest that this is a reasonable assumption (Figure 2-8). Other years and sites show good correlations, but with fewer data points for comparison (Figure 2-9 to 2-9).

Figure 2-12 shows the frost table position for all sites and years beginning on the first day of thaw. The frost table is expected to decline rapidly at first, subsequently slowing if the upper layers drain and insulate the underlying soils (Vasilenko and Zhuravin, 1997; Hinkel et al., 2001). Woo and Xia (1996) theorized that wet sites maintain greater thermal gradients near the surface, thus sustaining faster thaw rates due to the higher heat capacity of water over air. This occurs because water does not lose heat as readily during cooling periods, maintaining warmer subsurface temperatures, stronger temperature gradients and delivering heat more efficiently to the frost table for thawing.

At Granger, ground slope results in the drainage of the thawed soil and a decline in thermal conductivity (Figure 2-4B) providing better insulation and possibly causing shallower thaw depths (Figure 2-12). Deeper thaw is expected and observed at Scotty

(Figure 2-12) due to higher values of thermal conductivity (Figure 2-4) and heat capacity (Figure 2-5) as a result of persistent saturation of the soil due to the lack of slope.

2.6.3 The ΣQg-ΣTs Relationship

The ΣQg - ΣTs relationship and linear regression lines are plotted for each year of record for both sites (Figure 2-13). In all cases the plots show an initially rapid increase in Qg, after which the rate of accumulation decreases and plots become more linear as thaw progresses. Regression lines for Granger and Scotty in 2002 had R^2 values of 0.75 and 0.88, respectively, while in 2003 Scotty had the lowest R^2 value (0.55) with Granger for 2003 only slightly higher at 0.59 (Table 2-4). In all cases the linear regression initially underestimates the rapid increase in Qg, but later, a closer agreement is achieved although there is a consistent overestimation of Qg by the regression equation. An improved fit may be achieved by fitting two linear regressions, one to the initially rapidly increasing portion of the curve and one to the more linear later portion. However, inspection of the graphs indicate that the initial increase appears significantly different in all plots, and the selection of a consistent transition point would be difficult. On average, the regression lines show a final prediction of accumulated Qg to agree within 12% of calculated ΣQg (Table 2-4) with all the coefficients lying within 10% of the average coefficient value. Similarities in the regression coefficients suggests that a linear ΣTs-ΣQg relationship is reasonably portable between these two sites for estimating total accumulated energy, but with limited power to accurately predict the position of the frost table, especially during the early stages of thaw.

Figure 2-14 to 2-17 show the results of fitting the power equation [2-12] to the ΣTs-ΣQg relationship for each year at each site. Inspection of the curves suggested that a

one dimensional form of Fourriers law could potentially offer a better fit. Values of K, predictions of Qg, and error values are given in Table 2-5. The power relationship results in a better overall prediction of the trend in Qg, with better representation of the rapid initial increase. Root mean squared error (RMSE) values for the power equation are lower than their corresponding linear regressions and overall predictions of Qg are closer to the calculated values. Overall the results suggest that the power relationship is a better and more transferable representation of the accumulation of ΣQg as a function of ΣTs. However, the current linear representation of soil thaw in CRHM doesn't allow the power relation to be tested in the model.

In future research some physical meaning could be attached to the coefficient (K); perhaps trends in soil moisture, thermal conductivity, heat capacity or other moisture dependant variable. Continued accumulation of Qg, however, may show a significant departure from the power curve if the plot were to be extended beyond the current range considered in this study as the nature of the square root curve results in smaller and smaller increases in Qg with Ts. However, during the critical snowmelt period the power equation [2-12] better represents the thawing trend with a greater degree of accuracy compared to the linear relationship (Table 2-5).

2.6.4 Partitioning of Qg

The soil pits were excavated to measure the energy fluxes during thaw in the surface organic layer. Because total active layer thickness extends below the deepest sensors, calculated Qg is only a measure of the energy transferred in the upper organic portion of the soil profile at Scotty, but includes the shallow mineral soil at Granger. As such, the scope of this study is limited to the period during which the zero degree

isotherm is above the lowest temperature sensor. Despite a relatively close agreement between the ΣQg-ΣTs relationships at both sites, energy partitioning is very different. Values reported in the literature are compared to those calculated for this study in Figure 2-18 (Woo and Xia, 1996; Carey and Woo, 1998; Quinton and Gray, 2001).

Both sites show similarity in the partitioning of energy between years (Figure 2-18). At Scotty Creek, Qi accounts for the large majority (85-89%) of Qg. Qs is also relatively large, at 9% and 11%, at each site, respectively, compared to an average of 5% for all the data presented. Granger shows a different partitioning of energy, but with no significant difference between years. Qs is almost the same for both years, while Qp and Qi are slightly different. In 2002, Qi and Qp account for 68% and 30%, respectively, while in 2003, Qi accounts for only 63% and Qp for 34%.

Both years at Granger yield similar magnitudes of total accumulated Qi in MJ/m^2 (Figure 2-19) because of similar soil moisture contents. This occurs because the ice volume in the soil is assumed to be equal to the porosity minus the volumetric water content. Thus the unfrozen water is the only factor influencing the volume of ice and, subsequently, the magnitude of Qi. As a result, the total volume of ice thawed is roughly the same for 2002 and 2003 at Granger and, therefore, differences in the partitioning of Qg are accounted for by the magnitude of the Qp and Qs fluxes. Most of this difference is a result of a larger Qp in 2003, likely due to the stronger temperature gradient at the base of the soil pit (Figure 2-20). Scotty, on the other hand, has larger values of Qi because of deeper total thaw depth in 2003, larger porosity values throughout the profile and no mineral soil within the range of the soil pit. Larger Qs values at Scotty are a result of higher soil moisture content resulting in higher heat capacities. While smaller values

of Qp are a result of the smaller thermal conductivity of peat at Scotty over the mineral soil at Granger.

2.6.4.1 Transferability of Energy Partitioning

Between the two sites there is a significant difference in energy partitioning values. The majority of the difference is encompassed in Qp and Qi which vary by about 25-30% between Scotty Creek and Granger. Granger seems to be slightly more indicative of drier northern soils, with higher Qp and lower Qi values. Scotty is a wetter site with much higher Qi and very small Qp. On the whole, Qs values are uniformly small across all sites from both this study and the literature, while Qp and Qi vary by up to 60%. The majority of this variation is likely due to assumptions regarding ice content, thermal conductivity, heat capacity and soil moisture. These results indicate that the partitioning of energy is not transferable between these two sites.

2.6.5 Frozen Soil Infiltration

When the ground becomes snow free, subsurface temperatures at both Scotty and Granger are at or near $0^{o}C$ (Figure 2-21). One possible explanations for this is the percolation of snowmelt water into the soil profile prior to ground exposure, raising soil temperatures to just below freezing by latent heat transfer (McGaw et al., 1978; Hinzman et al., 1993). Soil moisture increases following a rise in soil temperature to just below 0 $^{\circ}C$, possibly indicating an initial percolation and refreezing of a few millimeters of water into all layers prior to snowcover disappearance. The refreezing of this water would explain why the CS615 data do not initially indicate an increase in unfrozen water content as soil temperatures increase. In this case, prior to thawing; frozen layers are not

initially saturated; however, the percolation and refreezing of meltwater may fill and seal some or all available pores (Woo and Steer, 1983; Woo, 1986). Another possible explanation is the conduction of heat downward from the isothermal snowpack into the soil. In this case, the soil will be warmed to 0°C, the temperature of mature melting snow, until the snow cover disappears and the soil is exposed. In either case the isothermal conditions in the soil profile create an ideal scenario for CRHM, where initial layer temperatures play an important role in energy requirements for Qs.

2.6.6 CRHM: Model Fit

The linear regression coefficients derived from the ΣQg-ΣTs relationships were used in CRHM to simulate soil thaw. Soil properties were set equal to those used in the thermo calorimetric calculations for each site. The association between predicted and measured thaw depth are reflected in all the predicted curves, but with a major departure during initial thaw (Figure 2-8 to 2-9). CRHM underestimates early values and eventually overestimates thaw rate at all sites except Scotty in 2002. For Granger in 2002 and 2003, CRHM accurately predicts the time that thaw began, but underestimates the thaw rate due to a rapid initial decline of the frost table. The refreezing at Granger in 2003 brings the zero degree isotherm points closer to the CRHM curve. However, subsequent rapid thawing between May 24th and 30th leads to a significant discrepancy between the two. In all cases, except Scotty in 2002, CRHM closely approximates the final position of the frost table within about 0.05-0.1 m. However, in no case does CRHM accurately represent the entire season.

2.7 CONCLUSIONS

One of the major drawbacks in the current representation of soil thaw is the assumption of constant energy partitioning throughout the thaw period. Initially, the majority of Qg is consumed in Qi (Figure 2-22 to 2-27). Following this, energy partitioning is largely dependant on ice content and soil moisture, with higher values of each corresponding to higher energy consumption in Qi and Qs. Figure 2-12 shows the progression of thaw at Granger and Scotty. At Scotty, thaw proceeded at a greater rate through most of the study period, likely due to wetter soil conditions and possibly more incoming radiation. Granger, on the other hand, located on a north facing slope, could experience slower thaw because of the insulating effect of dry soils or the reduced incoming solar radiation due to slope and aspect.

Differences in soil ice content are also likely to contribute to the variation in initial thaw rate. Once thaw progresses below 0.2 m at Granger, both years exhibit a similar rate, possibly because ice contents in both years are at saturation, with the lower porosities being more easily filled with ice. However, at Scotty, the first 17 days of thaw show a closer agreement between years, with an increasing difference once thaw progresses below 0.2 m; this could be attributed to differences in late season soil moisture and possibly rain events.

The use of a linear index model for Qg provides a reasonable approximation of thaw depth, but in all cases, rapid early thaw is underrepresented. One possible explanation lies in the assumption that the soil is both frozen and saturated. If highly porous near-surface soils are unsaturated, then the calculations of Qi and Qg largely overestimate energy consumption. As a result, simulations in CRHM, which assumes

soils are saturated when frozen, take longer to thaw ice, which, in reality, is not present in the soil. The power relation showed potential to improve the Qg-Ts relationship, with a better overall fit to the calculated values. Though both relations show a reasonable transferability between sites (Table 2-4), the energy partitioning does not, and it would be advantageous to be able to attribute both the curve fitting coefficients and the partitioning of energy to some physical qualities of the soils.

Although CHRM does a reasonably accurate job of modeling the final frost table, as well as the general trend, it consistently underestimates the actual thaw rate throughout the snowmelt period. However, CRHM does not partition Qg to the three components through the soil profile. Instead, incoming energy first warms the soil to zero degrees and then melts the ice. This essentially means Qs is neglected in layers once they are warmed to zero degrees, and Qp is not accounted for at all. As a result, CRHM will continue to thaw the soil until a model run is terminated and thawing will continue indefinitely, provided Ts is positive.

2.8 RECOMMENDATIONS

Based on the above results and discussion, a few recommendations for CRHM, future research and improvements for modeling thaw in organic soil are suggested. Models of the types of organic soils involved in this study should be sensitive to water content and should include measurements of unfrozen water content (when the soil is frozen). Energy partitioning could be improved by including information on soil moisture, where increasing wetness corresponds to larger Qs partitioning. The linear association between Qg and Ts in the CRHM model should be replaced by the power equation [2-12] and hopefully future research will find some physical meaning associated

with the coefficient. Finally, it is recommended that the calculation of Qg be automated in CRHM to allow a quick determination of this relationship for every year of record. The soil pits used in this study are still collecting data, and subsequent data sets should serve to strengthen the conclusions of this study.

2.9 ACCURACY AND ERRORS

In order to estimate the magnitude of error involved in calculating ground heat flux and its components, a simple sensitivity analysis was performed on the variables of the equations that have some associated uncertainty. The uncertainty in these variables is discussed, as well as other sources of error that may be more difficult to quantify.

2.9.1 Heat Capacity

The heat capacity of the organic soil as well as bulk heat capacity of the soil and its various constituents (air, ice and water) were increased by 10%, 20%, 50% and 100% to determine the sensitivity of the partitioning of energy and the magnitude of total ΣQg (Table 2-6). Because the heat capacity term is only used in the calculation of Qs, the smallest partition of Qg, a 50% increase in the bulk heat capacity results in an increase of only 1.4% in total ΣQg. However the values of heat capacity for water, ice and air are relatively reliable and the majority of the uncertainty exists in the values for peat. Increasing the heat capacity for peat resulted in only small changes in ΣQg and its components (Table 2-6).

2.9.2 Thermal Conductivity

Thermal conductivity was increased by 10%, 25%, 50% and 100% to determine the effect on ΣQg and its components (Table 2-7). DeVries (1975) reported that errors of

~10% for saturated and ~25% for dry soil can be expected in the equations used for this study. Increasing thermal conductivity has a pronounced effect on ΣQg and it's components, with increases of 10% and 25% resulting in 3.3% and 8.1% increases in ΣQg, respectively. There are a number of other uncertainties associated with the estimation of k because the value is dependant on the size, shape, arrangement and mode of packing of the soil and its constituents. The degree of saturation and the resulting connected pathways provided by liquid water and ice within the soil also influence the true thermal conductivity of the bulk soil volume. The equations for this study involve assumptions regarding the connectivity of these pathways (Farouki, 1981), however DeVries (1975) claims that k can be determined with a fair degree of accuracy within the limits of error outlined above. The k of the mineral soil was also varied under the assumption that the k of air, ice and water are relatively reliable. Increasing the k of the mineral soil by 10%, 25%, 50% and 100% resulted in less than 0.03% change in ΣQg.

2.9.3 Air Content

The degree to which the soil is saturated in its frozen state is uncertain, as there is no independent measure of this value. As outlined above, the soil was assumed saturated when frozen with the ice content equal to porosity less the unfrozen water content. This may not be true, in which case, if the CS615 data are taken as accurate, the uncertainty in ice content lies in the air volume that is potentially present in the soil. Air content was increased by 5%, 10% and 20% to examine the effect on ΣQg and its components. The result of this perturbation is a reduction in the ice content in the soil and the latent heat required to melt it. This had the most significant effect with a 5% increase in air content resulting in a 6.25% decrease in ΣQg (Table 2-8).

2.9.4 Instrument Error

Four instruments were used for the calculation of ΣQg, the SR50 snow depth sensor, the Apogee IRTS-P Infra-Red temperature sensor, CS107B soil thermisters, and the CS615 water content reflectometer. Documentation for these instruments outlines the expected error. The SR50 has a reported measurement error of 2.54 cm. This instrument also requires calibration and can be sensitive to strong winds. The data returned contained spikes which are possibly a result of movement of the mounting arm or animals moving through its field of view. Personal observations at the Granger Basin site indicated that the snow cover was patchy (~50%) on the day when Ts rose above zero, while the snow depth sensor approached zero due to its areal average measurement of snow cover height. Data from Scotty Creek show that the snow depth sensor indicates zero within a few days of Ts increasing above zero (Figure 2-5).

The IRTS-P has a reported measurement error of ±0.5°C. This instrument also takes an average reading with 90% taken from within a field of view of 52° and is assumed to be representative of the soil area above the soil pit. However the depth to which the sensor measures is uncertain and the exact thickness of the surface zone captured by the IR is unknown. The CS107B have a reported measurement error of ±0.4°C, and the CS615 has a reported measurement error of ±2%. Because these measurements were averaged daily, the individual errors may cancel out. Assuming the reported instrument errors are accurate for these soils, the effect of the combined error from these instruments on the ΣQg-ΣTs relationship was negligible. To test this further, the instrument errors were exaggerated by doubling and tripling them, however, results still indicated the thermo-calorimetric method is relatively insensitive to these errors.

However, it should be noted that large errors in the soil moisture sensors will greatly affect the results as outlined above regarding soil moisture and ice content of the soils.

2.9.5 Other Sources of Error

Qi, the largest component of Qg, makes use of estimates of ice content and the rate of frost table decline. Although the cryofront has been reported to reasonably approximate the frost table (Carey and Woo, 1998; Hinkel et al., 2001), the actual rate of decline was linearly interpolated between the temperature sensors. The spacing of the temperature sensors (at most 0.1 m) indicates that the error in estimation must be less than this distance; however, the actual location of the frost table at any point between the sensors is unknown. Also, during the phase change from ice to water, the soil temperature should remain at 0°C during melt. This could cause problems in determining the exact position of the frost table based purely on temperature. However, in all cases the soil temperature rose further above zero the day following the passing of the cryofront. This indicates a maximum potential temporal error of 1 day in predicting the position of the cryofront.

The two sites, Scotty and Granger, are similar in their organic soil cover, but are different in other ways. A major difference in site characteristics is that Granger is located above the tree line on a north facing slope, while Scotty is sparsely treed and on a flat peat surface. The assumption in this study is that the use of skin temperature (Ts) bypasses the energy exchanges involved in delivering heat to the surface and focuses on the energy that is entering the soil at the surface. Differences in location, elevation, slope, aspect and vegetation could contribute to the magnitude of errors in this study, and the possibility of finding any similarities between the sites.

2.9.6 Summary and Estimated Overall Error in ΣQg

The largest potential source of error in this study is associated with the moisture content of the soil. Because the thermal properties of organic soils are dependant on its water content, proper measurement and handling of this variable is crucial in studying the thawing of organic soils. Assuming reported instrument errors are accurate and a reasonable margin for error of 10-25% in calculations, and estimations of parameters for the calculation of Qg, the error in ΣQg is roughly estimated at 7-15% based on the assumptions and margins of error outlined above.

2.10 FIGURES

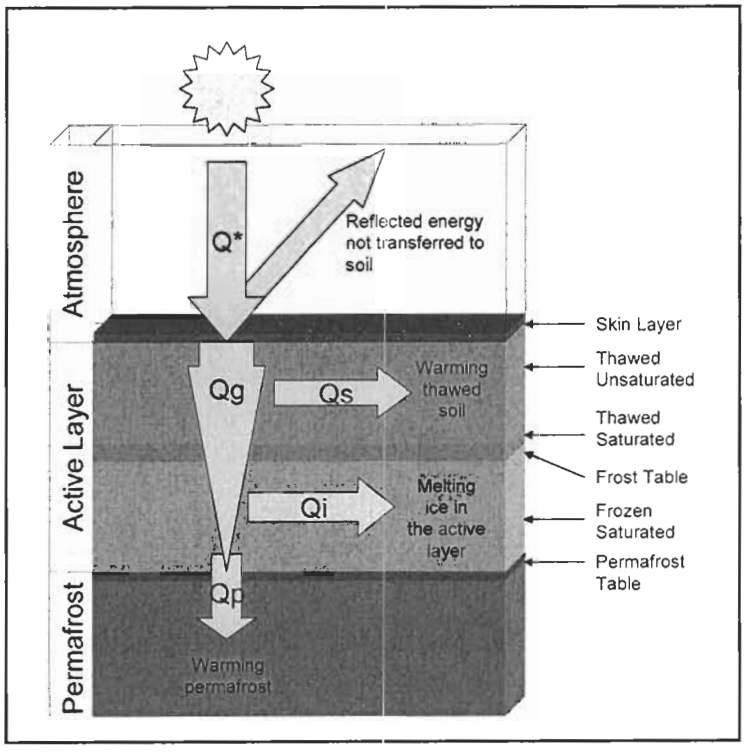

Figure 2-1. Simplified diagram of the partitioning of ground heat flux (Qg) to its three components: Qi (energy consumed to melt soil ice content), Qp (energy consumed to warm the permafrost) and Qs (energy consumed to warm the active layer after thawing) within the active layer and permafrost.

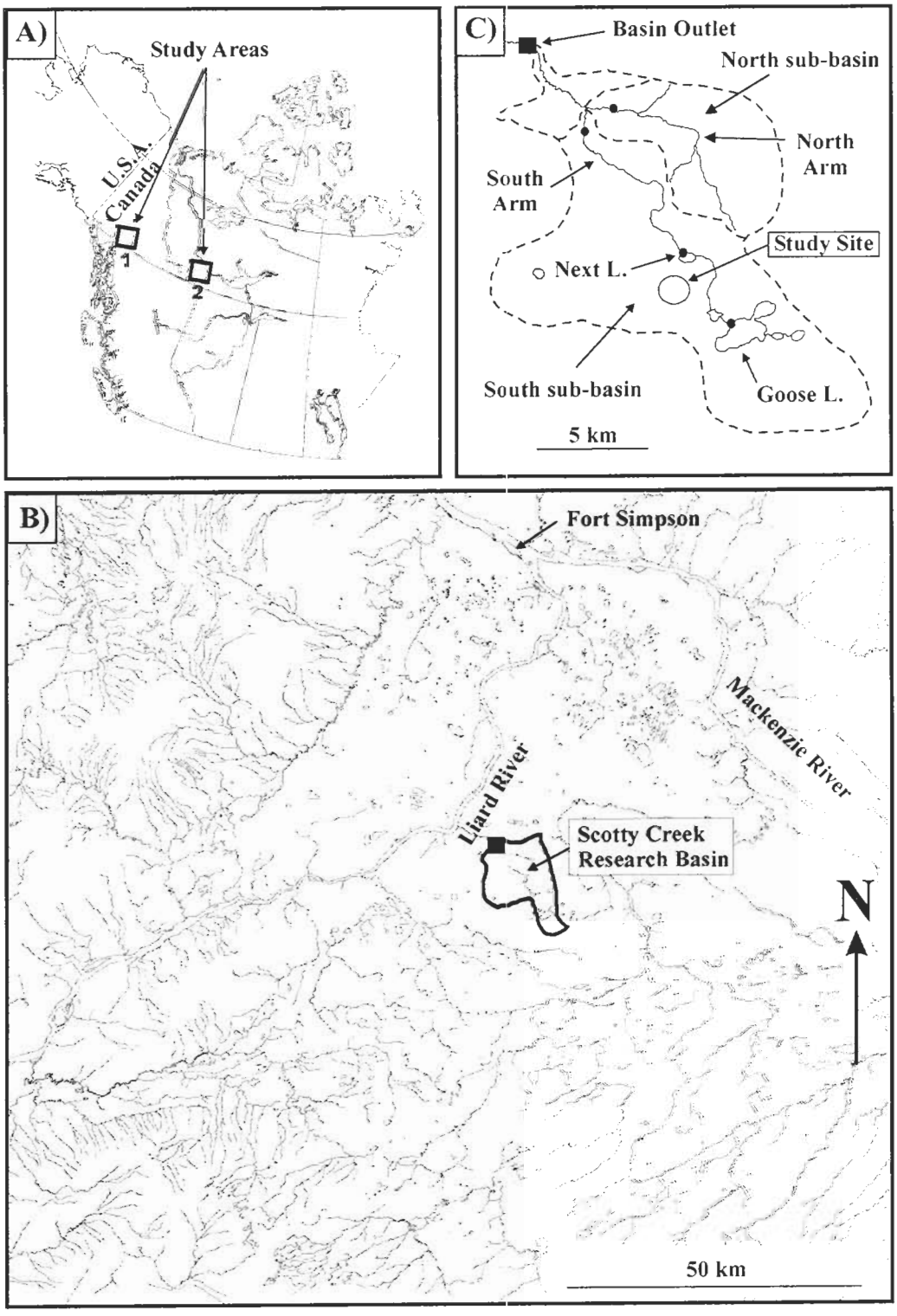

Figure 2-2. The location of the two northern sites (A) Granger Basin (1) and Scotty Creek (2) where field measurements were collected. The Scotty Creek site is located near fort Simpson in the lower Liard river valley (B). The study site where the soil pit was constructed and soil cores were extracted is located on a peat plateau in the south sub-basin (C).

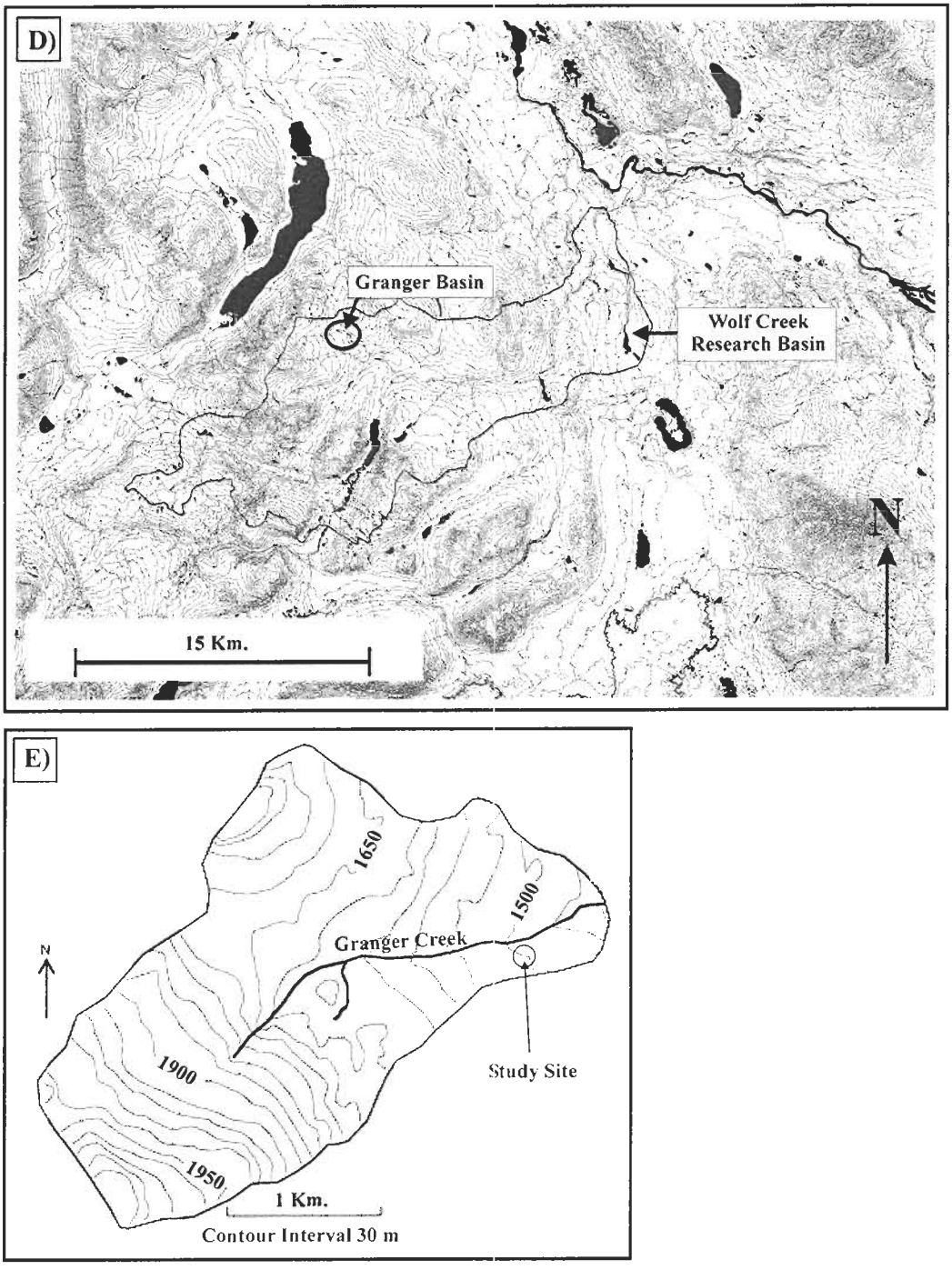

Figure 2-3. The Granger research site is located in the Wolf Creek Research Basin south of Whitehorse YT (D). The soil cores and soil pit data were acquired at a study site located on the north slope of the basin (E).

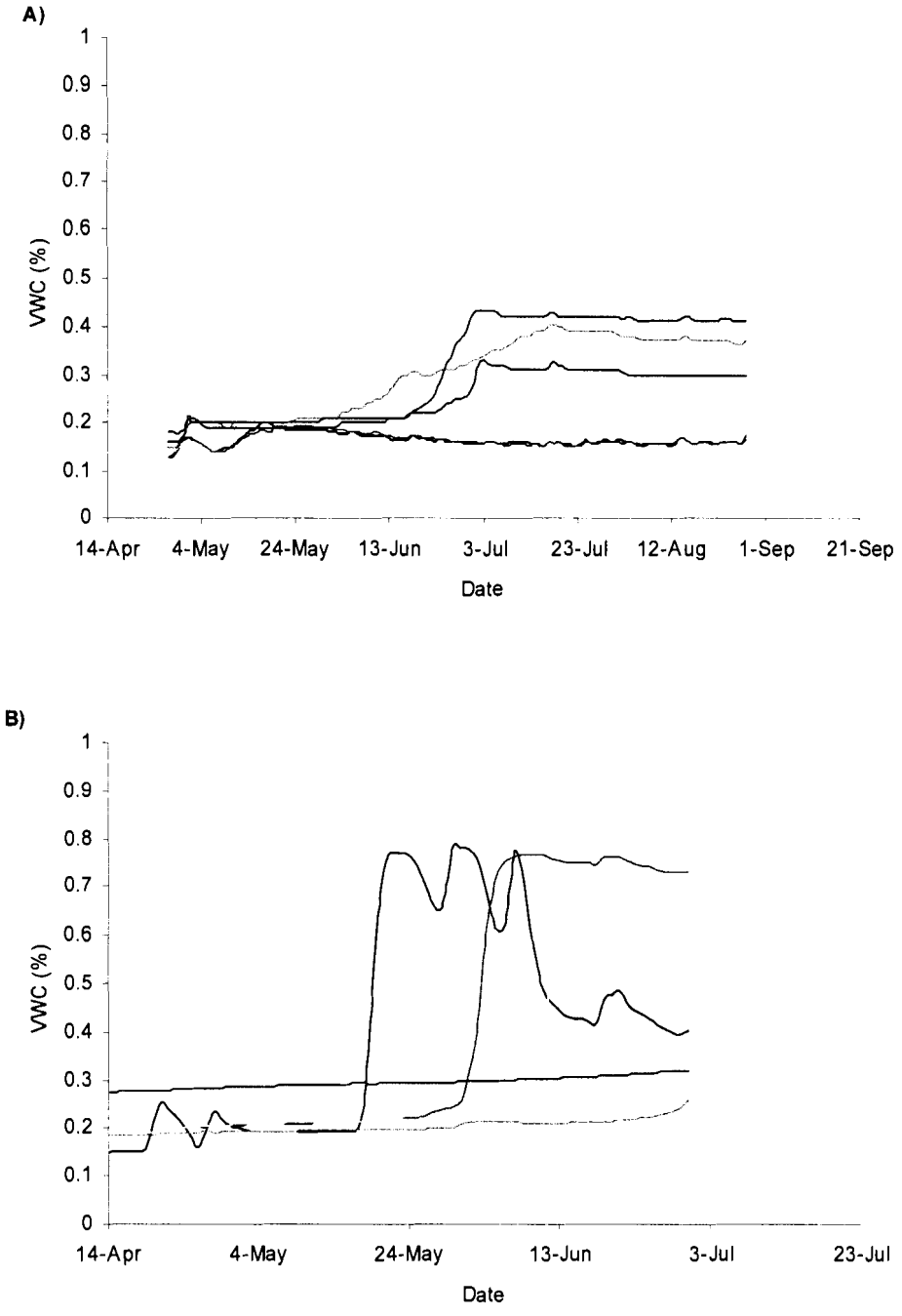

Figure 2-4. Volumetric water content (VWC) during the measurement period at Granger (A) and Scotty (B). The sharp increase in VWC occurs during the passing of the zero degree isotherm.

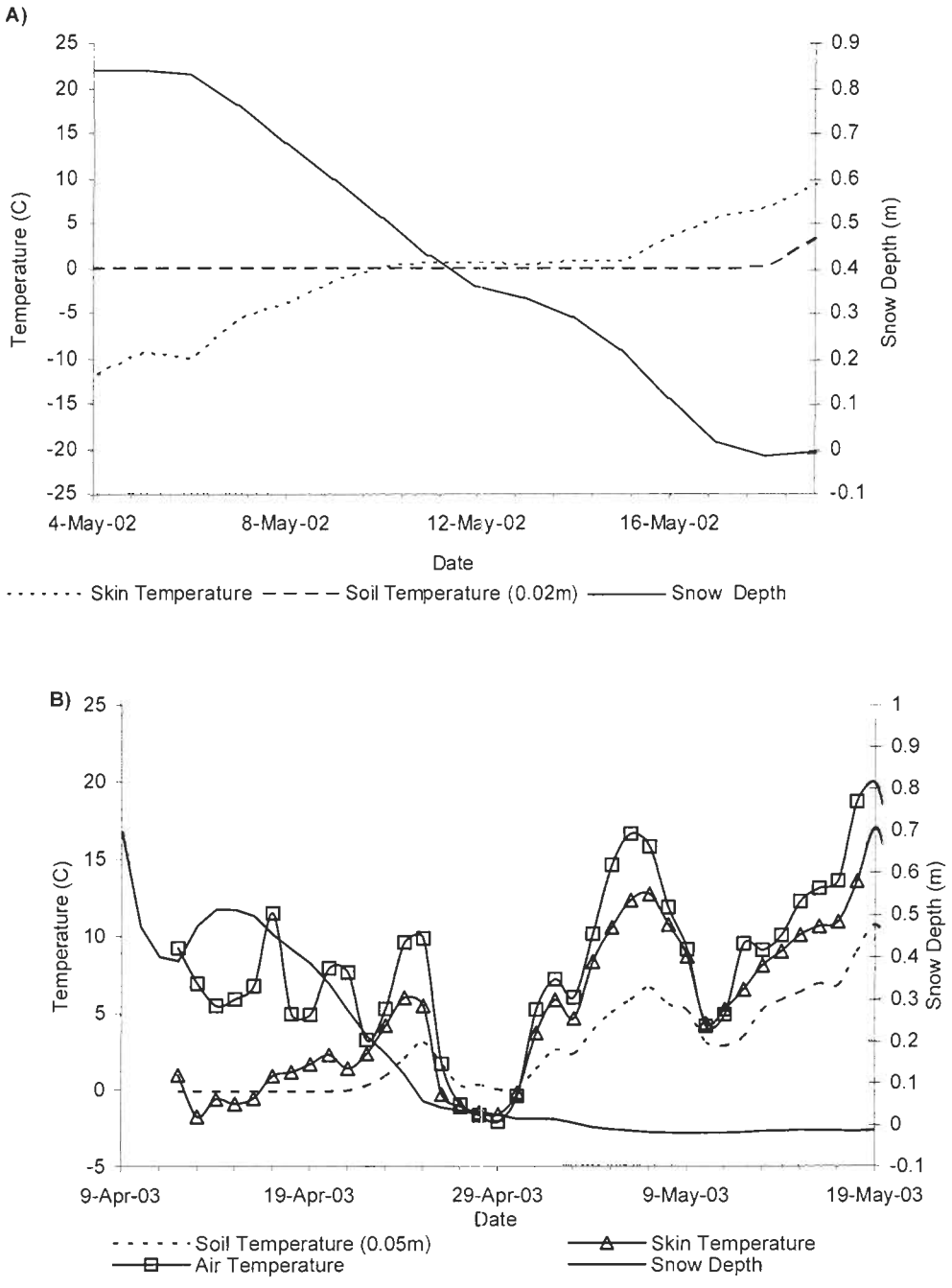

Figure 2-5. Skin temperature, near surface soil temperature (0.05 m depth), snow depth and air temperature for Scotty Creek in 2002 (A) and 2003 (B). Snow depth reaches zero within a few days of skin temperature increasing above zero. Also, following the disappearance of snow cover, skin temperature is more closely associated with air temperature (B). Note that even before snow depth reaches zero snow cover has been observed as patchy with exposed soil beneath the IR and SR50 sensors.

A)

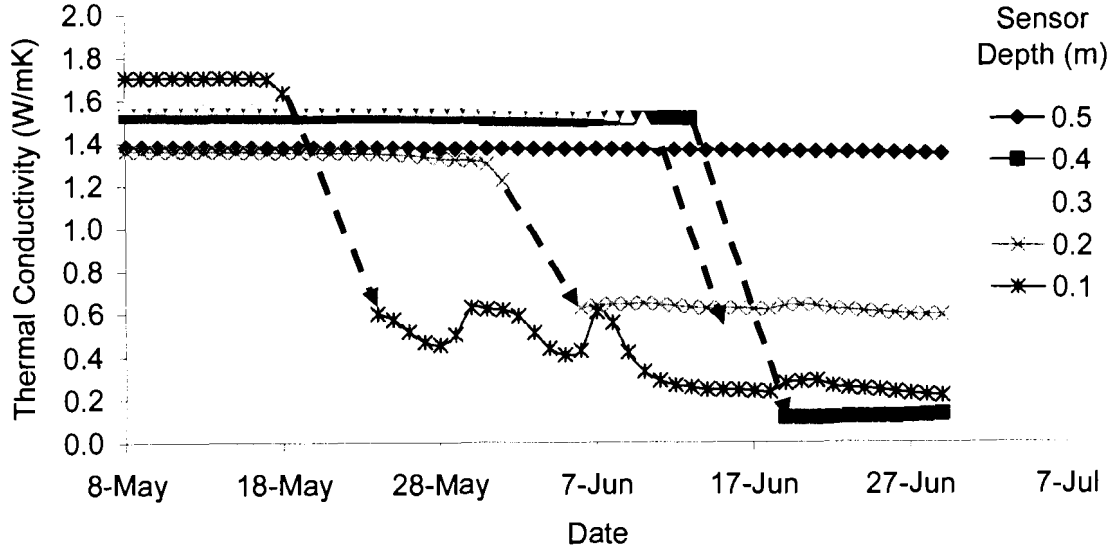

B)

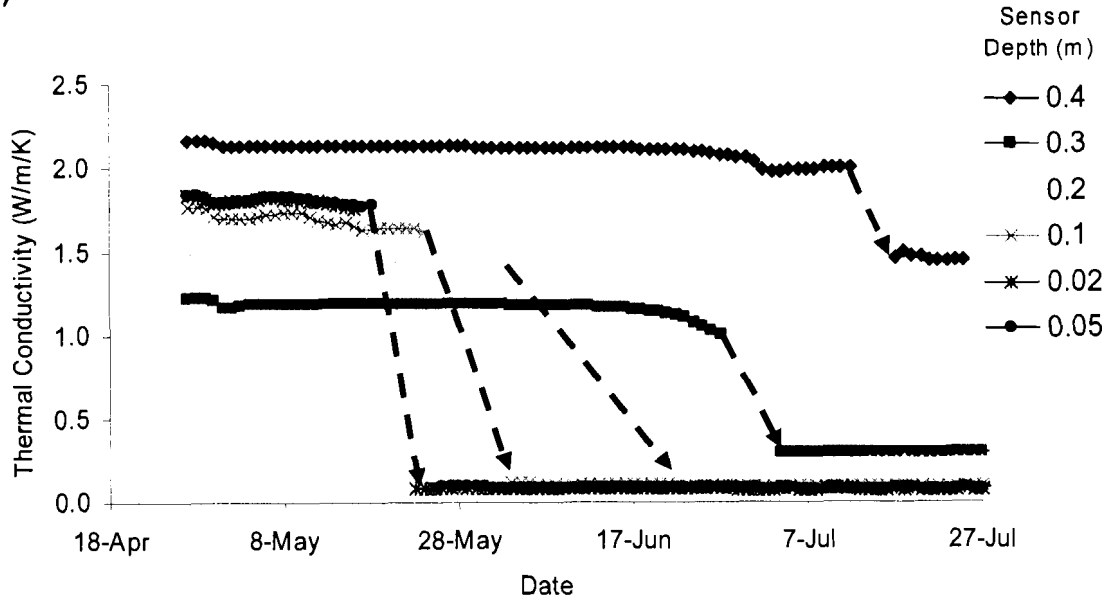

Figure 2-6. Thermal conductivity of soils for several depths at Scotty Creek (A) and Granger Basin (B) for the 2002 thaw period. Both plots indicate an abrupt decline in thermal conductivity as pore water changes state from ice to water and drains to be replaced by air. Due to a lack of data on soil air content, the transition from ice to air as soil thaws and drains has been indicated by the arrows.

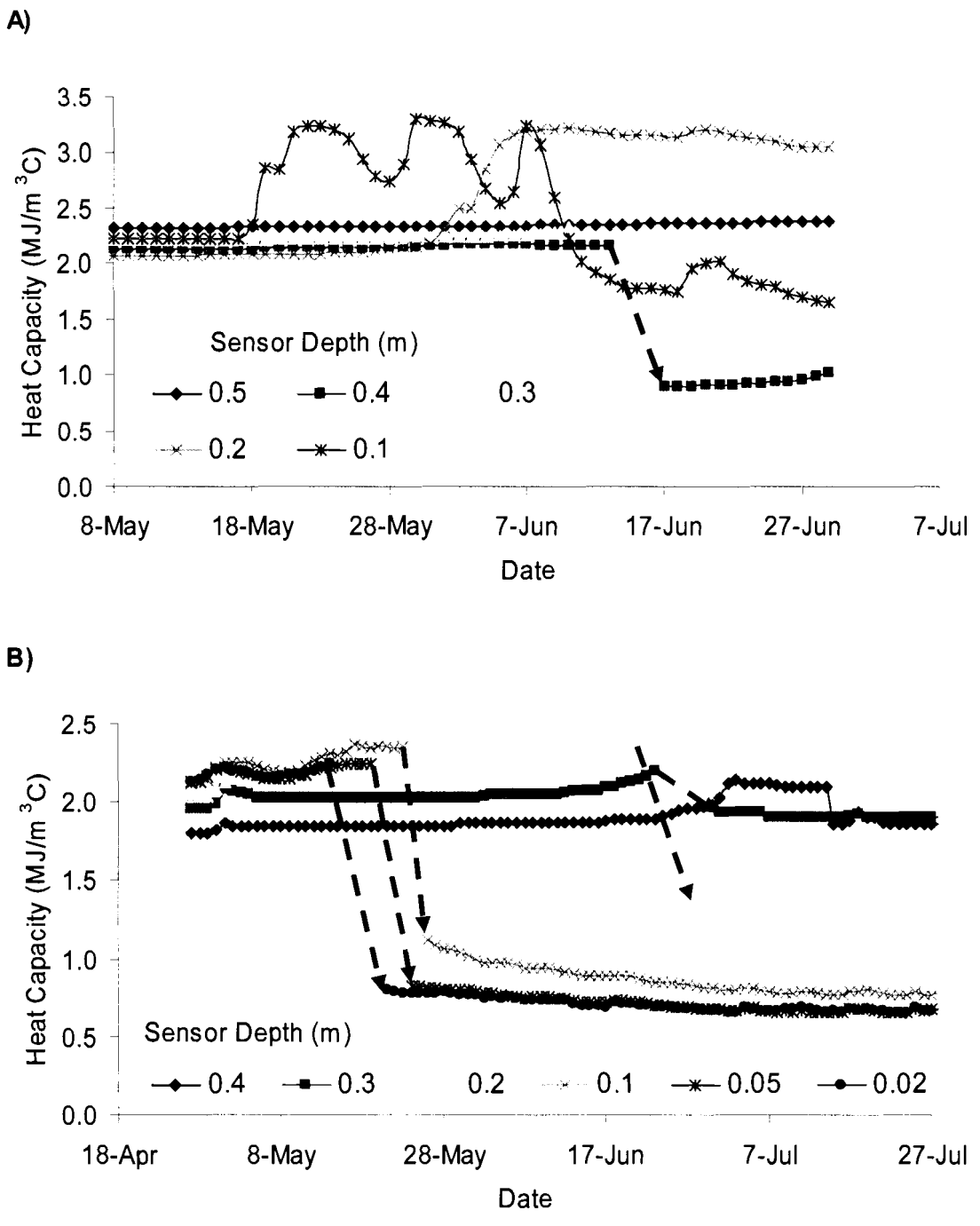

Figure 2-7. Heat capacity of soils for several depths at Scotty Creek (A) and Granger Basin (B) for the 2002 thaw period. Due to a lack of data on soil air content, the transition from ice to air as soil thaws and drains has been indicated by the arrows.

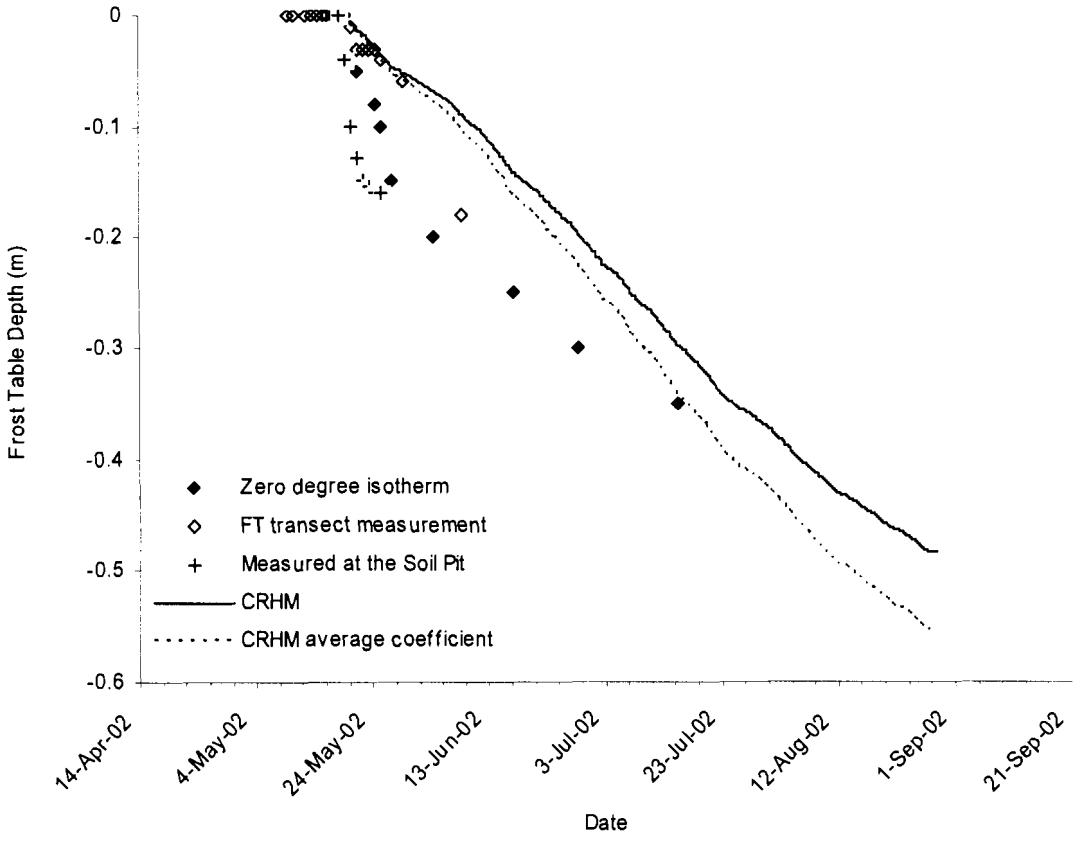

Figure 2-8. Frost table position for Granger Basin, 2002. Points show estimated position from the interpolated zero degree isotherm and measured using a graduated steel rod from points near the soil pit on the frost table transect (frost table transect points), and at the soil pit. Lines show model output from the CRHM soil thaw module for the coefficient derived from this year and the average coefficient for all sites/all years, respectively.

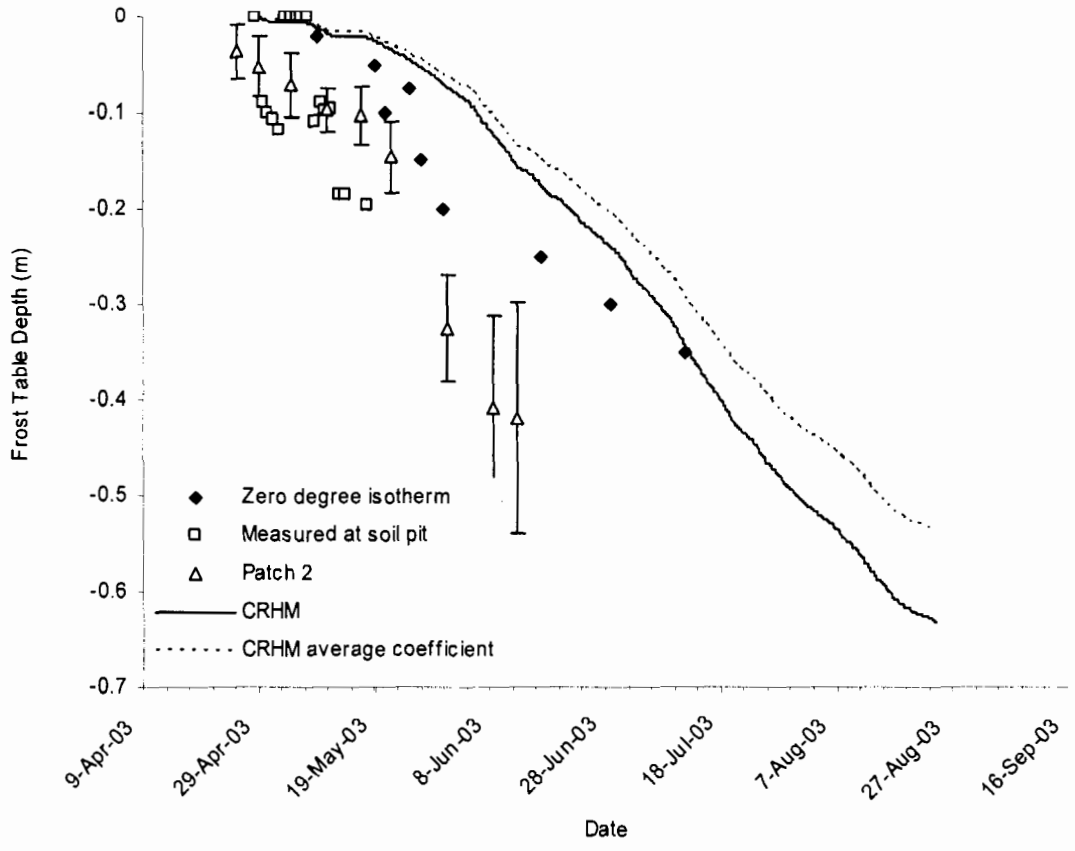

Figure 2-9. Frost table position for Granger Basin, 2003. Points show estimated position from the interpolated zero degree isotherm and measured at the soil pit and in a snow free patch nearby using a graduated steel rod. Data for measured points were taken from Shirazi (2005). The error bars indicate one standard error. Lines show model output from the CRHM soil thaw module for the coefficient derived from this year and the average coefficient for all sites/all years, respectively.

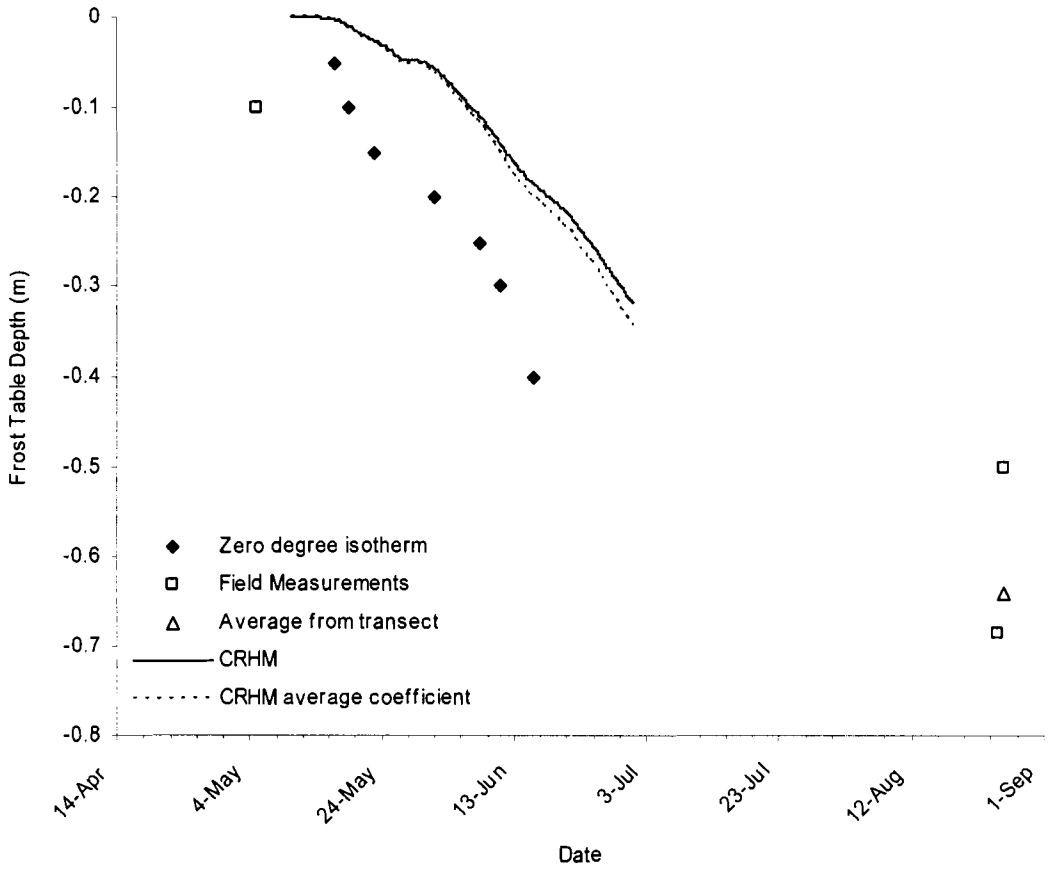

Figure 2-10. Frost table position for Scotty Creek, 2002. Points show estimated position from the interpolated zero degree isotherm and field measurements using a graduated steel rod (Hayashi, Personal Communication; Wright, Personal Communication). Lines show model output from the CRHM soil thaw module for the coefficient derived from this year and the average coefficient for all sites/all years, respectively.

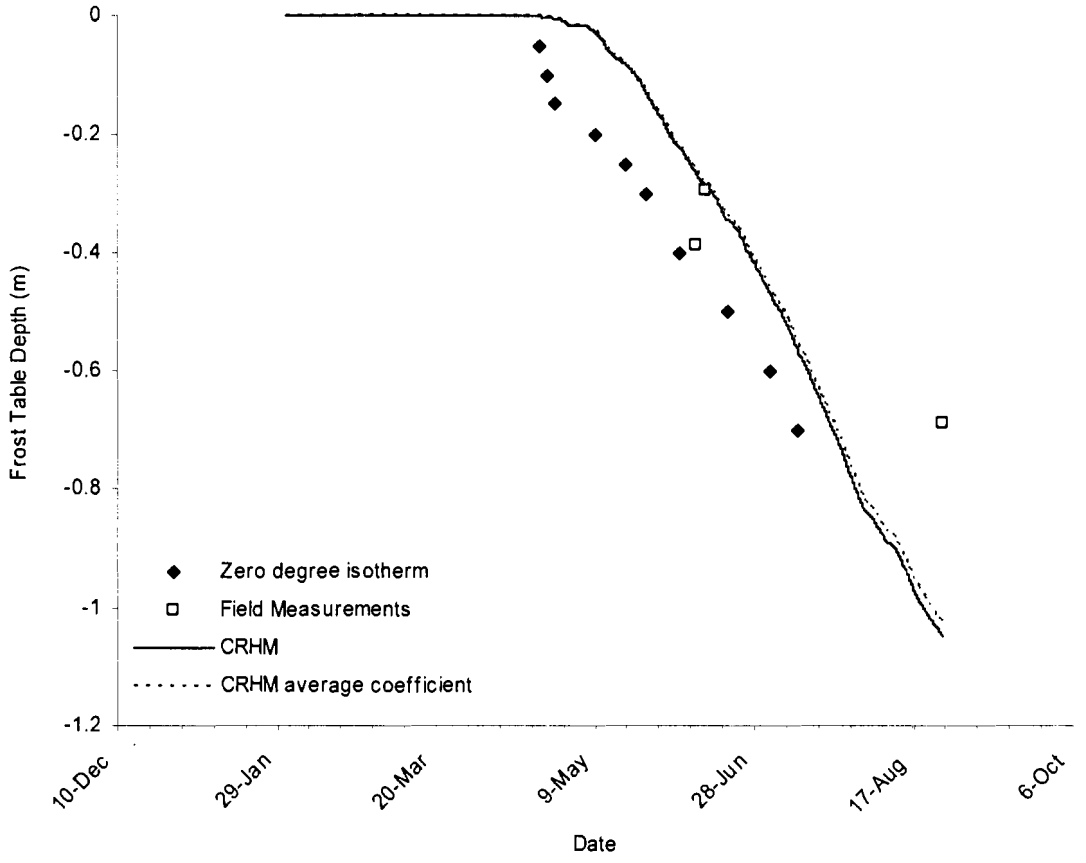

Figure 2-11. Frost table position for Scotty Creek, 2003. Points show estimated position from the interpolated zero degree isotherm and field measurements using a graduated steel rod (Hayashi, personal communication). Lines show model output from the CRHM soil thaw module for the coefficient derived from this year and the average coefficient for all sites/all years, respectively.

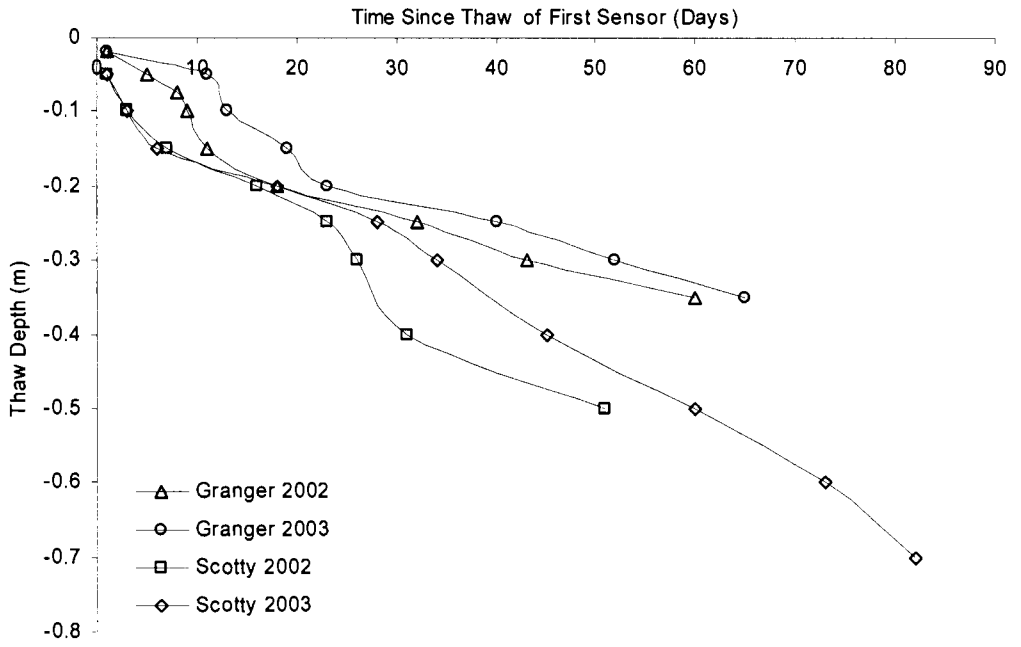

Figure 2-12. Position of the cryofront, considered to be indicative of the depth to the frost table. Points indicate the position of the zero degree isotherm as the first day the average daily soil temperature equalled or exceeded zero degrees Celsius. All plots are set to time zero on the day the first sensor thawed, for both sites, both years.

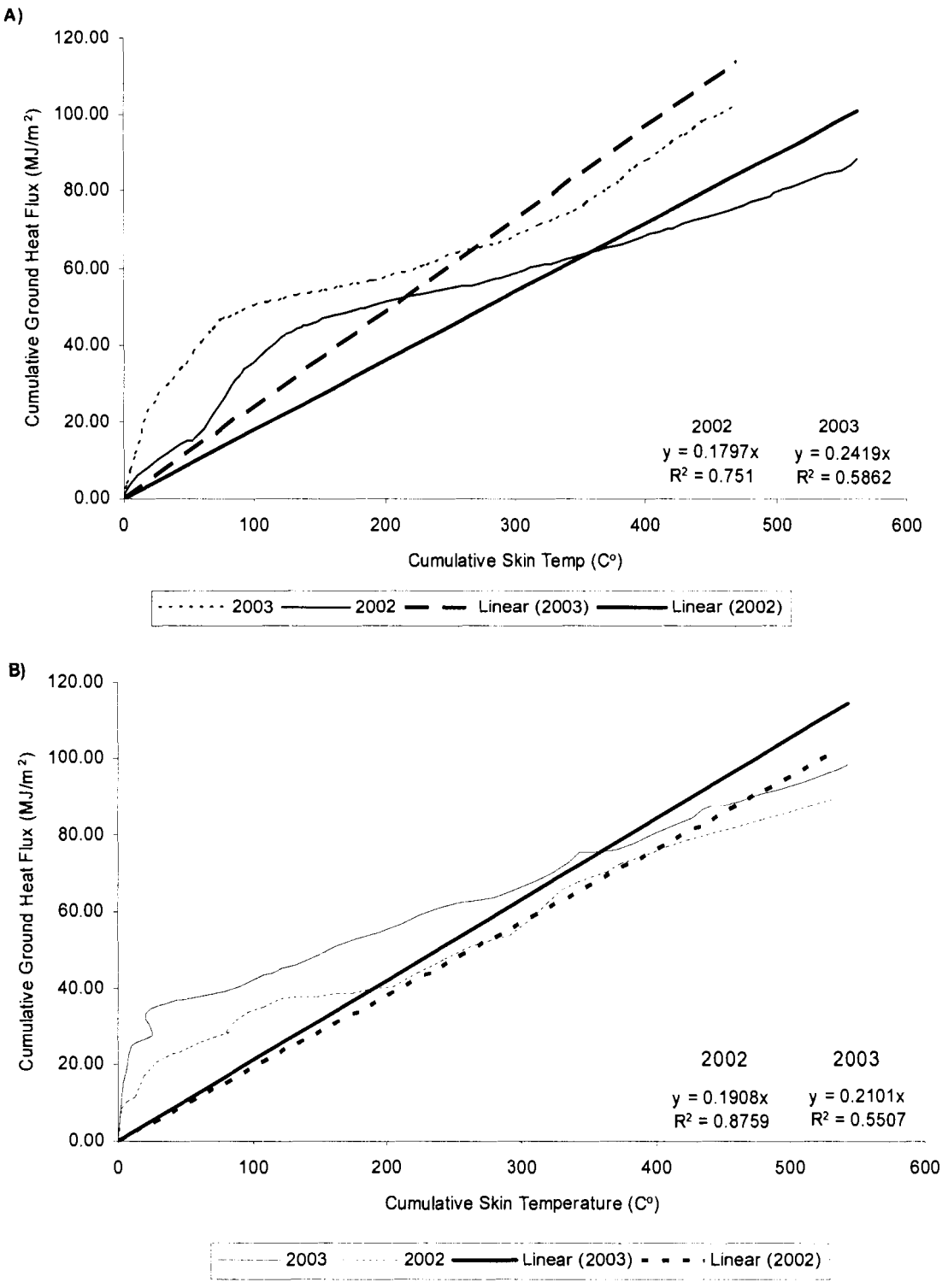

Figure 2-13. Cumulative daily ground heat flux (ΣQg) calculated using the thermo-calorimetric method plotted against cumulative skin temperature (ΣTs) for Granger (A) and Scotty (B). Regression lines, coefficients and R-squared values are shown.

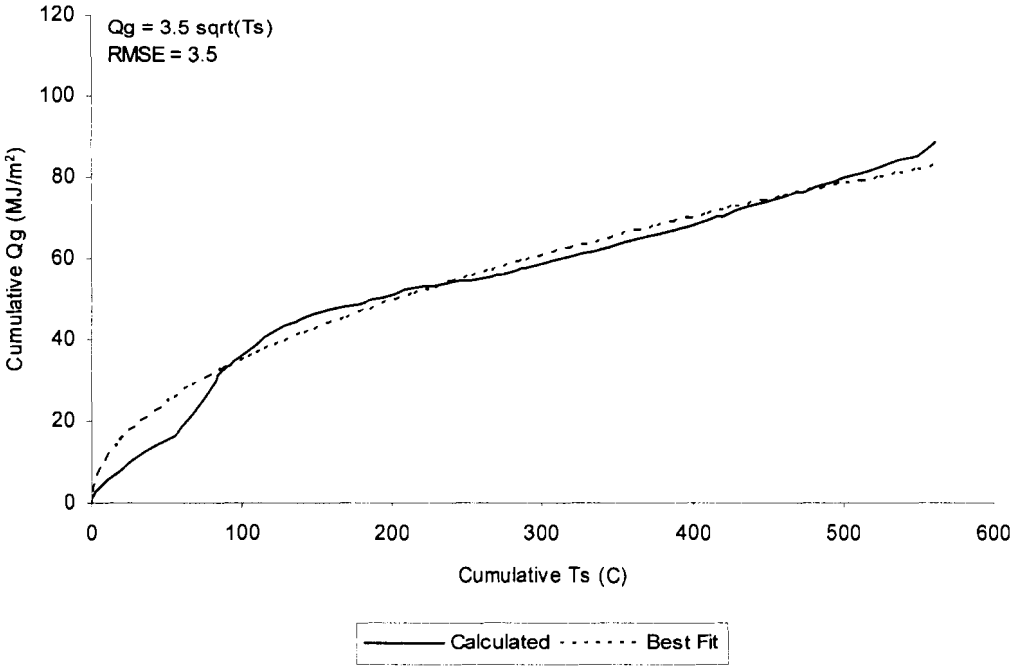

Figure 2-14. The ΣQg-ΣTs relationship with best fit power equation for Granger in 2002. Coefficient and root mean squared error values are shown.

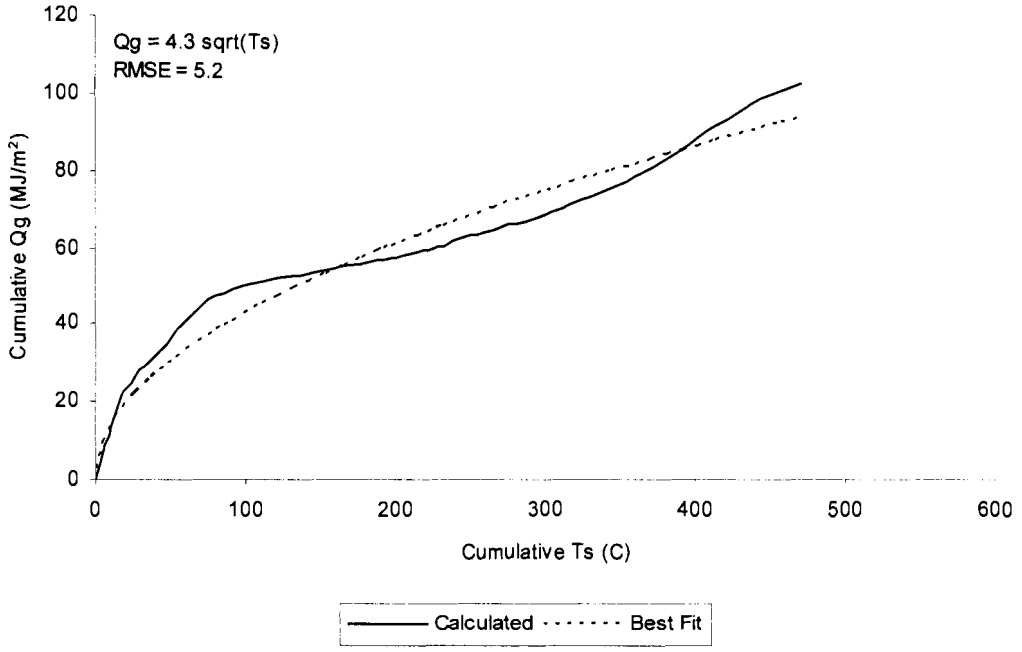

Figure 2-15. The ΣQg-ΣTs relationship with best fit power equation for Granger in 2003. Coefficient and root mean squared error values are shown.

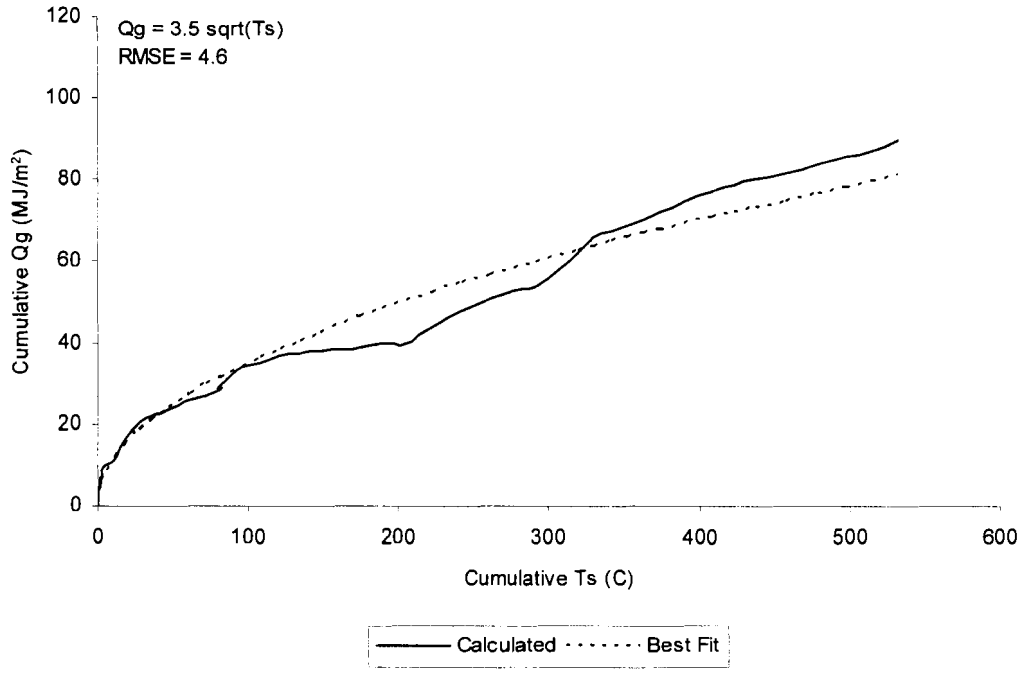

Figure 2-16. The ΣQg-ΣTs relationship with best fit power equation for Scotty in 2002. Coefficient and root mean squared error values are shown.

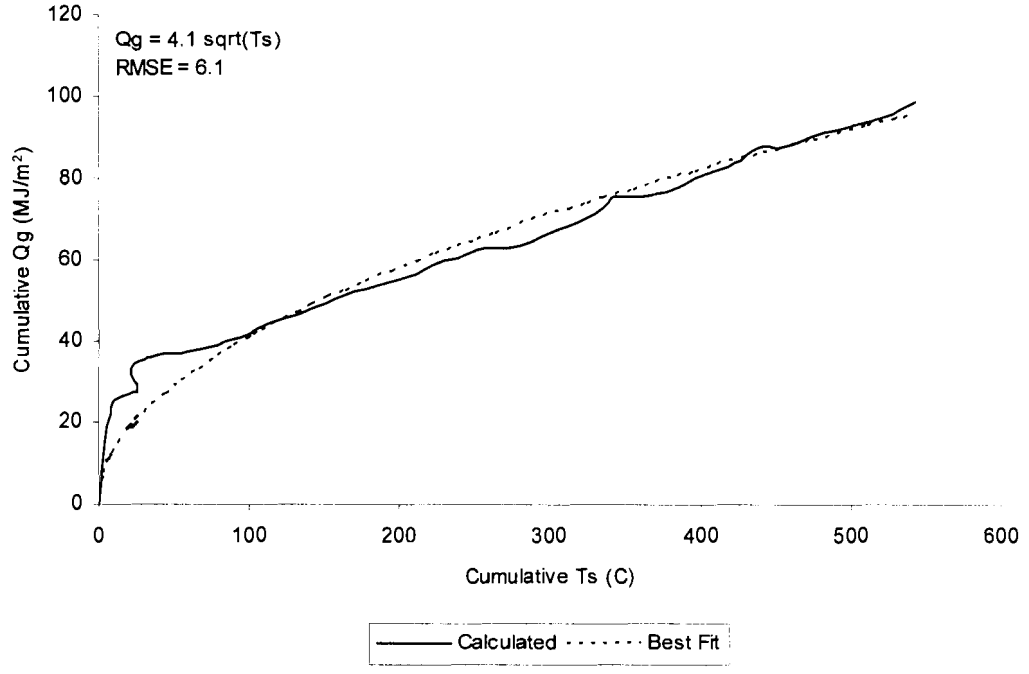

Figure 2-17. The ΣQg-ΣTs relationship with best fit power equation for Scotty in 2003. Coefficient and root mean squared error values are shown.

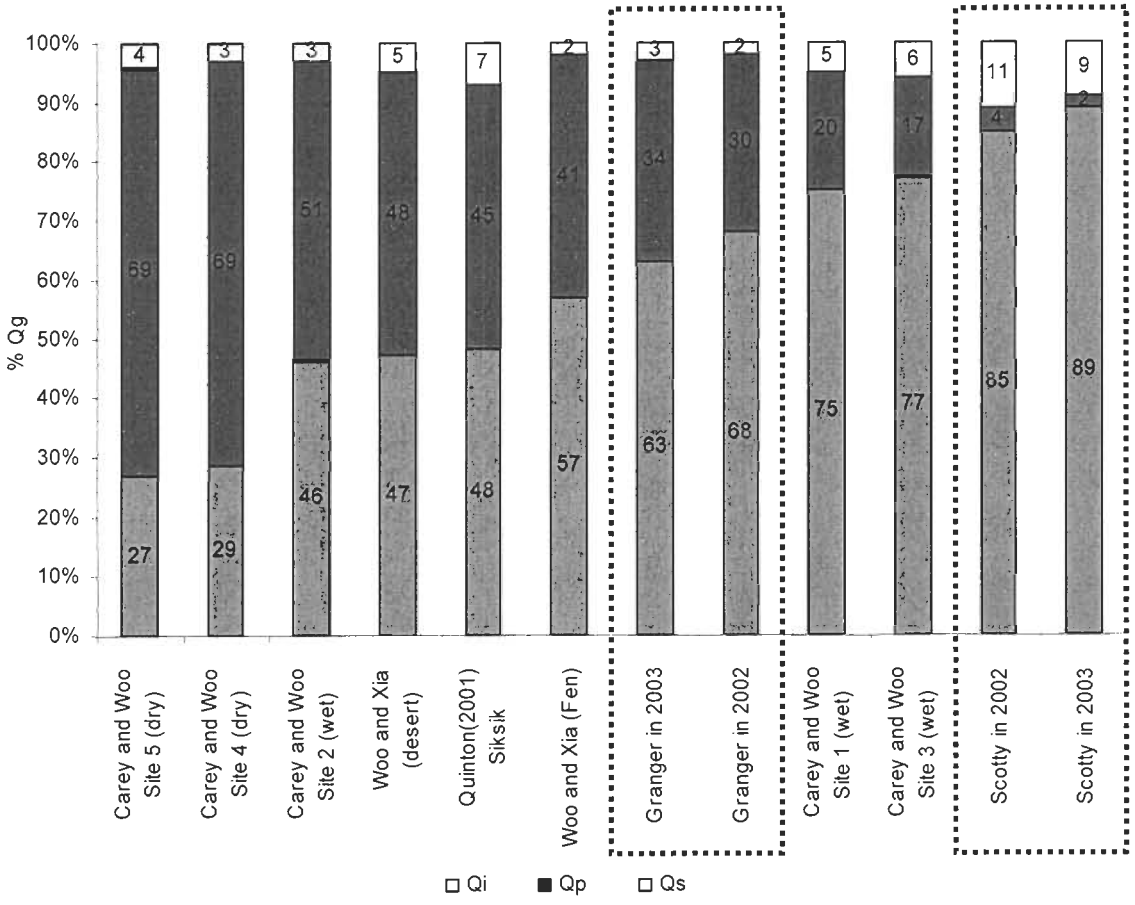

Figure 2-18. Energy partition summary for all sites showing the percentage of Qg accounted for by each component, Qs, Qp and Qi. The two study sites are indicated by the dashed boxes. Includes data from: Carey and Woo (1998), Woo and Xia (1996) and Quinton (2001). Site descriptions of other data sources are given in Table 2-9.

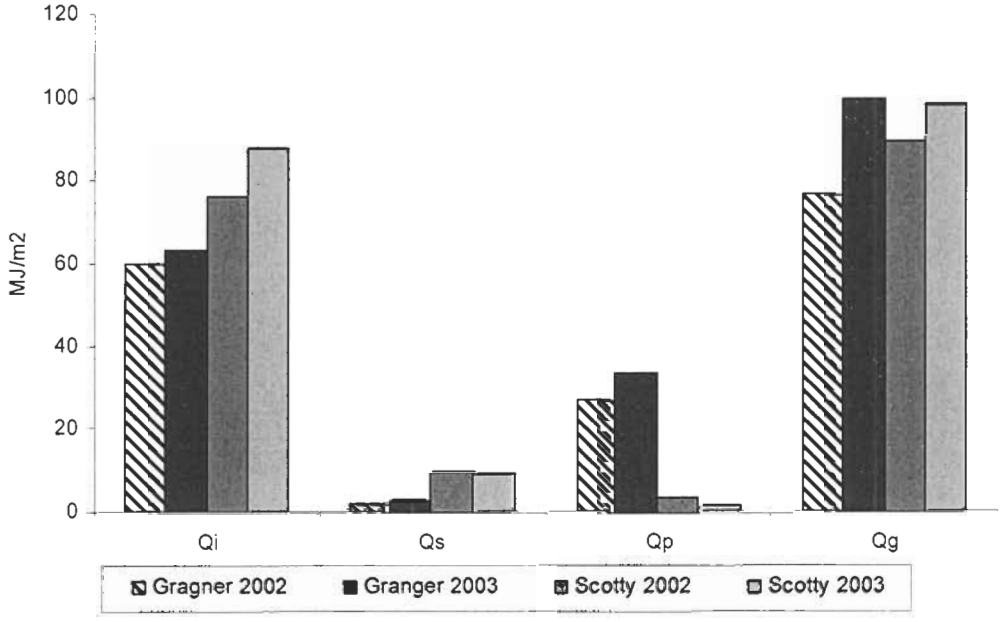

Figure 2-19. Final magnitude of Qg and its components in units of MJ/m^2 each year at both sites.

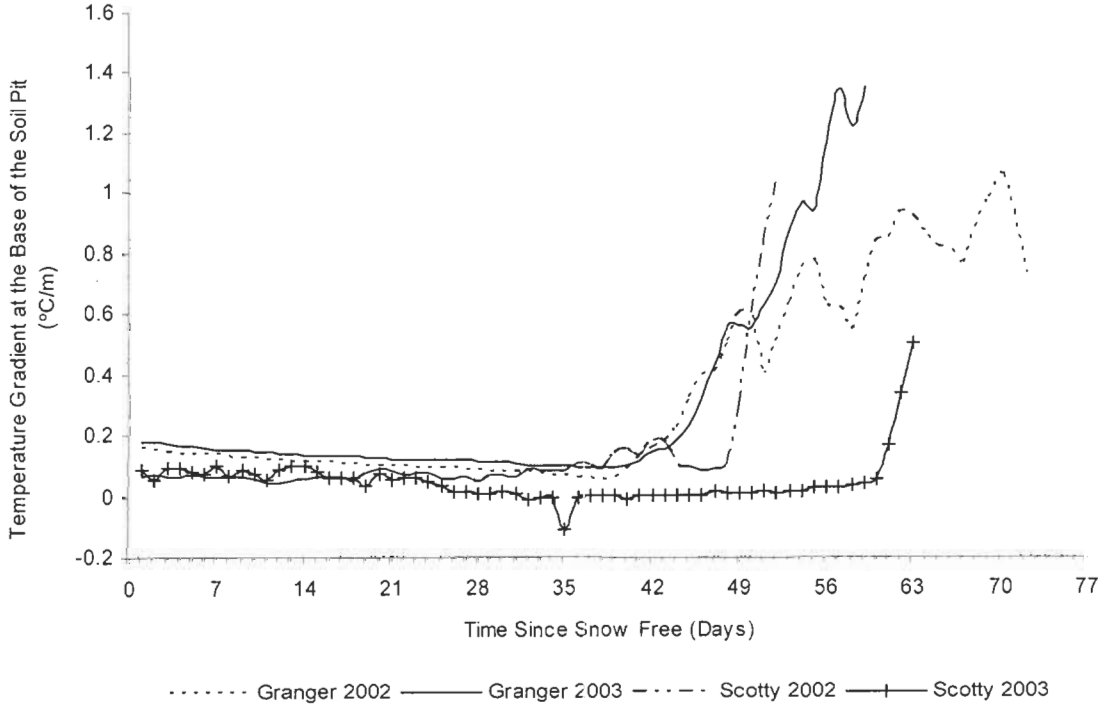

Figure 2-20. The temperature gradients at the base of the soil pit for Granger and Scotty. Both years used in the calculation of Qp.

A)

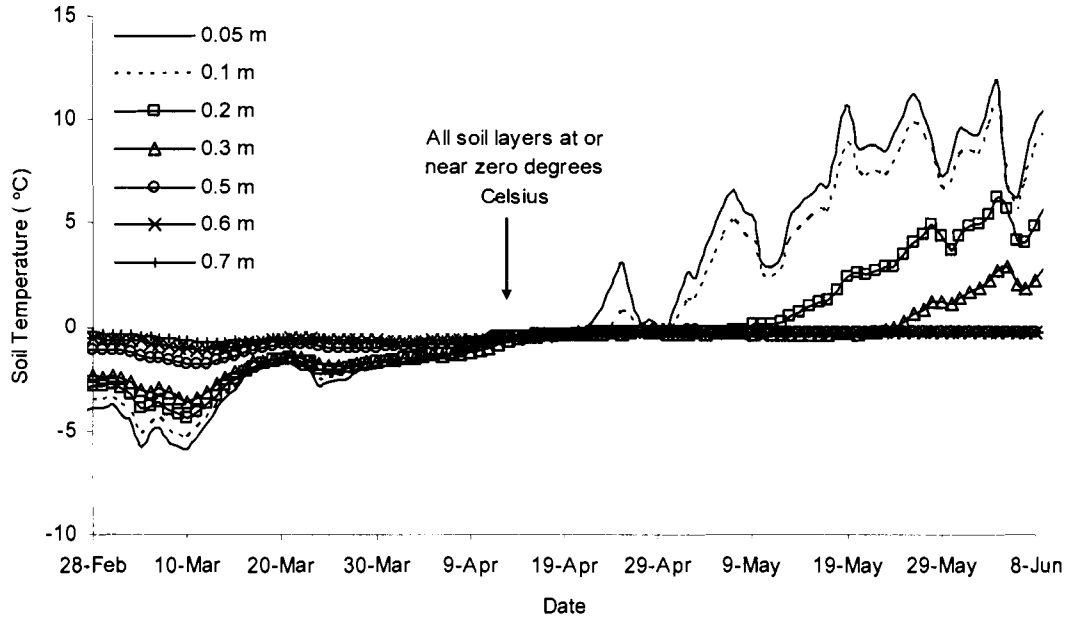

B)

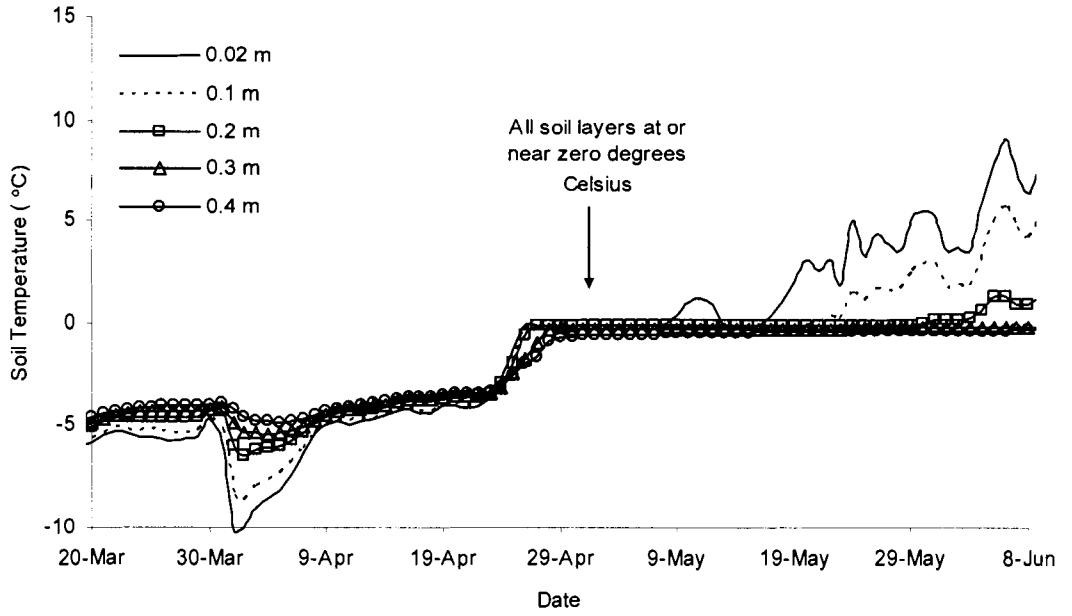

Figure 2-21. Soil temperatures at Scotty Creek (A) and Granger Basin (B) in 2003 showing soil temperatures in all layers are at or near zero degrees prior to the initiation of thaw suggesting either snowmelt water percolation and refreezing or conductive heat transfer from an isothermal snowpack.

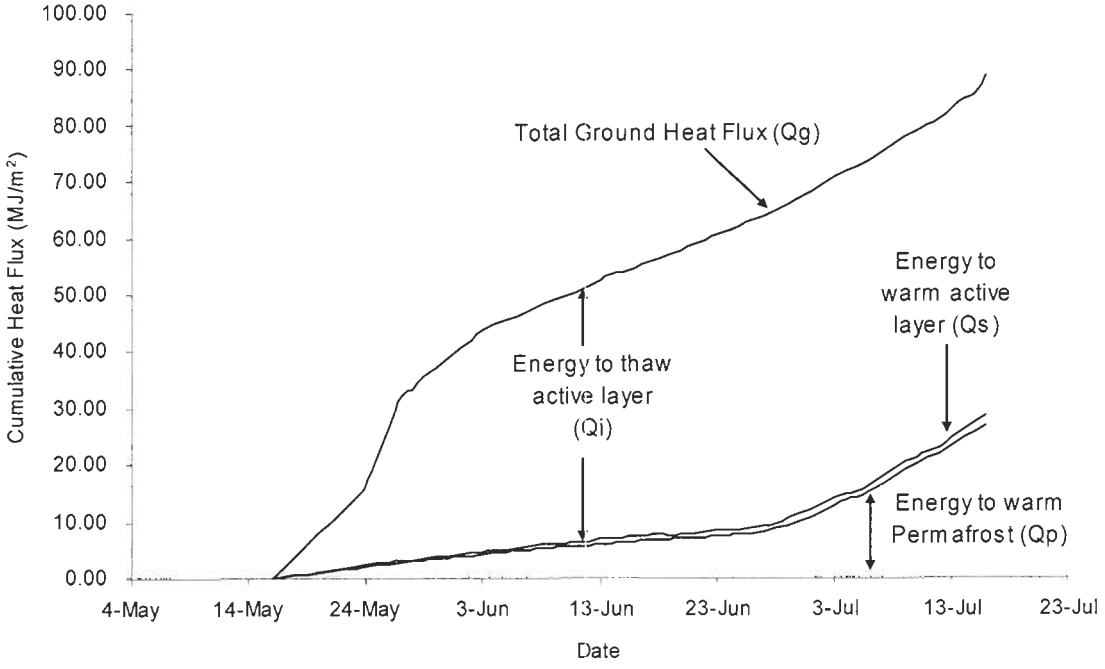

Figure 2-22. Cumulative values of ΣQs, ΣQp, ΣQi and ΣQg for Granger Basin in 2002. The area between the lines represents the energy consumed for each purpose.

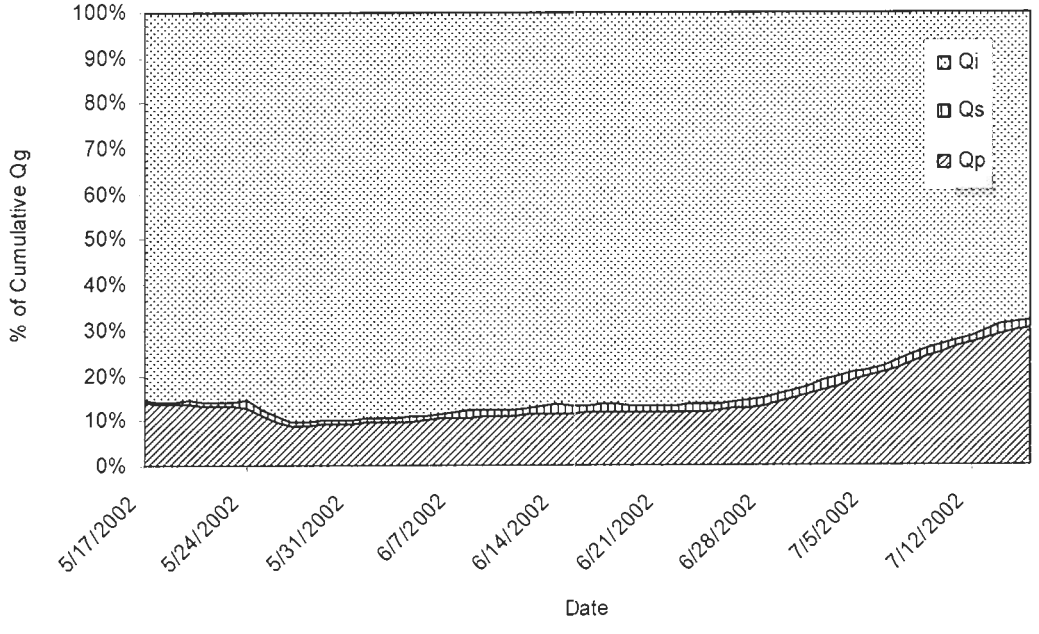

Figure 2-23. Partitioning of energy during the thaw period at Granger in 2002.

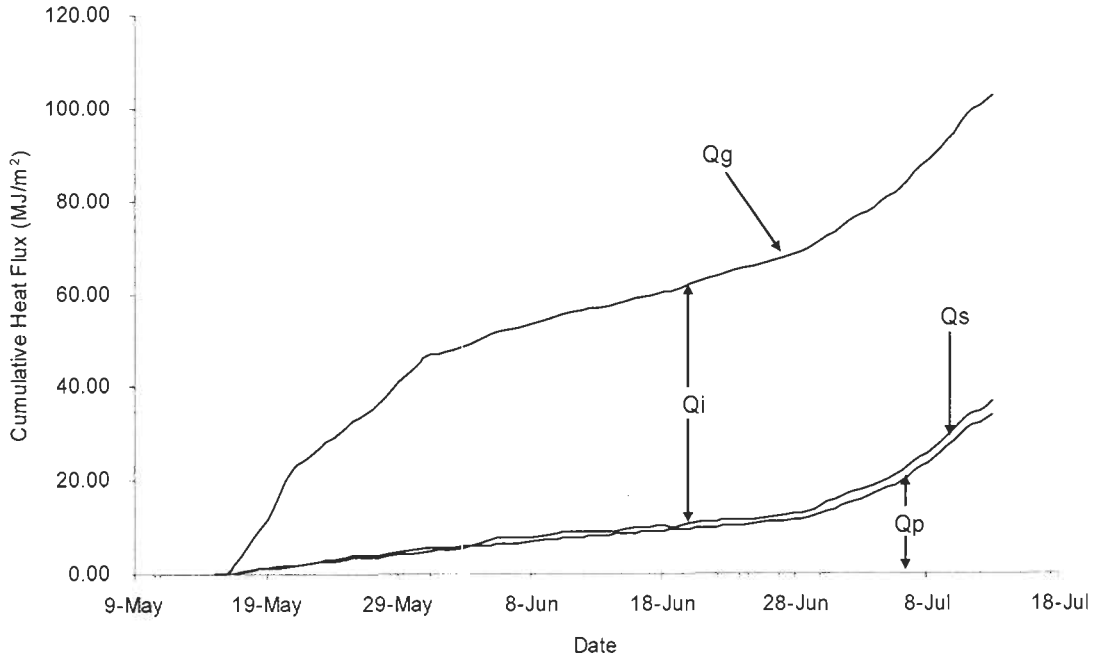

Figure 2-24. Cumulative values of ΣQs, ΣQp, ΣQi and ΣQg for Granger Basin in 2003. The area between the lines represents the energy consumed for each purpose.

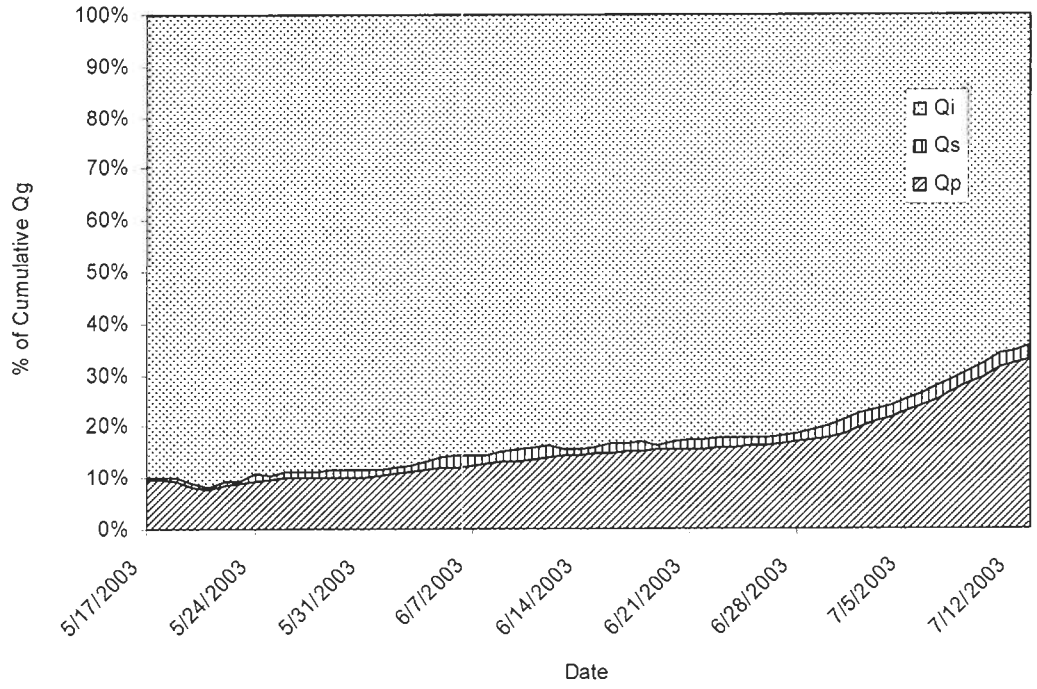

Figure 2-25. Paritioning of energy during the thaw period at Granger in 2003.

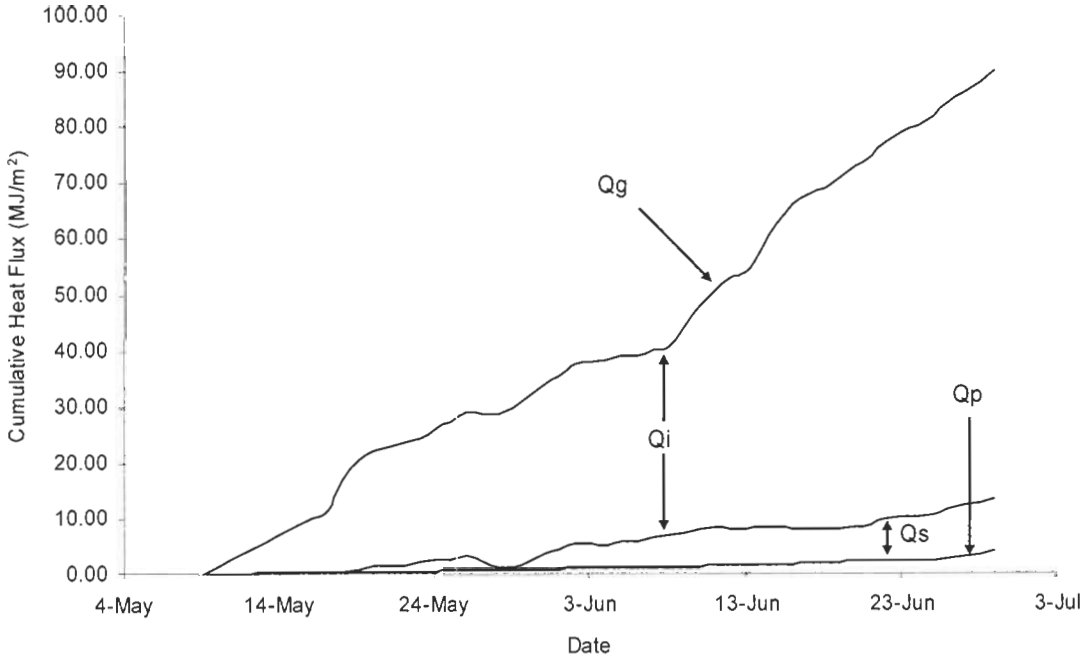

Figure 2-26. Cumulative values of ΣQs, ΣQp, ΣQi and ΣQg for Scotty Creek in 2002. The area between the lines represents the energy consumed for each purpose.

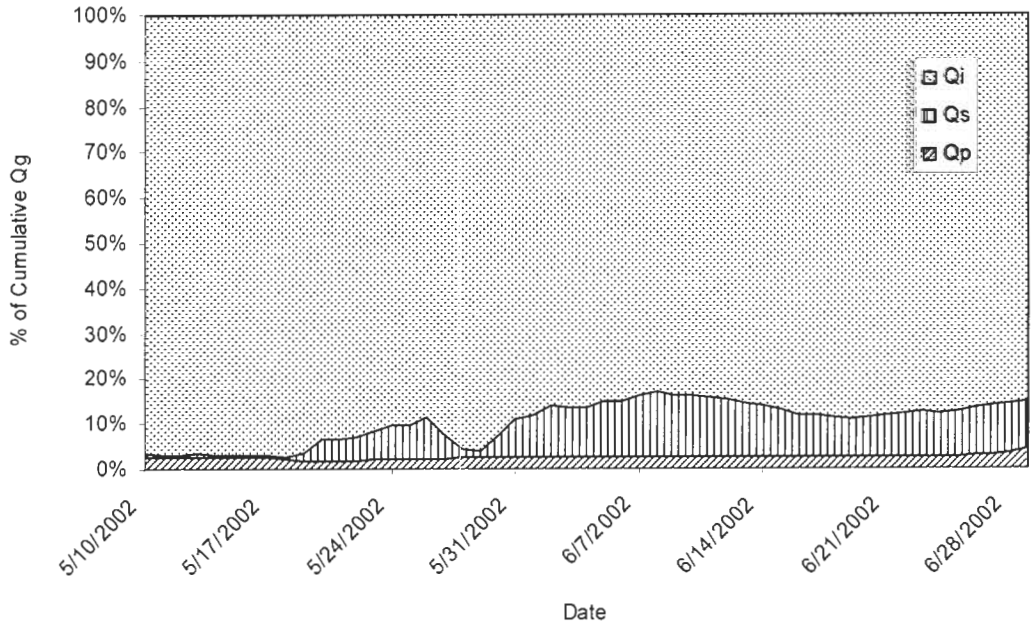

Figure 2-27. Partitioning of energy during the thaw period at Scotty in 2002.

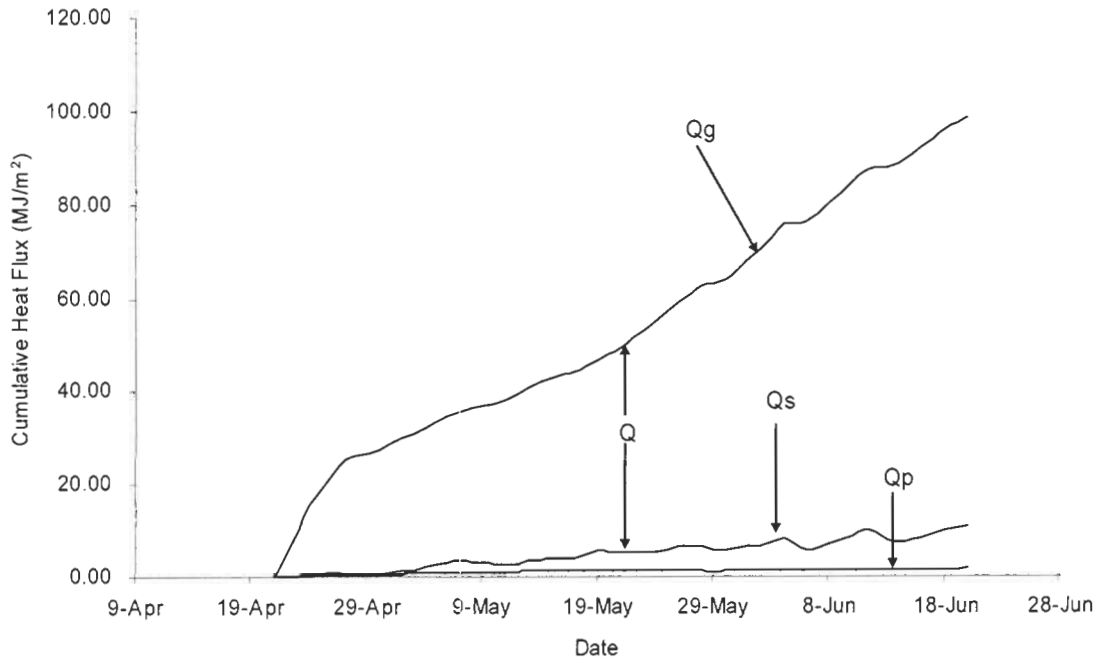

Figure 2-28. Cumulative values of ΣQs, ΣQp, ΣQi and ΣQg for Scotty Creek in 2003. The area between the lines represents the energy consumed for each purpose.

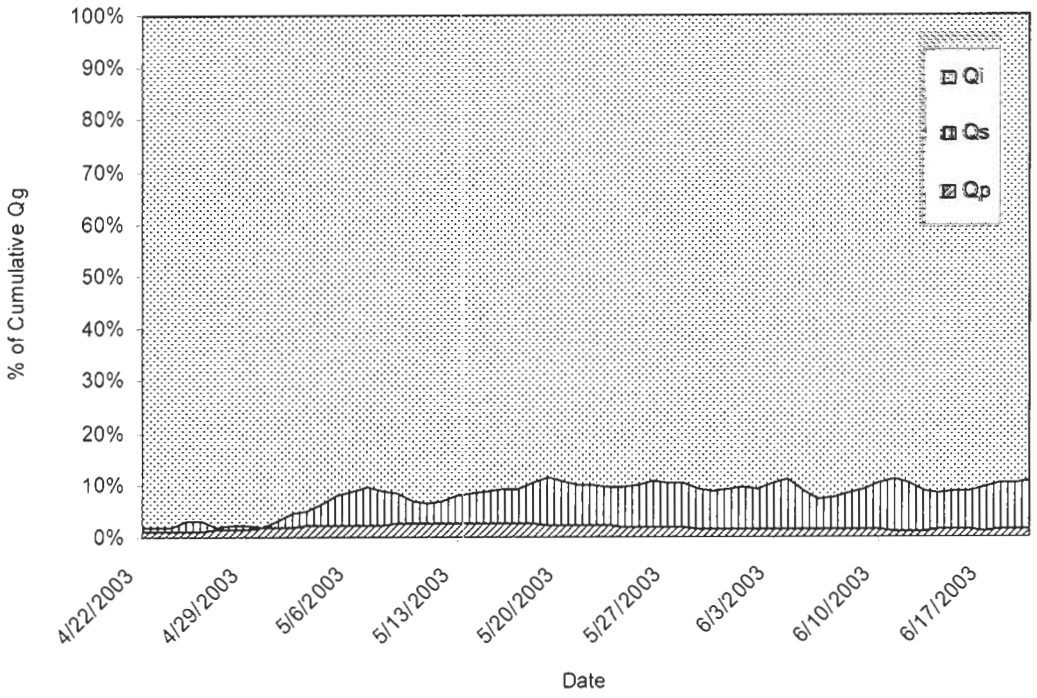

Figure 2-29. Partitioning of energy during the thaw period at Scotty in 2003.

2.11 TABLES

Granger Basin		Scotty Creek	
Temperature Sensor Depths (m)	Soil Moisture Sensor Depths (m)	Temperature Sensor Depths (m)	Soil Moisture Sensor Depths (m)
0.02	0.02	0.05	0.1
0.05	0.05	0.1	0.2
0.75	0.1	0.2	0.3
0.1	0.2	0.3	0.4
0.15	0.3	0.4	0.5
0.2	0.4	0.5	
0.25		0.6	
0.3		0.7	
0.35			
0.4			

Table 2-1. Location of soil temperature and soil moisture sensors in the soil pits at Granger Basin and Scotty Creek.

Granger			Scotty		
Soil Pit Layer	Temp Sensor Depth (m)	Soil Moisture Sensor Depth (m)	Soil Pit Layer	Temp Sensor Depth (m)	Soil Moisture Sensor Depth (m)
0-0.03	0.02	0.02	**0-0.15**	0.1	0.1
0.03-0.07	0.05	0.05	**0.15-0.25**	0.2	0.2
0.07-0.15	0.1	0.1	**0.25-0.35**	0.3	0.3
0.15-0.25	0.2	0.2	**0.35-0.45**	0.4	0.4
0.25-0.35	0.3	0.3	**0.45-0.55**	0.5	0.5
0.35-0.45	0.4	0.4			

Table 2-2. Locations of soil pit layers, temperature sensors and moisture probes (m) at Scotty Creek and Granger Basin.

Material	Depth (m)	Porosity (%)	Specific Heat (J kg^{-1} $°C^{-1}$)	Thermal Conductivity (W m^{-1} K^{-1})	Density (kg m^{-3})	Volumetric Heat Capacity (J m^{-3} $°C^{-1}$)
Air			1010	0.025	1.2	1212
Ice			2120	2.24	920	1950400
Water			4185	0.57	1000	4185000
Granger Basin Soils						
Peat	0.02	0.94	1920	0.21	39.8	76416
Peat	0.05	0.94	1920	0.21	68.3	131136
Peat	0.1	0.92	1920	0.21	80.5	154560
Peat	0.2	0.85	1920	0.21	141.3	271296
Peat	0.3	0.75	1920	0.21	289.8	556416
Mineral	0.4	0.49	890	2.5	1104	982560
Scotty Creek Soils						
Peat	0.05	0.89	1920	0.21	88.68	170266
Peat	0.1	0.92	1920	0.21	88.41	169747
Peat	0.2	0.82	1920	0.21	233.9	449088
Peat	0.3	0.89	1920	0.21	134.27	257798
Peat	0.4	0.87	1920	0.21	127.44	244685
Peat	0.5	0.86	1920	0.21	135	259200

Table 2-3. Porosity, specific heat, thermal conductivity, density and volumetric heat capacities for the soils at Granger Basin and Scotty Creek and the constituents: air, ice and water. Reproduced from Quinton et al. (2001).

Site	Regression Coefficient	R^2	% Difference predicted vs. calculated Qg	% Difference using avg. coefficient
Granger '02	0.1794	0.7510	12	23
Granger '03	0.2419	0.5862	10	-6
Scotty '02	0.1908	0.8759	12	18
Scotty '03	0.2101	0.5507	14	12
Average	.2056		12	15

Table 2-4. Regression coefficients for the ΣTs-ΣQg relationship, R squared values for linear best fit curves, and the percentage difference between total calculated and predicted Qg. Percentage differences are indicated for both coefficients for each site/year and for average coefficient from all data sets as a percentage difference between final computed Qg and estimated Qg from regression lines.

	Granger 2002	Granger 2003	Scotty 2002	Scotty 2003	Average
Coefficient (power)	3.5	4.3	3.5	4.1	3.9
RMSE (power)	3.5	5.2	4.6	6.1	4.9
RMSE (power) Avg. Coefficient	7.3	7.5	6.8	6.9	7.1
% difference (a)	9	12	9	6	9
Final Qg	89	102	90	98	
Final Ts	561	471	532	543	
Predicted Qg	83	93	81	96	
% difference (b)	7	9	10	3	7
Predicted (Average Coefficient)	91	84	89	90	
%difference (c)	3	18	1	9	8
RMSE (linear)	11.6	15.3	9.3	17.2	13.4
RMSE (linear) Avg. Coefficient	14.1	17.7	10.0	17.3	14.8

Table 2-5. Coefficients for the best fit power curves to the ΣQg-ΣTs relationship for each site and year, and root mean squared error (RMSE) values for both the power and linear regression curves, expressed in units of MJ/m^2. Percentage differences are calculated between (a) the power coefficients for each site and year and the average coefficient, (b) the total cumulative Qg predicted by the power curve and the calculated Qg and (c) the total cumulative Qg predicted using the average power coefficient and the calculated Qg.

Bulk C (%)	Total Qg (%)	Qs (%)	Qi (%)	Qp (%)	Qg (MJ/m^2)
10	0.3	0.3	-0.2	-0.1	0.28
20	0.5	0.5	-0.3	-0.2	0.55
50	1.4	1.3	-0.9	-0.5	1.38
100	2.7	2.6	-1.7	-0.9	2.75
Peat C					
10	0.01	0.01	0	0	0.01
20	0.01	0.01	-0.01	0	0.01
50	0.03	0.03	-0.02	-0.01	0.03
100	0.06	0.06	-0.04	-0.02	0.06

Table 2-6. The effect of increasing peat and bulk heat capacity on the magnitude of Qg and each component in percent of total accumulated energy, errors are expressed as a percentage of the original value.

K (%)	Total Qg (%)	Qs (%)	Qi (%)	Qp (%)	Qg (MJ/m^2)
10	3.3	-0.1	-2.1	2.2	3.38
25	8.1	-0.2	-4.9	5.2	8.45
50	15.6	-0.4	-9.2	9.6	16.90
100	28.9	-0.7	-16	16.7	33.79
Mineral Soil K					
10	0	0	0	0	0
25	0.01	0.01	-0.01	0	0.01
50	0.02	0.02	-0.01	-0.01	0.02
100	0.03	0.03	-0.02	-0.01	0.03

Table 2-7. The effect of increasing bulk thermal conductivity on the magnitude of Qg and each component in percent of total accumulated energy, errors are expressed as a percentage of the original value.

Air Content (%)	Total Qg (%)	Qs (%)	Qi (%)	Qp (%)	Qg (MJ/m^2)
5	-6.25	-0.18	-2.36	-2.18	-6.05
10	-12.9	-0.38	-5.04	-4.66	-12.10
20	-27.57	-0.88	-11.7	-10.82	-24.20

Table 2-8. The effect of increasing the air volume in the frozen peat during thaw on the magnitude of Qg and each component in percent of total accumulated energy, errors are expressed as a percentage of the original value.

Source	Site	Site Description
Carey and Woo (1998)		All sites have an organic layer made up of peat, mosses, lichens and vascular plants overlying a sandy loam (organic soil), measurements were taken on 3x3 m plots
	Site 1	Saturated zone frequently reaching the surface
	Site 2	Saturated zone frequently reaching the surface
	Site 3	Saturated zone frequently reaching the surface
	Site 4	Dried out partially in the summer
	Site 5	Dried out partially in the summer
Woo and Xia (1996)		Both sites are located near Resolute on Cornwallis island NWT
	Desert	A dry site underlain by a mixture of pebbles and loam
	Fen	Surface layer of living moss and peaty materials overlying a silty clay
Quinton and Gray (2001)	Siksik	Site is located near Siksik creek on the northerm fringe of forest tundra transition zone near Inuvik in continuous permafrost. Soils consist of 0.2-0.5 m of organic soils overlying mineral soils

Table 2-9.Descriptions of other sites where data was collected for figure 2-18.

CHAPTER 3 COMPARING IMAGE ANALYSIS AND PRESSURE PLATE EXTRACTOR DATA

3.1 INTRODUCTION

Organic soils are hydrologically important because the saturated hydraulic conductivity (Ks) decreases with depth (Ingram, 1978; Loxham and Burghardt, 1986; Hoag and Price, 1997; Quinton and Marsh, 1999). This depth-dependency is also a characteristic of other soil physical properties such as pore size, bulk density, decomposition, and others (Verry and Boelter, 1978; Ingram, 1981; Quinton et al., 2000). Quinton et al. (2000) pointed out that northern peat differs from Ivanov's 1957 classification of temperate peat because the lower layer of northern peat often becomes unsaturated, and thus, available for hydraulic conduction. This is important because it means the volume and timing of runoff is a function of saturated layer depth and thickness (Boelter, 1965; Ingram, 1981; Hoag and Price, 1997; Quinton et al., 2000). Ivanov (1957) proposed an equation for K_s as a function of depth in temperate peat using empirical constants that were found to vary with the type of microtope (the actively growing, upper layer of a bog consisting of the living parts of *Sphagnum* and into which vascular plants are rooted) (Ingram, 1981). Quinton et al. (2000) proposed a more recent model for cold regions that considers the peat profile to have continuous depth-varying resistance properties (Quinton et al., 2000). Estimation of these resistance properties can be achieved through the use of various methods, including pedo-transfer functions.

The term "pedo-transfer function", coined by Bouma and Van Lanen in 1987, is the name for equations translating basic soil data into functional (e.g., hydraulic or thermal) properties (Leij et al., 2002). A number of pedo-transfer functions are available for calculating Ks using various physical parameters, such as porosity, pore size or pore size distribution. Some of these data can be gathered indirectly from pressure plate extractor tests or other bulk measures, but a potentially richer and more complete source of data could be acquired from direct observations of soil and pore structure using image analysis.

3.2 IMAGE ANALYSIS

The use of image analysis for direct observation and measurement of soil physical properties can be used to calculate functional soil properties. However, this method assumes that two dimensional (2D) images are representative of the true three dimensional (3D) structure (Vogel and Babel, 1992). To evaluate this assumption, pore size data from image analysis (2D) are compared to similar data derived from pressure plate extractor tests (3D). This chapter compares the data sets obtained using these two methods for organic soil samples to determine the viability of image analysis to characterise soil physical structure.

Digital image processing software can provide improvements in replication, consistency, potential for automation and speed over traditional microscope methods of analysis (Heydorn, 2000; Minasny, 2000). A number of available software packages are capable of performing a range of processing and measurement procedures on soil images. However, there are problems associated with image analysis of 2D soil blocks or thin sections.

The automated procedures in image analysis programs rely on algorithms, which cannot discriminate between different objects for measurement; for example, two pores connected by a small channel will be measured as one object (Berryman and Blair, 1987; Ringrose-Voase, 1994). As well, during analysis images are filtered, thresholded and converted to binary (two-colour images; pores are one colour, soil is another) in order to better distinguish pore and non-pore spaces. Binary conversion is achieved by splitting an intensity histogram at some point, usually between peaks, or at an inflection point on a curve decided by the user (Schaap and Lebron, 2001). Despite the automation of image analysis measurements, some user-controlled filtering, thresholding and binary conversion are often necessary, and these subjective processes introduce biases (Berryman and Blair, 1987; Giminez et al., 2000; Heydorn, 2000; Pachepsky et al., 2000). Although, Thompson et al. (1992) point out that the introduction of errors actually begins with field sampling. Some other common problems associated with image analysis are: edge effects, image orientation, image resolution (Ringrose-Voase, 1994), external illumination problems (Bodziony et al., 1993), a lack of standardized data and methods (Stoops, 2003), hardware and software discrepancies (Bruand et al., 1996; Coleou et al., 1999), the translation of 2D objects to 3D (Bodziony et al., 1993), and sample damage (Mooney et al., 1998; Heydorn, 2000). Several studies have also found that image measurements are subject to error because the resolution cannot define features smaller than the detection limit (Mooney et al., 1998; Schaap and Lebron, 2001). But Schaap and Lebron (2001) argued that only a certain magnification is necessary to define a pore shape because of the sensitivity of pedo-transfer functions to pore wall features (Berryman and Blair, 1987; Schaap and Lebron, 2001). For example, hydraulic

radius (r_h=2A/P) measurements increase with higher magnifications. However, smoother perimeter to area ratios give better predictions in permeability relations (Berryman and Blair, 1987; Giminez et al., 1997; Schaap and Lebron, 2001).

The primary uncertainty in the image analysis of soil is the relationship between the 2D measurements and the actual 3D pore geometry. Bouabid (1992) noted that the extrapolation of 2D properties to 3D can be undertaken in some cases, but not all, and care should be taken in drawing conclusions from these results. More specifically, Velde et. al. (1996) and Heydorn (2000) noted that the range of pore orientations can lead to measurement errors of up to 40%. Pore size distributions can be obtained by both image analysis and the water retention characteristic curve from pressure plate extractor tests. Those derived from the water retention characteristic curve are an integrated measure of soil physical properties, whereas pore morphology measured in 2D using image analysis is independent of pore continuity and pore necks that affect water retention data (Vogel and Babel, 1992).

3.3 THE WATER RETENTION CHARACTERISTIC CURVE

An indirect and integrated method of measuring soil structure in 3D is through the use of the water retention characteristic curve; a plot of the volume of water held by capillary forces in a soil volume against matric potential. These curves are a principle tool in the indirect measurement of soil pore structure (Mishra et al., 1989; Vogel and Babel, 1992; Crawford et al., 1995). Several equations have been developed to fit a continuous function through a series of points measured using experimental methods.

Brooks and Corey (1964) concluded that the water retention characteristic curve can be reasonably well described by equation [3-1],

$$\theta(h) = (h / h_b)^{-\lambda} \qquad [3\text{-}1]$$

Where h is the matric potential, θ is the soil moisture content, h_b is the bubbling pressure and λ is the soil characteristic parameter (a function of the pore size distribution) (Brooks and Corey, 1964). h_b is the pressure at which water first begins to drain from a soil sample, which Brooks and Corey (1964) claim is related to the largest limiting pore size forming a complete network (Brooks and Corey, 1964).

More recently, Van Genuchten (1980) developed a relatively simple and widely used water retention characteristic function,

$$\theta(h) = \theta_r + \frac{(\theta_s - \theta_r)}{(1 + (\alpha h)^n)^m} \qquad [3\text{-}2]$$

with four independent parameters: residual moisture content, θ_r, saturated moisture content, θ_s, and the fitting parameters α, m and n, where m is defined as 1-1/n. Of these θ_r and θ_s are usually known from experimental analysis and the others are fitted by trial and error, or least squares error analysis (Van Genuchten, 1980). The above equations can be used to define a continuous water retention characteristic curve, and pore geometry can be inferred using the capillary equation, discussed below, which equates matric potential with pore size.

3.4 THE CAPILLARY EQUATION

The capillary equation can be used to convert the water retention curve to a pore size distribution (Mishra et al., 1989) by calculating the smallest pore size drained at a

given matric potential. The theory is based on the height of rise of water in a circular capillary tube. The equation balances the forces suspending a column of water (F_s) [3-3] against the force of gravity (F_g) [3-4].

$$F_s = 2\pi r\gamma \cos\alpha \qquad [3\text{-}3]$$

$$F_g = h\pi r^2 \rho_w g \qquad [3\text{-}4]$$

Balancing the suspending force F_s and the gravitational force F_g yields [3-5]

$$F_s = F_g \qquad [3\text{-}5]$$

$$\pi r^2 \rho_w g h = 2\pi r\gamma \cos\alpha \qquad [3\text{-}6]$$

$$h = \left(\frac{2\gamma \cos\alpha}{\rho_w g}\right)\left(\frac{1}{r}\right) \qquad [3\text{-}7]$$

$$\frac{1}{r} = \frac{\pi r}{\pi r^2} = \frac{\frac{1}{2}P}{A}, r = \frac{2A}{P} = HydraulicRadius \qquad [3\text{-}8]$$

where r is the radius of the capillary tube, γ is the surface tension, α is the angle of the meniscus to the tube wall, h is the height of the water column in metres, ρ_w is the density of water, and g is gravitational acceleration (Dingman, 1984). For mineral soils, α is assumed to be 0 degrees (Marshall and Holmes, 1988), but for the moderately hydrophobic organic soils it is estimated to be closer to 40 degrees (Bachmann et al., 2002; Bachmann et al., 2004).

Swanson and Peterson (1942) found the capillary equation to be satisfactory when compared to microscope analysis of pore sizes (Marshall and Holmes, 1988). They recommended the use of a drying curve as it is influenced more by the size of the

smallest opening on any connected path; a measurement that is of greater use in calculations of soil hydraulic properties (Marshall and Holmes, 1988). This is important as connectedness and flow in groundwater problems are limited by the diameter of pore necks (limiting diameter on any connected pore pathway) (Hillel, 1998). Using the capillary equation to derive water retention characteristic curves from image analysis and pore size distributions from pressure plate extractor tests allows comparison between the data sets generated by each method. Similarities between these data sets would suggest that the 2D measurements from image analysis are, to a reasonable extent, representative of the 3D soil structure.

3.5 HYDRAULIC CONDUCTIVITY AND PERMEABILITY

The general equation for flow through a porous medium is given by Darcy's law,

$$Q = K_s A \frac{\Delta H}{\Delta L} \qquad [3\text{-}9]$$

where,

$$K_s = \frac{k \rho g}{\mu} \qquad [3\text{-}10]$$

where Q is discharge [L^3/T], K_s is saturated hydraulic conductivity [L/T], A is cross-sectional area [L^2] and $\Delta H/\Delta L$ is the gradient of hydraulic head (Hillel, 1998). The magnitude of K_s depends on both fluid (density (ρ)[m/V] and dynamic viscosity (μ)[$F \cdot T/L^2$]) and media (permeability (k)[L^2]) properties. For groundwater flow, the fluid properties of water are well understood and it is the permeability (k) of the medium that determines K_s, and thus, flow rate for any specified gradient.

3.5.1 Permeability

The magnitude of permeability (k), depends on a number of soil physical properties, but there are a few that tend to explain the majority of the variation amongst different soils (Bouabid et al., 1992; Fetter, 1994; Arya et al., 1999; Mbonimpa et al., 2002). Some of the more relevant variables that can be quantified using image analysis are porosity (Garcia-Bengochea and Lovell, 1981; Thompson et al., 1987), effective porosity (Mathan et al., 1995; Leij et al., 2002), pore size, pore shape, spatial and relative distribution of pores, orientation, connectivity, shape factor (Brooks and Corey, 1964; Loxham and Burghardt, 1986; Rajani, 1988) and tortuosity (Childs and Collis-George, 1950; Loxham and Burghardt, 1986; Thompson et al., 1987; Marshall and Holmes, 1988).

However, the most useful relation, and the one that many studies indicate should be the dominant term in permeability calculations, is the variation of permeability with a mode or frequency of pore size(s) (Garcia-Bengochea and Lovell, 1981; Clymo, 1983; Thompson et al., 1987; Hillel, 1998; Arya et al., 1999). A number of measures have been used to characterize pore size, essentially the size of the openings in soil through which water will pass. At any given level of saturation, water movement is greatest in the largest channel available (Loxham and Burghardt, 1986; Thompson et al., 1987) and therefore, k is mainly determined by the structure of the largest water filled pores (Giminez et al., 1997). However, it is important to note that it is still the smallest pore in any connected network that limits the flow rate (Bouabid et al., 1992).

3.5.2 The Hagen-Poiseuille Equation

The Hagen-Poisueille equation forms the basis of many flow relations (Garcia-Bengochea and Lovell, 1981; Loxham and Burghardt, 1986). It is a physically based relationship originally developed to explain the flow of blood through capillaries. Its application to porous media requires modification because soil pores are neither cylindrical nor of constant radius (Leij et al., 2002).

Flow is considered in a straight circular tube having a velocity of zero at the walls and a maximum in the centre. The velocity of the fluid in cross section can be visualized as concentric rings sliding past each other resisted by viscosity (Hillel, 1998). The velocity profile is parabolic, proportional to the distance from the tube wall. A commonly reported form of the Hagen-Poisueille equation is:

$$q = \frac{\pi r^x}{S\mu} \frac{\rho_w g \Delta H}{\Delta l} \qquad [3\text{-}11]$$

where r is mean pore radius [L], ρ_w is the fluid density [M/L^3], g is the gravitational constant [L/T^2], ΔH is the pressure head [L], S is a dimensionless shape factor, q is the pore flow rate [L/T], μ is visocity [M/L/T] and Δl is the flow path length [L]. For cylindrical straight tubes, x=4 and S=8 (Leij et al., 2002). By assuming a unit gradient and assuming water at constant temperature, so that density and viscosity are fixed, the flux is a function of medial properties: $k = cr^x$ where k is permeability and $c = \frac{\pi}{S}$. In terms of permeability, this relationship uses pore radius (r), and for circular tubes reduces to $k = \frac{\pi}{8} r^2$. For soil pores, the exponent and coefficient values vary from those for

straight circular capillary tubes and reflect the combined effects of pore shape, roughness, tortuosity, interaction between pores and organization (Arya et al., 1999).

Because of the complex geometry of soil pores, a simple radius measurement does not adequately characterise pore geometry for use in the Hagen-Poiseuille equation for permeability. A potentially better representation of pore size is the hydraulic radius derived from the capillary equation [3-8] (Brooks and Corey, 1964; Giminez et al., 1997). The hydraulic radius is a better descriptor of the shape of non-circular pores and is a measure of the frictional surface area resisting flow in the pore network (Bouabid et al., 1992). Since image analysis can be used to determine a wide range of pore dimensional parameters, it may be possible to characterize pore size and hydraulic radius from the images for use in calculating permeability using a fitted a form of the Hagen-Poiseuille equation.

3.6 OBJECTIVES

The objective of this study is to demonstrate that measurements on 2D images of organic soil are representative of the 3D soil structure by comparing pore hydraulic radii distributions and water retention characteristic curves measured in 2D from image analysis to 3D data from pressure plate extractor tests.

3.6.1 Rationale

The structural properties of a soil can be measured directly and indirectly. Image analysis enables the direct measurement of pores and grain structure in 2D while pore size data can also be estimated in 3D from water retention characteristic curves using the capillary equation [3-7]. Because the pressure plate extractor tests are an integrated

measure of pore size in the soil samples, a close correlation between this and the image analysis measurements will support the use of image analysis to quantify soil physical structure for use in estimating functional properties. For the following method, knowledge of the water retention characteristic curve is required in order to process images for analysis. Although the image analysis method outlined here does not stand alone, the advantage is the richer source of data provided by being able to directly view and measure the structure of soil and its pores.

3.7 STUDY SITES

Data from the Scotty and Granger research basins were used for this study. For the complete description of these sites refer to section 2.3 page 14.

3.8 SAMPLE COLLECTION AND PREPARATION

Cores of organic soil were extracted using 50 cm lengths of PVC pipe with an inner diameter of 15 cm. These were inserted vertically into the ground, and the lower end was capped in order to retrieve the soil in the tube. Two sets of samples were prepared from the soil cores. 15 samples were cut from some of the tubes at several depths and sent for pressure plate extractor tests at the University of Calgary. Other soil cores were impregnated with fluorescent epoxy resin and left to harden. 15 blocks were cut from these cores at several depths, and a 'window' was polished to present a vertical soil face for photographing at the University of Guelph.

3.9 ANALYTICAL METHODS

The following methods describe the derivation of a cumulative pore size density distribution from a water retention characteristic curve and the derivation of both of these

from image analysis. Pore size density distributions were derived from similar samples for comparison of the two methods.

3.9.1 The Water Retention Characteristic Curve (3-D)

Water retention characteristic curves were plotted using data from standard pressure plate extractor tests performed at the University of Calgary. The samples were subjected to 8 levels of decreasing matric potential. At each level, the moisture content was allowed to reach equilibrium and the sample was weighed to determine the volumetric soil moisture. Measured volumetric soil moisture was then plotted as a function of matric potential, and the Van Genuchten equation [3-2] was used to fit a curve through the experimental points. Curves for each sample were plotted using the RETC program generously donated by Rien Van Genuchten. In all cases, the Van Genuchten curves fit the experimental data with an R^2 value of 0.97 or better indicating a very good fit.

3.9.2 Cumulative Pore Size Distribution and Representative Pore Size

In order to estimate a representative pore diameter from the water retention characteristic data, a cumulative pore size distribution was calculated using the capillary equation [3-7] and a contact angle of 40 degrees was assumed for organic soils based on values from the literature (Bachmann et al., 2002; Bachmann et al., 2004).

Pore water is held by surface tension similar to water drawn up in capillary tubes. This water will be retained until a sufficient matric potential is established to withdraw it, with smaller pores requiring greater suction to drain. Water retention by pores is limited by the smallest opening through which the water must pass in the continuous network. In

this way, the pressure plate extractor test is a good indication of the smallest pore size which must be overcome in order to pass water through the continuous pore network in a sample of soil.

The capillary equation [3-7] calculates the hydraulic radius of the smallest pore that will drain at a given suction. The actual shapes and sizes of pores calculated using this equation are unknown, but are assumed equal to 2A/P based on the capillary equation [3-8].

The matric potential applied to the samples can thus, be translated into the hydraulic radius of the smallest pore that is drained. Combining this with the volumetric soil moisture at each level of matric potential gives the volume of the pores of each size range as a fraction of the total pore volume. Each size class is assigned a median pore diameter, calculated as the mid point of the range. The pore size density was combined with the average size of the pores in each range and translated into a cumulative pore size density distribution.

Using the cumulative pore size distributions calculated above, a single value of geometric mean pore hydraulic radius was computed for each sample using:

$$\prod^{n} x_i^{w_i} \qquad [3\text{-}12]$$

where x_i is the pore diameter and w_i is the weight percent.

3.9.3 Image Analysis (2-D)

Sigma Scan pro 5 (SPSS Inc.) was used to perform the analysis on the images of the soil blocks. The process employed for this was limited to the most basic operations,

in order to keep the method consistent for all the images. This was also done in the interest of examining the potential for automation of this method. To this end no filtering to improve image definition was applied in order to limit any bias which may be introduced.

Sub-samples from the resin impregnated cores were extracted at certain depths and the vertically oriented faces (perpendicular to the ground surface) were polished. The images were photographed using a high resolution digital camera at the University of Guelph under normal and ultra-violet light. The UV illuminated images were used because they provided better contrast between pore and non-pore areas. The images were then converted to gray scale (Figure 3-7a); where each pixel is assigned a shade of gray between 0 and 255, where 255 = white and 0 = black; where the lighter areas are pores and the darker areas soil. Next a threshold was established to assign areas for the image analysis program to measure.

3.9.4 Thresholding

The process of thresholding, sometimes called image segmentation, is an important step in image analysis (Thompson et al., 1992). It requires a range of gray scale values to be specified so that each cell within the range is classed as part of the set of objects for measurement. If the intensity histogram, a plot of pixel intensity against number of pixels, is a bimodal distribution, a threshold is usually established by splitting the peaks assuming each indicates either pore or non-pore areas (Schaap and Lebron, 2001). However, this was not the case for the organic soil images (Figure 3-8) and another solution was needed in order to assign a proper threshold. This step is important

as too large a threshold will class soil areas as pores, while too small a threshold will underestimate pore sizes and areas (Ringrose-Voase, 1991).

Initially, measurements of total porosity taken from Quinton (2001) were used for each sample, but with values approaching 90% it was clear by visual inspection that the binary overlay included non-pore areas (Figure 3-7b). This problem occurs because pores smaller than several pixels in size are either not resolved or are artefacts of the imaging process (Thompson et al., 1992). The digital images have a resolution of 17 microns per pixel and all features close to, and smaller than, this size cannot be resolved.

By inspection of the water retention characteristic curves it is apparent that in all the samples a portion of the pore space is below the limits of image resolution and cannot be detected in the images. Therefore, the visible pore area in the images is smaller than the actual value of porosity. In order to establish a threshold value for each image, an estimate of the porosity visible in the images was required. In order to accomplish this, the water retention characteristic curves are required. First, a smallest detectable pore size (threshold size) was established as an object roughly 2X2 pixels square, which corresponds to a diameter of about 34 microns and a hydraulic radius of 8.5 microns. Next, the water retention characteristic curves were used to determine the volume of pores smaller than the threshold size. The difference between this value and the saturated moisture content gives the approximate pore volume for the samples most closely associated with the image samples. Although the samples for the images are different from the samples acquired for pressure plate extractor analysis, an effort was made to ensure that the samples were obtained from the same location and soil horizon. In all

cases, each image has two or three closely associated samples from the pressure plate extractor tests.

The pore volume above the threshold size obtained from the water retention characteristic curves was then used as the visible porosity for image thresholding. Using *Sigma Scan*, a binary image was created by filling up the lighter (pore) areas to the visible porosity. A visual inspection showed that these values gave more realistic results (Figure 3-7c).

A major drawback of the image analysis technique is the requirement that a threshold be obtained from the water retention curve to define the areas of the image that the program considers for measurement. Despite this dependence, image analysis provides much more detailed information about soil structure than can be obtained from the more integrated data available from water retention characteristic curves.

3.9.5 Pore Measurement

Sigma Scans measurement function was assigned to measure the area and perimeter of each pore. These data were then transferred to a spreadsheet program (*Microsoft Excel*) for processing.

For each measurement, a hydraulic radius (r_h) was calculated using the formula derived from the capillary equation [3-8]. The data were then sorted in order of increasing hydraulic radius. This was performed because *Sigma Scan* does not automatically discriminate pores by size or shape, and will measure and count all objects including those smaller than the minimum size considered (8.5 microns r_h). All pores smaller than the minimum hydraulic radius were removed from the data set.

3.9.6 Water Retention Characteristic Curve from Image Analysis

In order to calculate the water retention characteristic curve from the hydraulic radii measured in the image analysis a frequency distribution was calculated. The same pore size classes used to plot a cumulative pore size distribution from the pressure plate extractor samples were applied. The frequency distribution was then computed and plotted as a cumulative pore size distribution for comparison with plots derived from the water retention characteristic curves.

The frequency distribution of hydraulic radii was used to construct a theoretical moisture characteristic curve for each sample. An average pore size was established for each pore size class. Each class was then assigned a matric potential head corresponding to the tension required to drain this average pore size. A percentage of the pore space represented by each class was calculated as a percentage of the total pore space. The result is a set of increasing values of matric potential corresponding with decreasing pore size, and decreasing values of total pore area from 1 to 0. Next the pore area was normalized to the visible porosity for the image the data was derived from. This means that the maximum pore area is set to the saturated moisture content, and the minimum pore area is set to the residual moisture content at the smallest resolvable pore size (34 microns). Again, the capillary equation [3-7] was used to calculate a matric potential for each pore size with an assumed contact angle of 40 degrees. The resulting function was then plotted with matric potential on the vertical axis versus theoretical moisture content (the normalized visible porosity) on the horizontal axis. This function then plots as a moisture characteristic curve and was plotted alongside the Van Genuchten curves of the closest associated samples from the pressure plate extractor tests.

3.10 RESULTS AND DISCUSSION

The pressure plate extractor tests offer indirect evidence of the 3D structure of the pore networks, while the image analysis offers a direct 2D view of pore shape and size. These results compare the measurement of soil pores using both methods. Similarities between the data sets will support the use of the capillary equation [3-7] to translate soil matric potential to pore hydraulic radius and that its measurement in 2D is representative of the true 3D dimensions of the pore network. This research is intended to support further work in linking soil physical properties to functional properties by determining if image analysis is an effective tool for measuring soil structure. The results and discussion included below focus specifically on two samples, one near surface and the other deeper in the soil profile. These samples are taken as indicative of the results of this study and exemplify the effect of the depth dependant pore properties of the peat soil.

3.10.1 Physical Properties

The following is a discussion of soil physical properties identified by each method and a comparison between the two.

3.10.1.1 Maximum Pore Size

In the pressure plate extractor tests, the air entry pressure (the matric potential at which water is first removed from the sample) is an indication of the largest limiting pore size on a continuous path available for flow (Figure 3-1 to 3-8) (Brooks and Corey, 1964). At both sites, the increase in air entry value (greater matric potential) with depth indicates a decrease in the size of the largest available pore.

The largest pore size indicated by the pressure plate extractor test exceeded the largest pores visible in the images (Figure 3-9 and 3-10). There are a number of possible explanations for this. The image analysis values for largest pore size are limited by the field of view of the images, orientation of the sample and number of samples. The largest values of pore size are rare and difficult to capture with this method due to the specific viewing area (location and orientation) that is acquired in the sampling and imaging process.

3.10.1.2 Cumulative Pore Size Distribution and Porosity

Cumulative pore hydraulic radius curves measured from one core at several depths using image analyses were plotted for Granger (Figure 3-11) and Scotty (Figure 3-12). The general trend expected at both sites is a shift to smaller pore sizes with increasing depth. However, at Granger, an increase in pore size at a depth of 0.09 m is either an anomaly or possibly indicates the low density zone just below the surface reported for some peats (Ingram, 1981; Hoag and Price, 1997; Heydorn, 2000). Scotty also has smaller pores at 0.27 m than at 0.38 m, however the similarity in these curves suggest that they both lie in the lower peat layer and are an indication of the variation possible among samples at similar depths in the profile.

Figure 3-13 and 3-14 show cumulative pore hydraulic radius curves derived from the pressure plate extractor samples for the three sampled depths at Granger (0.04, 0.06 and 0.15 m) and four depths at Scotty (0.09, 0.25, 0.29 and 0.4 m). Again, the trend is towards an increase in smaller pores with depth; however, at Scotty the pore size distribution at 0.4 m shows slightly larger pore sizes than at 0.29 m possibly for the same reasons described above.

Cumulative pore hydraulic radius distributions from image analysis were compared with the pressure plate extractor test samples. Comparison of the curves shows a good agreement between the image analysis and pressure plate methods within the range of image resolution (Figure 3-9 and 3-10). The resolution of the images prevents the detection of pores smaller than 8.5 microns (the detection limit). As a result, the image analysis curves exhibited a better fit for shallower depths where a larger portion of pores are above the detection limit (Figure 3-9).

Deeper samples have a smaller volume of pore sizes above the detection limit and, as a result, the data from image analysis plots only a small portion of the curve (Figure 3-10). Figure 3-9, at a depth of 0.04 m, indicates that about 10% of the pore sizes fall below the detection limit, while in Figure 3-10, at a depth of 0.4 m, about 90% of pore sizes are not detected.

3.10.1.3 Geometric Mean Pore Diameter and Permeability

In an effort to obtain a single value of pore size to characterize each sample, a geometric mean pore hydraulic radius was calculated for both the image analysis and pressure plate extractor samples (Figure 3-15). Having a much narrower range of pore sizes and a lower limit of detection, the image analysis samples have a consistently larger geometric mean hydraulic radius than those from the experimental samples at equal depths. However, the overall trend in the plot of pore sizes does show an exponential decrease with depth, similar to the trend observed in hydraulic conductivity using tracer tests (Quinton et al., 2000). Since the two methods result in significantly different geometric mean pore hydraulic radius values (Figure 3-15), the application of a simple permeability-pore hydraulic radius relationship will be influenced by the method of pore

measurement. The use of image analysis would be relatively effective if the undetectable pores have little effect on permeability.

3.10.1.4 The Capillary Equation

Root mean squared error values comparing cumulative hydraulic radius curves plotted using image analysis and those from pressure plate extractor data within the range of image resolution are given in Table 3-1. Error values indicate a good fit between the data sets above the detection limit for image analysis, with an average root mean squared error of 8.8% and a maximum of ~20% pore volume/area. On average, error values are lower for deeper samples because there are fewer points for comparison. This suggests that the derivation of 2A/P as hydraulic radius is a reasonable approximation of pore size and that image analysis is a useful tool for the measurement of soil pores.

3.10.2 Drainage Properties

The following is a comparison of the water retention characteristic curves generated by each method and the information on pore structure they provide.

3.10.2.1 Water Retention Characteristic Curve

The fit of the estimated water retention characteristic curve from image analysis to the experimental curve is also depth dependent with shallower samples (Figure 3-17) showing a better association than deeper samples (Figure 3-18). Since the maximum and minimum volumetric water contents are fit by the water retention characteristic curves, it is the shape of the curve in between these points that is of interest.

In the shallow samples, the air entry pressure, analogous to the largest pore size, is slightly greater than the experimental value, again owing to the lack of equally large

pores in the images (Figure 3-17). Above this point, the curves follow a similar trend as the experimental curves until reaching the minimum detection limit (water content) at a matric potential of ~0.3 m. The range of plotted values for imaged samples depends on the sampling depth and, in all cases, the shallower the sample the more pores available for measurement above the detection limit. This again demonstrates that the primary limitation of the image analysis is the resolution of the image; however, the method of measurement and calculation seem to give good results.

Root mean squared error values comparing the fit of the water retention characteristic curves from image analysis to experimental curves are given in Table 3-1. The average error of all plots was 4.8%, with a maximum error of 13.1% volumetric water content. The fit was better for deeper samples where fewer points were available for comparison due to image resolution. Thus, the shallower samples give a better indication of the reliability of the image analysis method.

3.10.2.2 Pore Connectivity and the Limiting Pore Size

The pressure plate extractor removes water through the continuous and complex network of pores giving a bulk estimate of pore size. Water movement is limited by the smallest pore on any continuous path and the resulting dimension calculated from the capillary equation [3-7] is an indication of this size. The images do not allow the direct observation of these limiting dimensions, but instead display the pores at a single point in the network. Similarities between the image analysis and pressure plate extractor data suggest that the distribution of pore sizes is similar at most points in the medium and the location and orientation of sampling may not be as important as the image analysis procedure (e.g. resolution, threshold, measurement etc.).

Permeability is dependant not only on the pore size distribution, but on the connectivity in a network of pores and their limiting pore size. Only the open and continuous pores contribute to flow in the medium, making the pressure plate extractor test data ideal for characterization of the pore networks used for flow and their limiting pore size. However, the capillary equation [3-7] is only an idealization of the association between matric potential and pore size. The image analysis confirms that the distributions of directly measured hydraulic radii are closely correlated with those derived from water retention characteristic curves indicating that the image analysis is an effective method of pore measurement.

The resin impregnation process also offers some indication of pore connectivity. Deeper samples showed the increased volume of closed and dead end pores by an inability of the resin to infiltrate unconnected or very small pores. This rendered some of the samples useless for image analysis as they were full of cracks and bubbles, and were, as a result, very brittle. The images also display a much more closed and discrete pore structure; whereas the shallow samples were very open and connected (Figure 3-16). This agrees with other studies regarding decreasing pore size and connectivity in peat with depth (Loxham and Burghardt, 1986; Hoag and Price, 1997); (Heydorn, 2000).

3.10.3 Applications of Image Analysis

Images of soil blocks contain much more detailed information about soil structure than is available by other more integrated or bulk methods of analysis. The image analysis process could generate data for application to a number of other purposes, such as the calculation of thermal conductivity, tortuosity, pore surface area, ice and water

locations in frozen soil, water transmission and storage, solute diffusion and the modelling of soil responses to such things as freezing and thawing.

As outlined in chapter 2, the calculation of thermal conductivity makes use of certain assumptions regarding the orientation and connectivity of the soil, water, air and ice phases in order to estimate the bulk value for a soil volume. These assumptions are estimated using the empirical equations [2-4 to 2-8] of DeVries(1963). Using image analysis, it is possible to directly observe and quantify the connected pathways provided by the soil in the dry state. By modelling these connections through which heat is conducted in soil and the influence of varying water/ice/air content it may be possible to more accurately calculate the thermal properties of the bulk soil volume and determine how thermal conductivity changes with the saturation and state of soil moisture.

3.11 CONCLUSIONS

The comparison of pore hydraulic radius data derived from image analysis and the pressure plate extractor tests indicated that the image analysis technique is an effective method for measuring soil pores, provided the size of the pores of interest fall above the detection limit (image resolution). Because of the depth dependency of peat's physical properties the effectiveness of image analysis decreases with increasing depth of a sample in the peat profile. Thus, the effectiveness of applying this technique is highly dependent upon the size of the features of interest and the resolution of the images used for measurement. The application of this technique in assessing permeability of organic soil is also depth dependant. In the near surface soils where the majority of the pores are visible for measurement, the image analysis technique is a viable method for measuring

pores and estimating permeability. However, this technique is not applicable to deeper soils where a large portion of the pores are not detectable.

One of the major difficulties in the image analysis of soil pores is selecting which dimensions of the pores to measure. Matric potential head from the water retention characteristic curve data is translated into a pore hydraulic radius using the capillary equation [3-7]. However, the hydraulic radius term in this equation requires some physically measurable parameters to quantify using image analysis. The capillary equation [3-7] is an established relationship for circular capillary tubes, however, its application to irregular pores requires some modification. In this study, pore hydraulic radius is derived from the capillary equation as a function of the pore area and perimeter [eq. 3-8], two easily measurable physical properties of the soil pores. Plots of cumulative pore hydraulic radii calculated using measurements from images corresponded well with the data from pressure plate extractor tests. With an average root mean squared error of 9% between the curves, results suggest that this method of calculating hydraulic radius is representative of the complex pore shape influencing soil drainage.

The major drawback identified in this study is the requirement of thresholding information that can only be obtained from pressure plate extractor data. This means that the image analysis technique is not a stand alone method for the measurement of soil physical structure. Another limitation is the requirement of saturated and residual water content values, data which cannot be quantified solely from image analysis. However, digital images of resin-impregnated soil blocks provide a richer source of soil physical and structural data that is not available from indirect methods such as pressure plate extractor or drainage tests.

Average root mean squared error values of 4.8% for the water retention characteristic curves and 8.8% for the cumulative pore size distribution curves indicate a good agreement between the two methods of acquiring pore size data. This suggests that the images of soil pores are a reasonable representation of the 3D pore structure and could be used for the measurement of other soil physical properties; assuming that the pressure plate extractor data provide a good indication of the true 3D structure of the pore network.

3.12 RECOMMENDATIONS

This study was carried out with 15 pressure plate extractor samples and 15 images. The results from this study are encouraging, but could be strengthened by a larger sample set for both pressure plate extractor testing and image analysis. A larger set of image samples and soil cores would provide a better representation of the peat profile allowing more solid conclusions to be drawn regarding the reliability of these methods. The relatively simple procedure used in the analysis of these samples means that it is easily automated for quick processing, and could be carried out on a large scale with little programming. However, the use of image analysis is still limited by the requirement for the water retention characteristic curve to be known in order to threshold the image for measurement. A vast improvement to this method would be to eliminate this need.

The image resolution employed in this study is approximately 1500 pixels per inch (ppi), but higher resolution scanning and imaging systems are available. A quick assessment of the data indicates that an increase in resolution of at least an order of magnitude is required to significantly extend the range of pores measured in deeper samples. Neglecting software, hardware and optical limitations, it appears that higher

resolution images, which may be able to capture the micropores that went undetected in this study are possible. The highest resolution scanning found in an internet search of commercial scanning equipment can define a 3 micron spot (http://www.aztek.com/). This technology, using the same criteria applied in this study, could detect a pore of 3 micron hydraulic radius. This corresponds to a matric potential head of 4 m and in deeper samples would enable plotting curves which include nearly 90% of the data available from the pressure plate extractor tests.

3.13 FIGURES

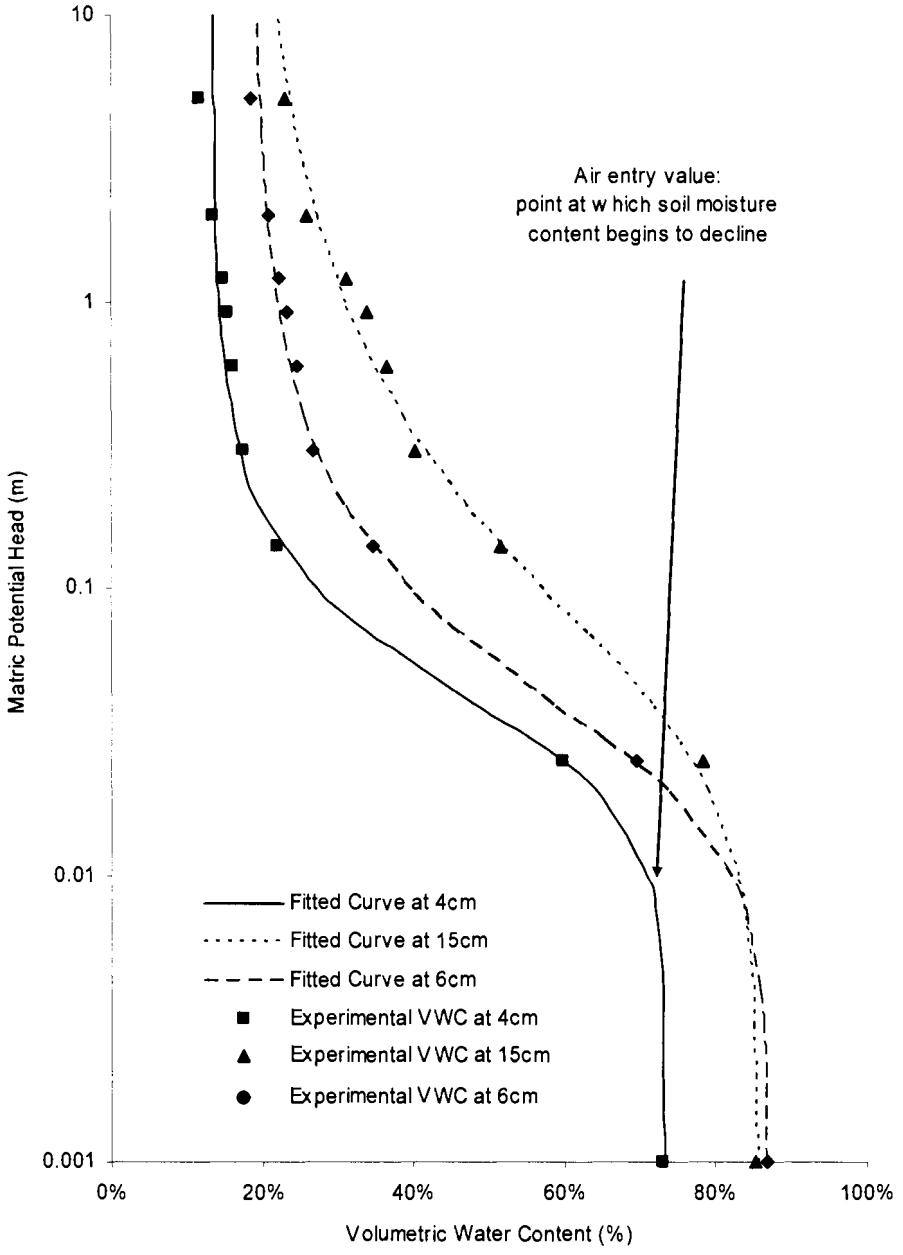

Figure 3-1. Variations in volumetric water content (VWC) with matric potential head for soils sampled from Granger basin. Best fit curves are plotted using the VanGenuchten equation (Van Genuchten, 1980).

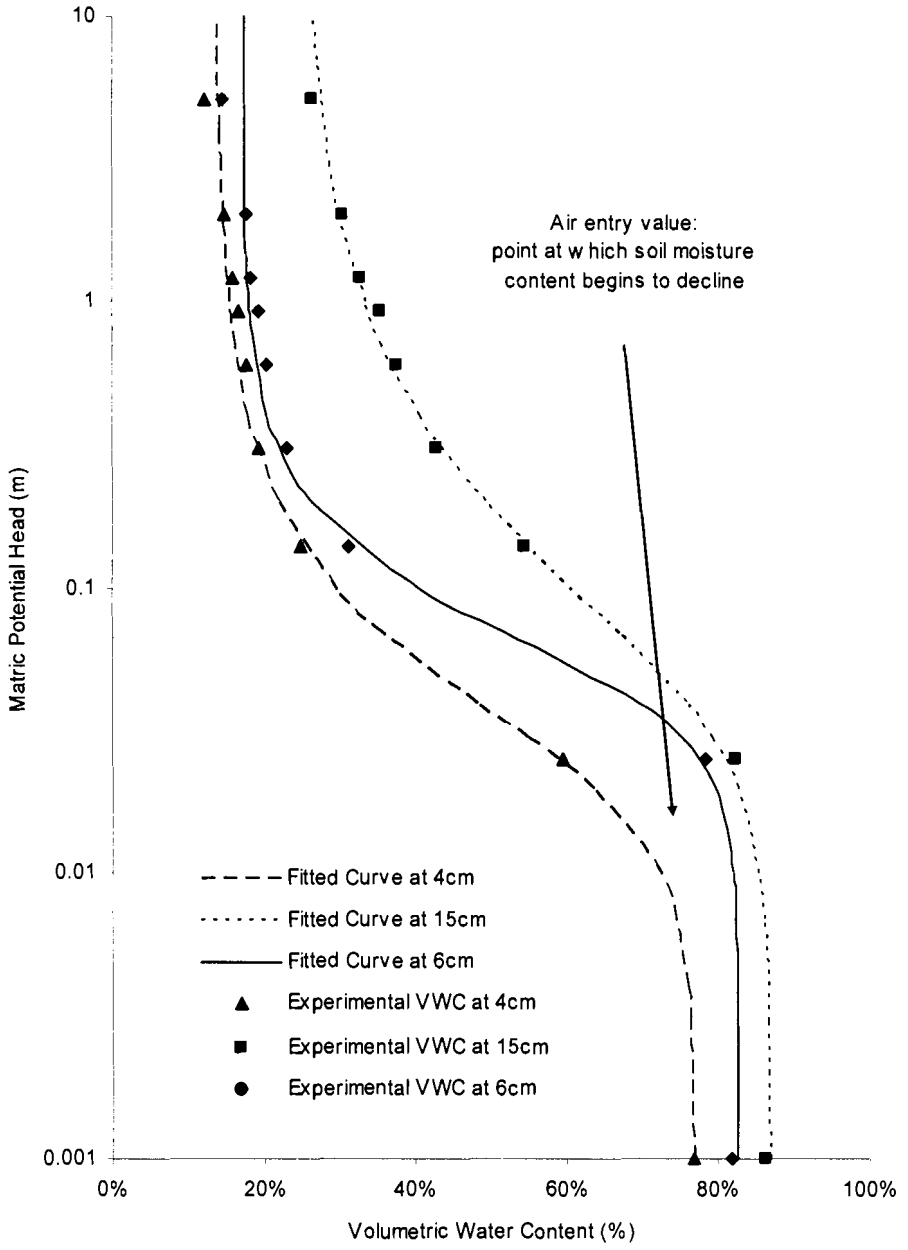

Figure 3-2. Variations in volumetric water content (VWC) with matric potential head for soils sampled from Granger basin. Best fit curves are plotted using the VanGenuchten equation (Van Genuchten, 1980).

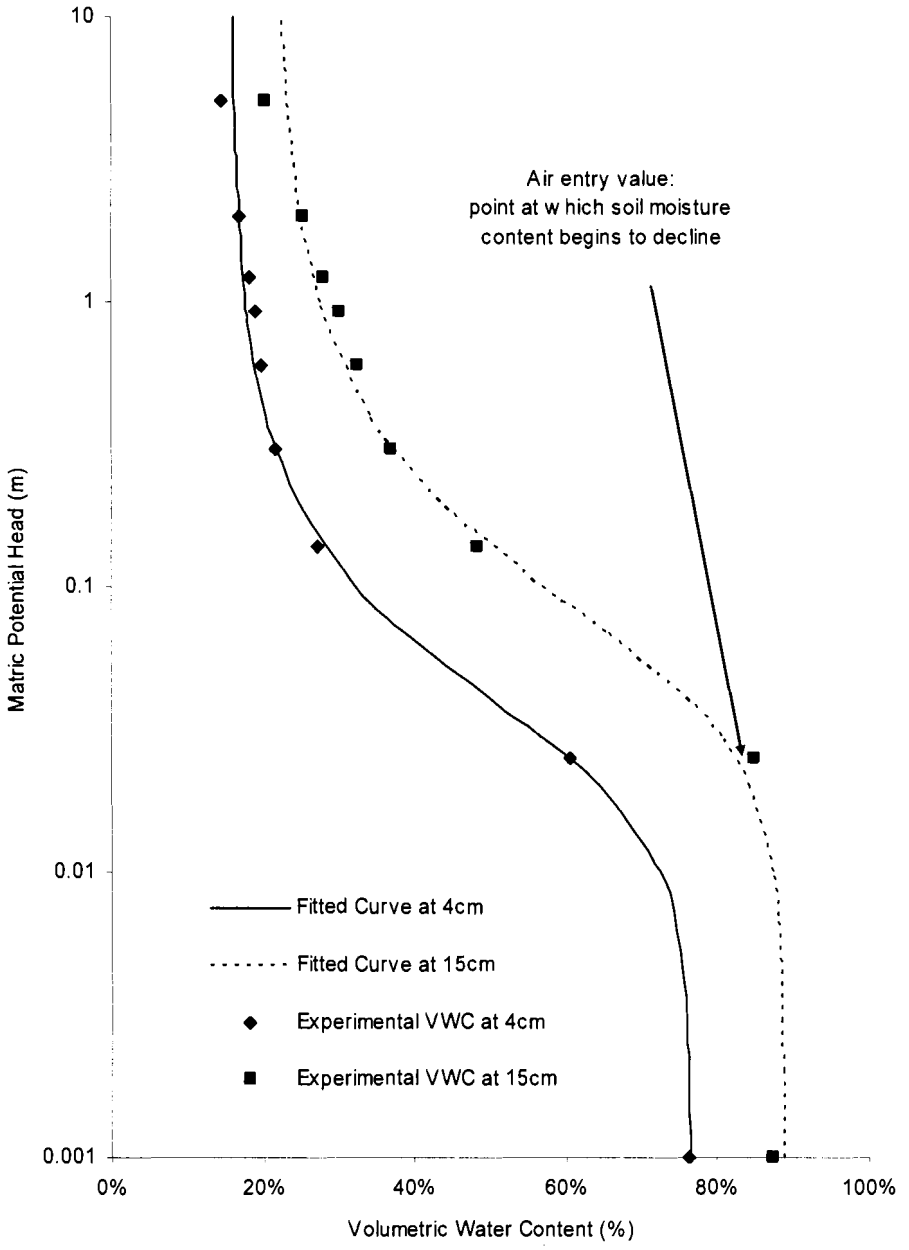

Figure 3-3. Variations in volumetric water content (VWC) with matric potential head for soils sampled from Granger basin. Best fit curves are plotted using the VanGenuchten equation (Van Genuchten, 1980).

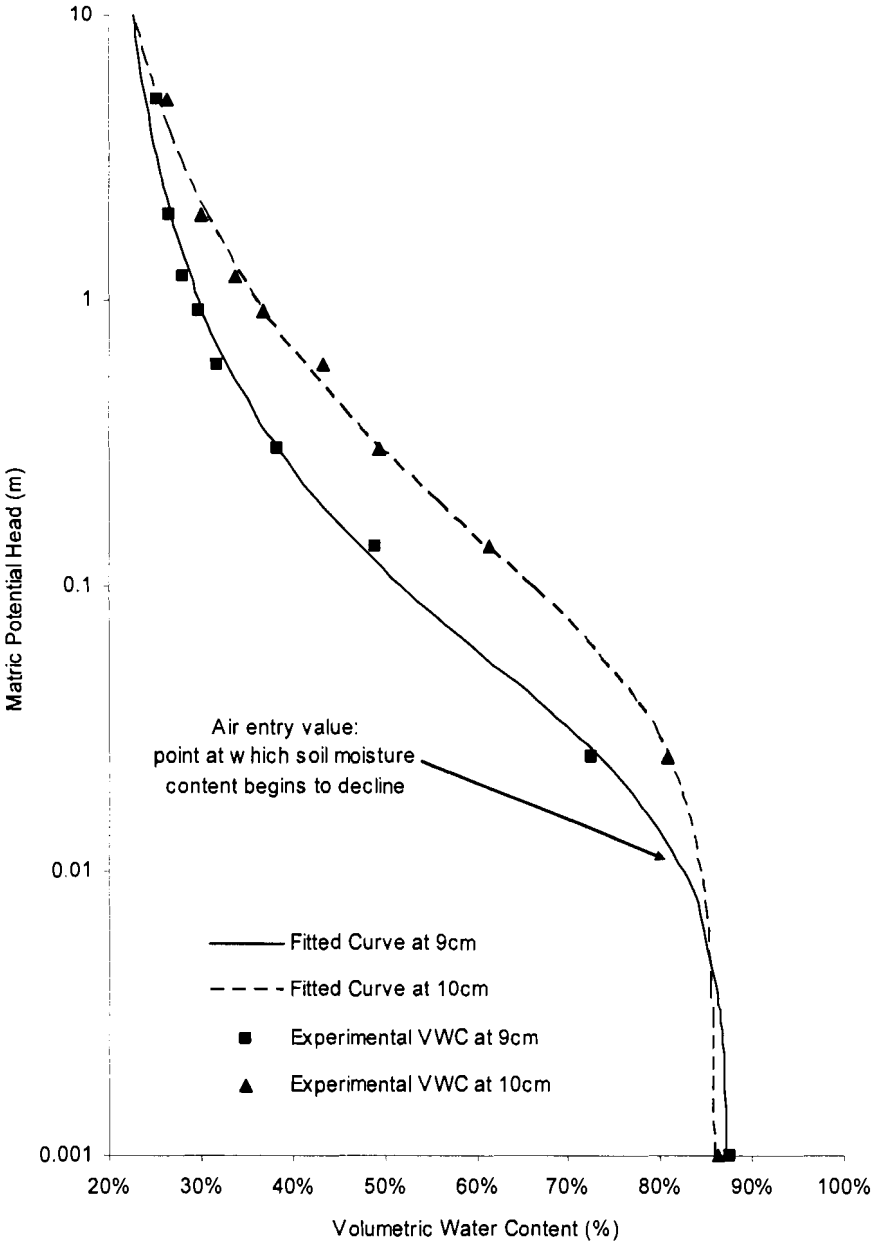

Figure 3-4. Variations in volumetric water content (VWC) with matric potential head for soils sampled from Scotty Creek. Best fit curves are plotted using the VanGenuchten equation (Van Genuchten, 1980).

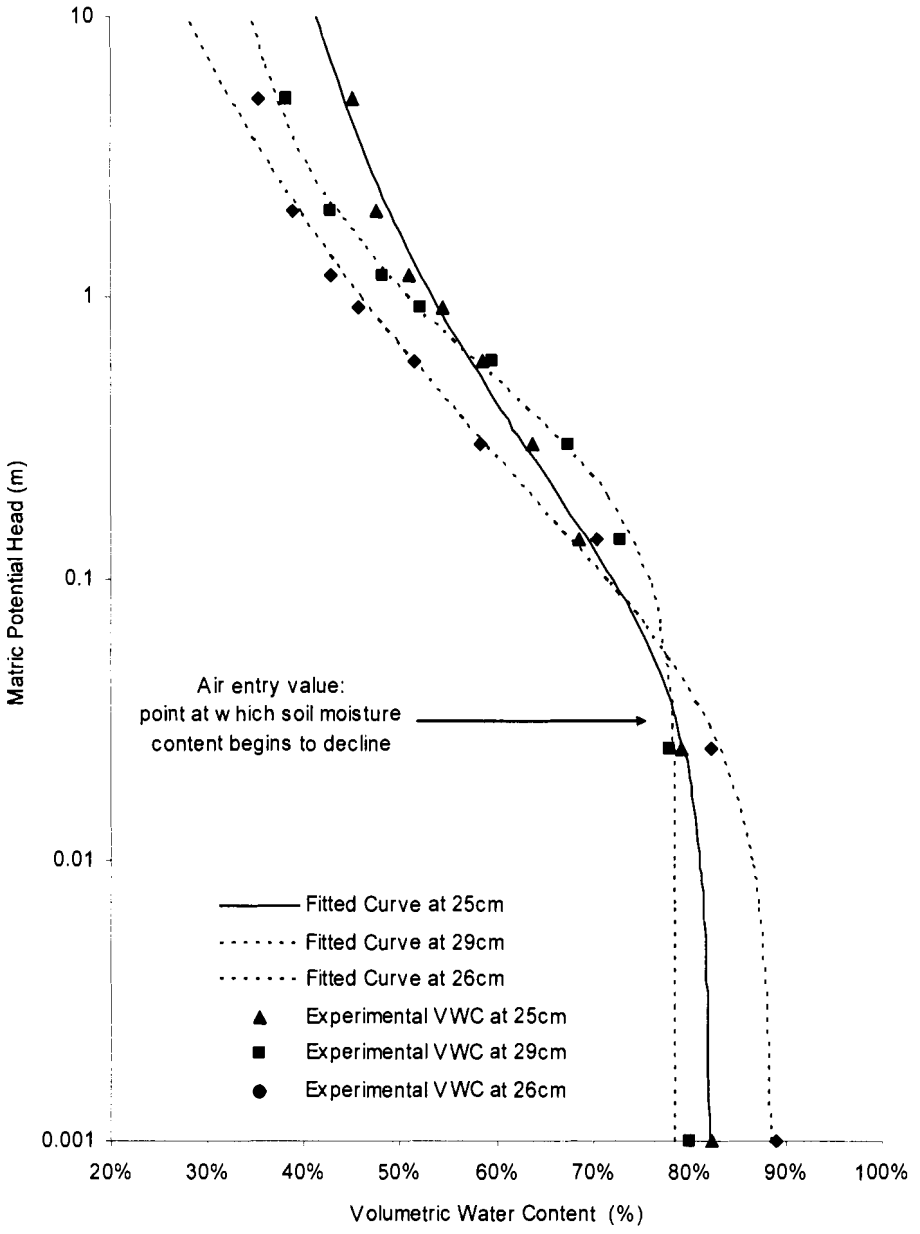

Figure 3-5. Variations in volumetric water content (VWC) with matric potential head for soils sampled from Scotty Creek. Best fit curves are plotted using the VanGenuchten equation (Van Genuchten, 1980).

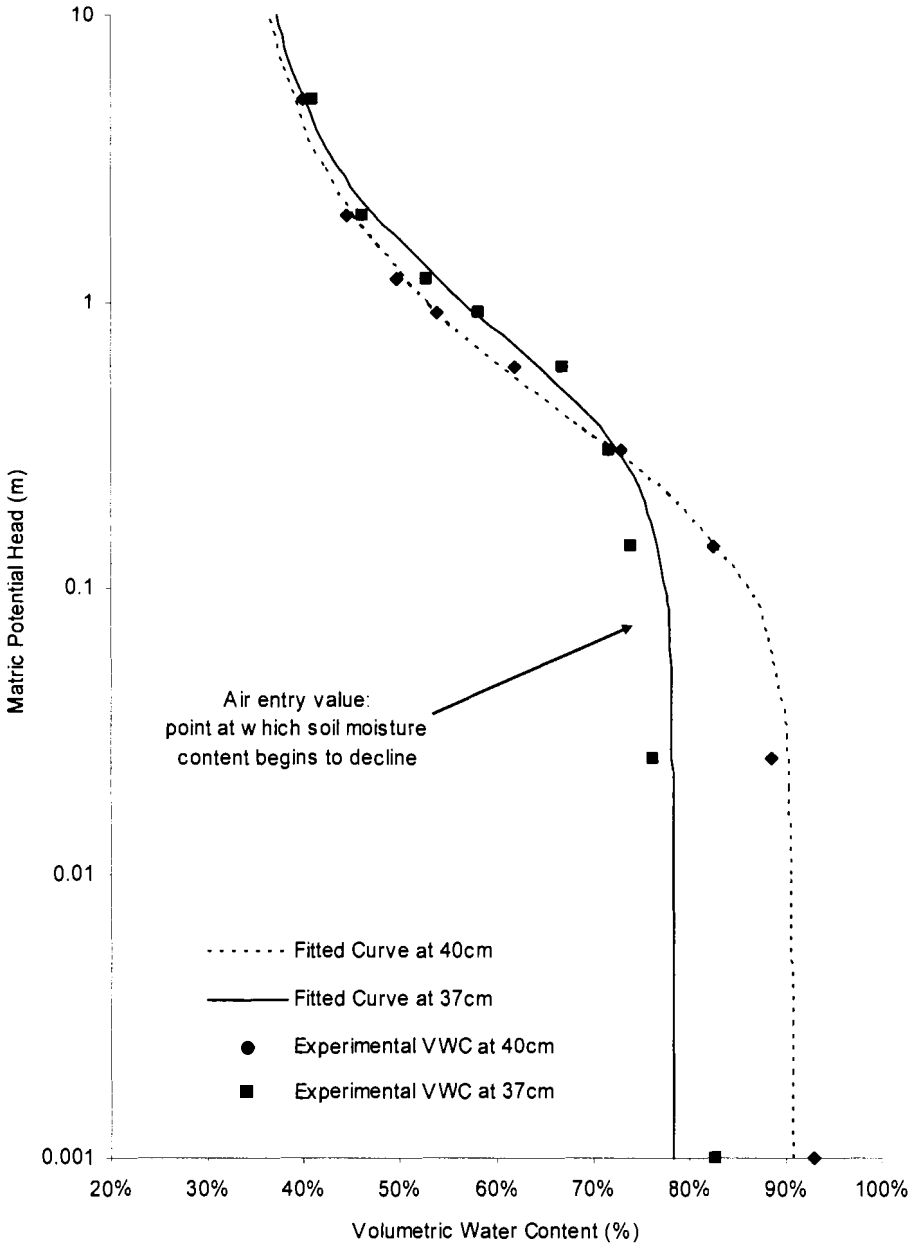

Figure 3-6. Variations in volumetric water content (VWC) with matric potential head for soils sampled from Scotty Creek. Best fit curves are plotted using the VanGenuchten equation (Van Genuchten, 1980).

A) Original black and white image

B) Image thresholded at porosity

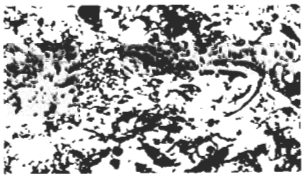

C) Image thresholded with modified porosity

Figure 3-7. The original black and white image (A), the result of thresholding this image at porosity (B) and using the modified threshold (C) of porosity equal to pores theoretically visible above the assumed lower limit of detection for the images.

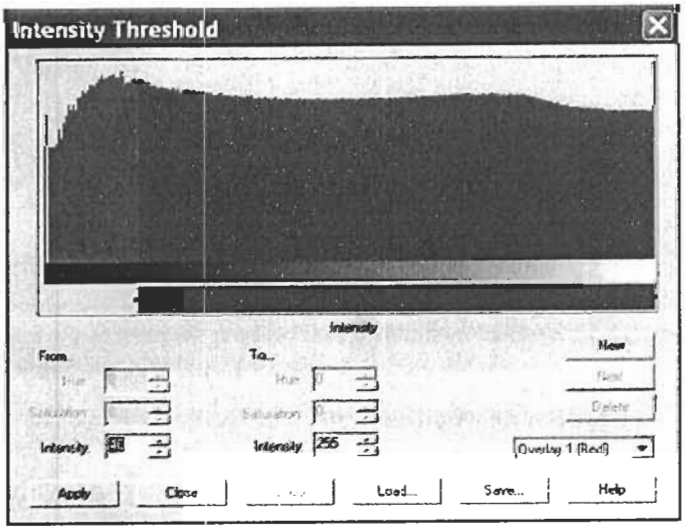

Figure 3-8. An intensity histogram used to define a threshold in *sigma scan*. The distribution of pixel values does not appear as a strongly bi-modal distribution which would allow the threshold to be defined as the minimum between the peaks. The red area is the range of gray scale values to be filled by the overlay for measurement.

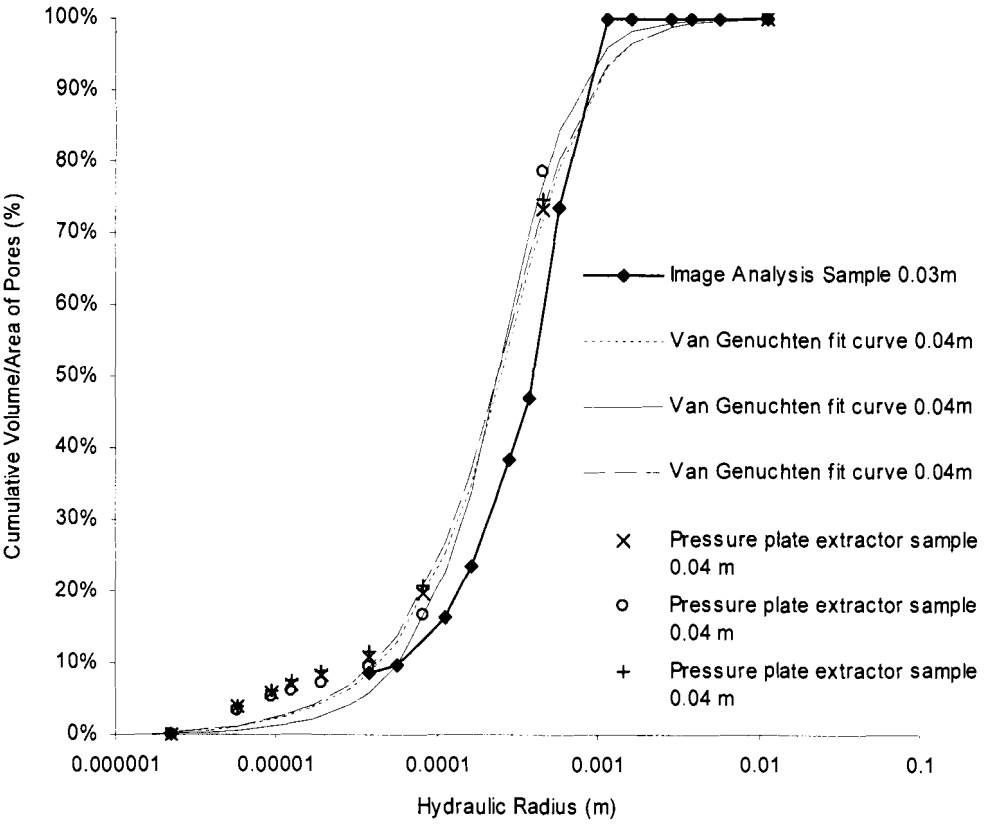

Figure 3-9. Cumulative pore hydraulic radius distributions comparing data points generated from pressure plate extraction tests (pore volume) and curves fit using the Van Genuchten equation to points measured using image analysis (pore area) for a shallow sample.

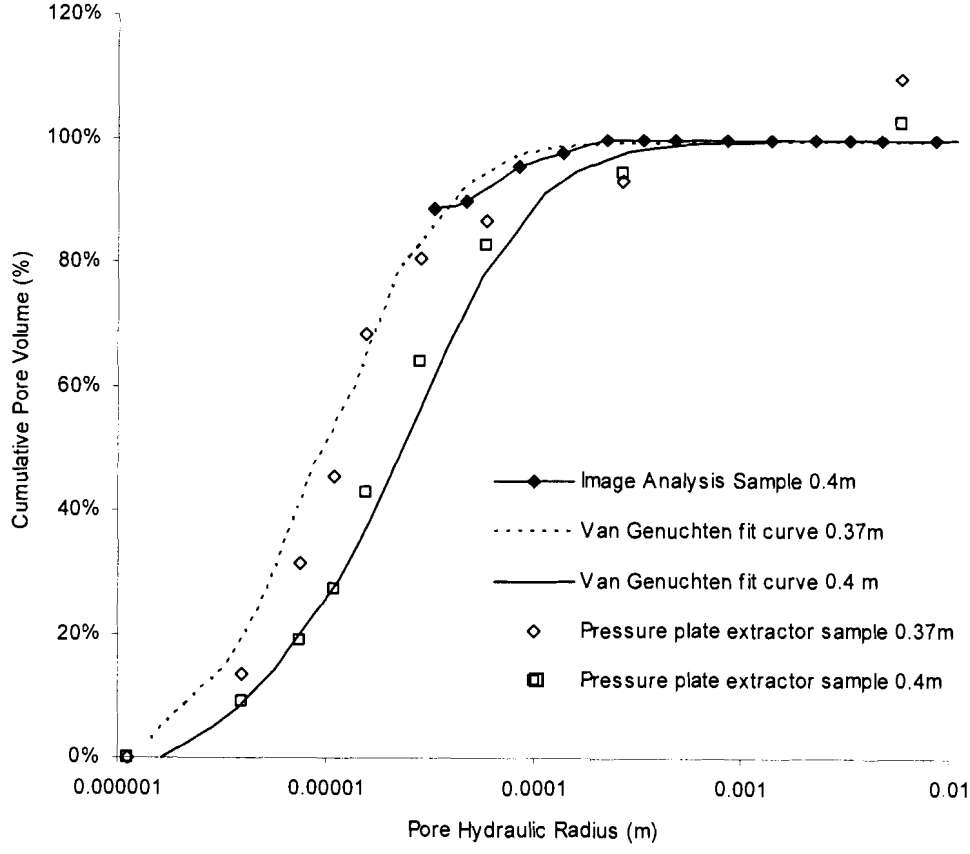

Figure 3-10. Cumulative pore hydraulic radius distributions comparing data points generated from pressure plate extraction tests (pore volume) and curves fit using the Van Genuchten equation to points measured using image analysis (pore area) for a deep sample.

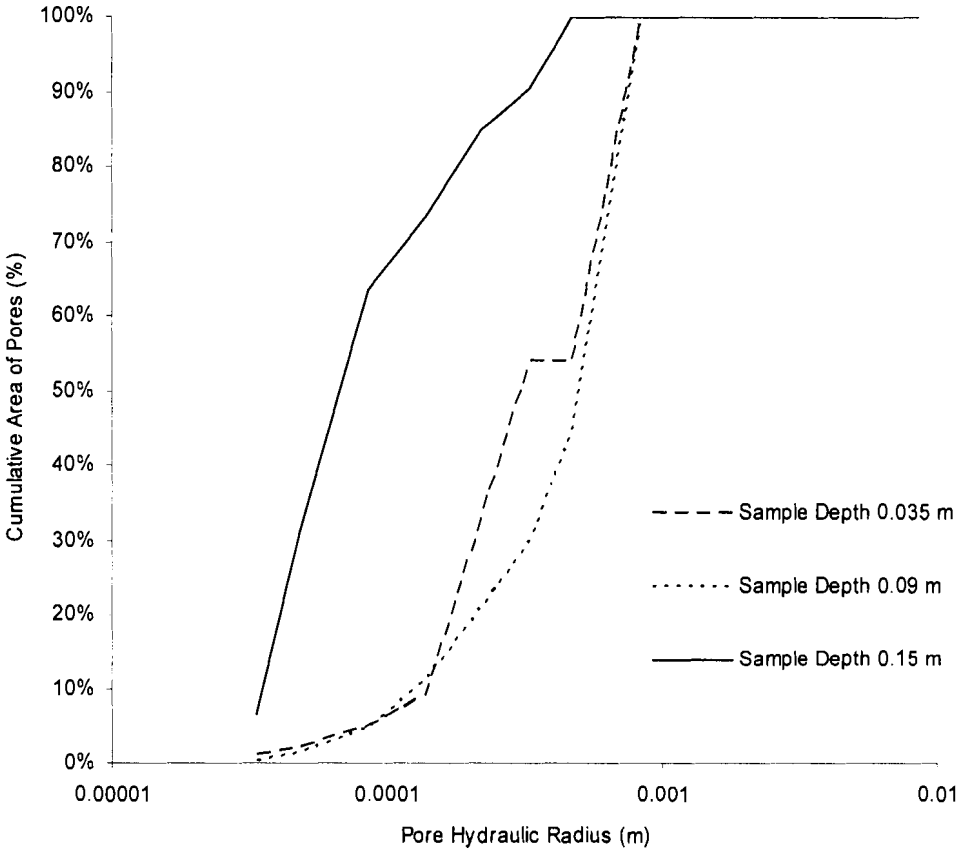

Figure 3-11. Cumulative pore hydraulic radius distributions plotted using image analysis data for core #3 from Granger Basin at 3 depths in the soil profile showing decreasing pore size with depth. Larger pores at 0.09 m may indicate the low density zone just below the surface reported for some peats.

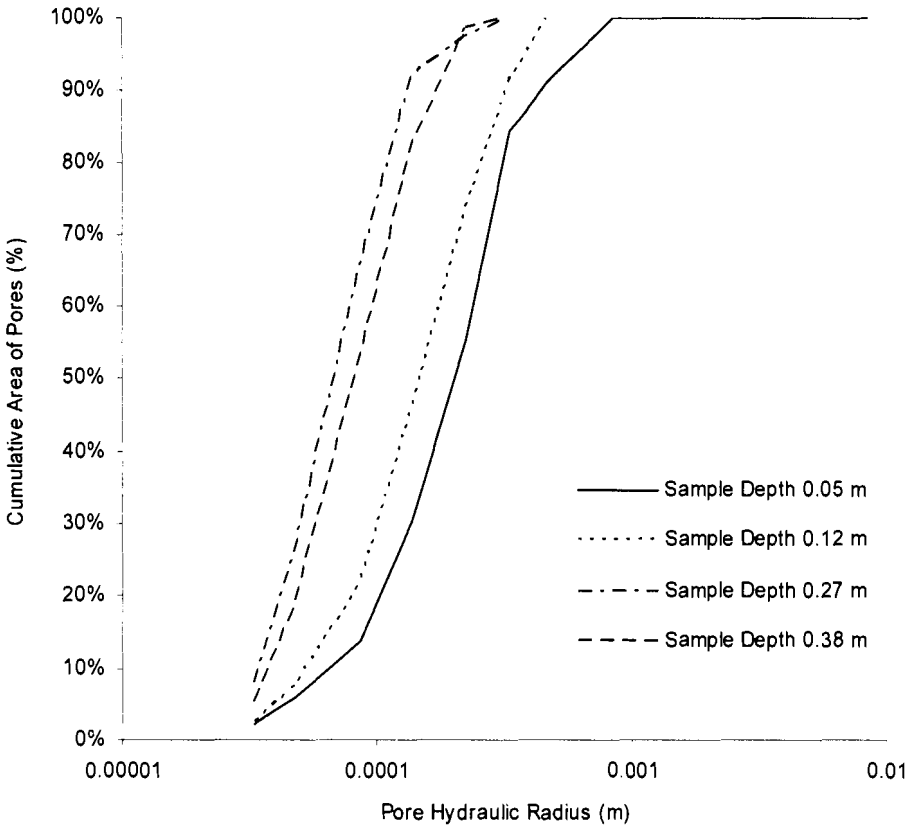

Figure 3-12. Cumulative pore hydraulic radius distributions plotted using image analysis data for core #5 from Scotty Creek at 4 depths in soil profile showing decreasing pore size with depth.

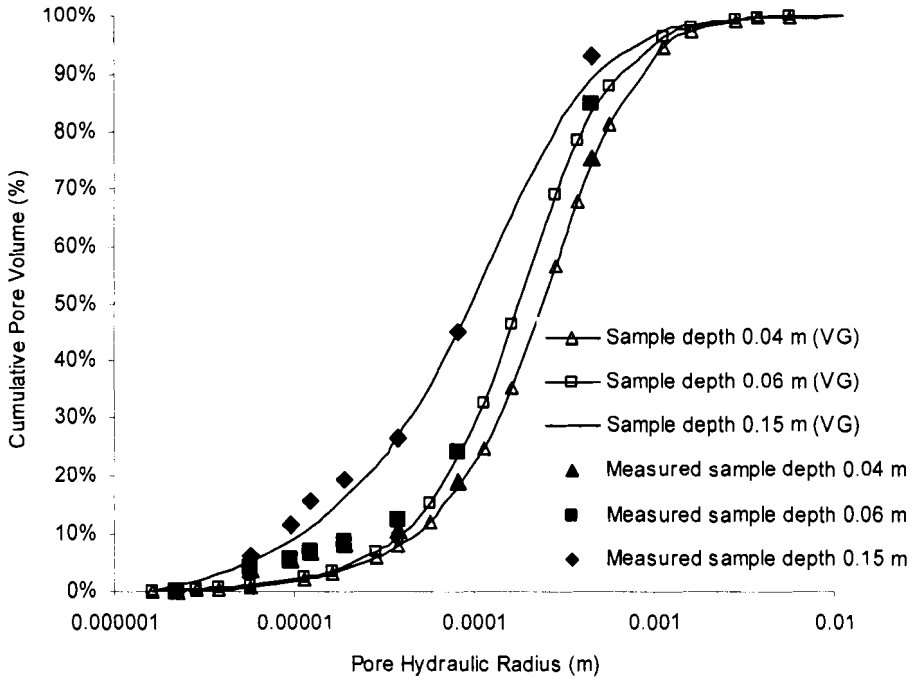

Figure 3-13. Cumulative distribution of pore hydraulic radii for 3 sampled depths at Granger Basin. Points are plotted from pressure plate extractor data and lines are plotted using best fit curves calculated using the Van Genuchten (VG) equation.

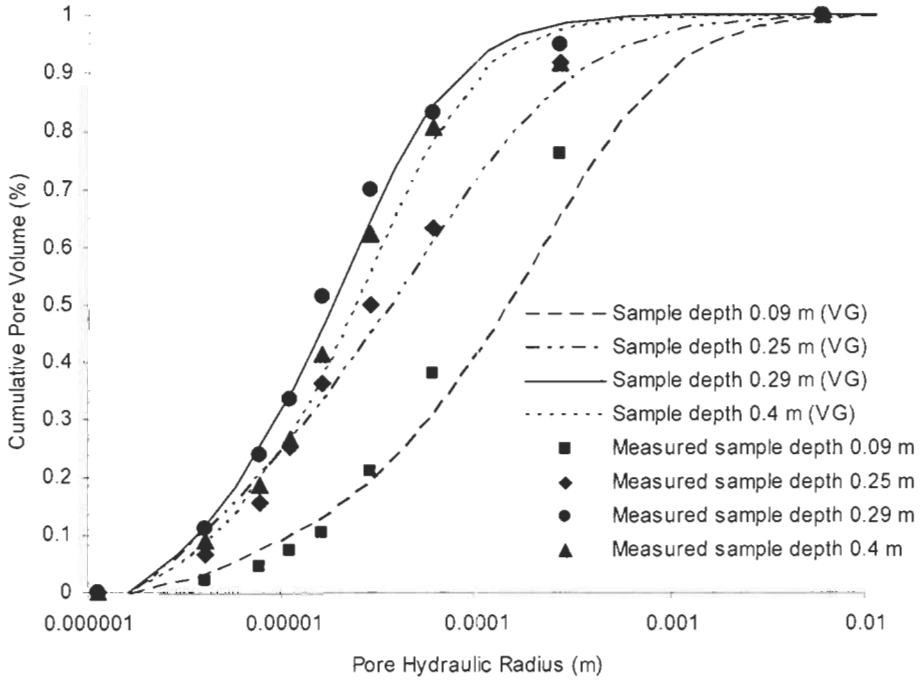

Figure 3-14. Cumulative distribution of pore hydraulic radii for 4 sampled depths at Scotty Creek. Points are plotted from pressure plate extractor data and lines are plotted using best fit curves calculated using the Van Genuchten (VG) equation.

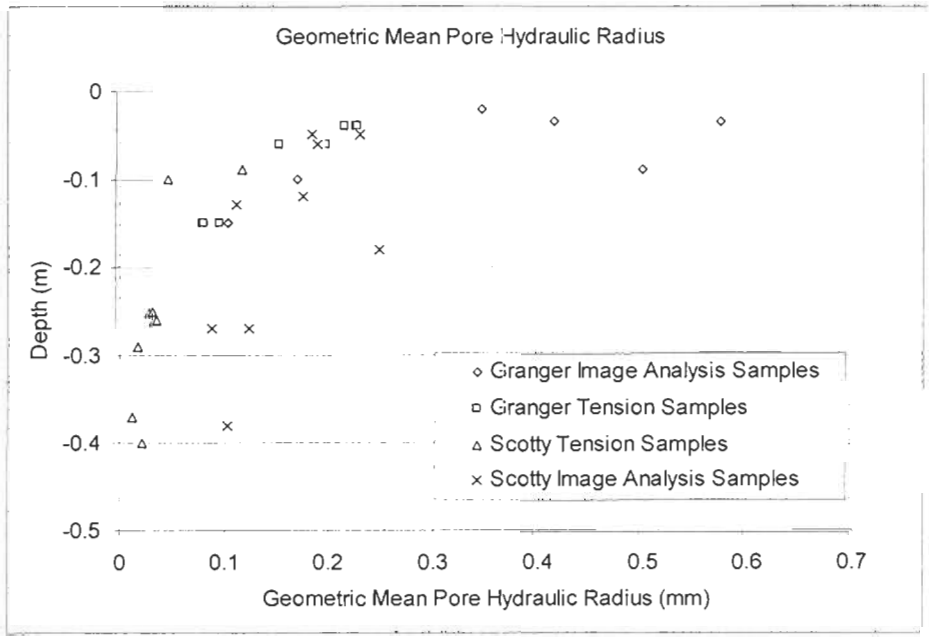

Figure 3-15. Variation in geometric mean pore hydraulic radius with depth for pressure plate extractor and image analysis samples at Granger Basin and Scotty Creek.

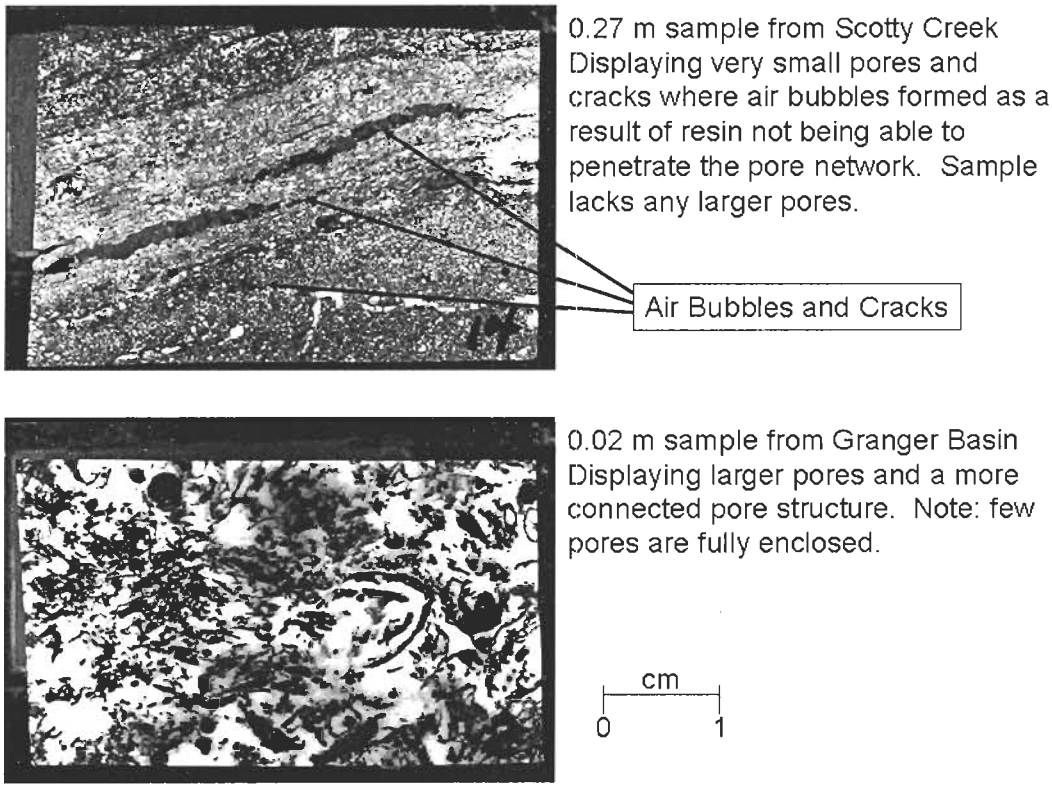

Figure 3-16. Two image analysis samples from different depths. The shallow sample (0.02 m) has an open and connected pore structure with high porosity. The deeper sample (0.27 m) has a lower porosity, smaller pores and is less connected. As a result the fluorescent resin was not able to penetrate pores resulting in the sample being brittle and full of air bubbles.

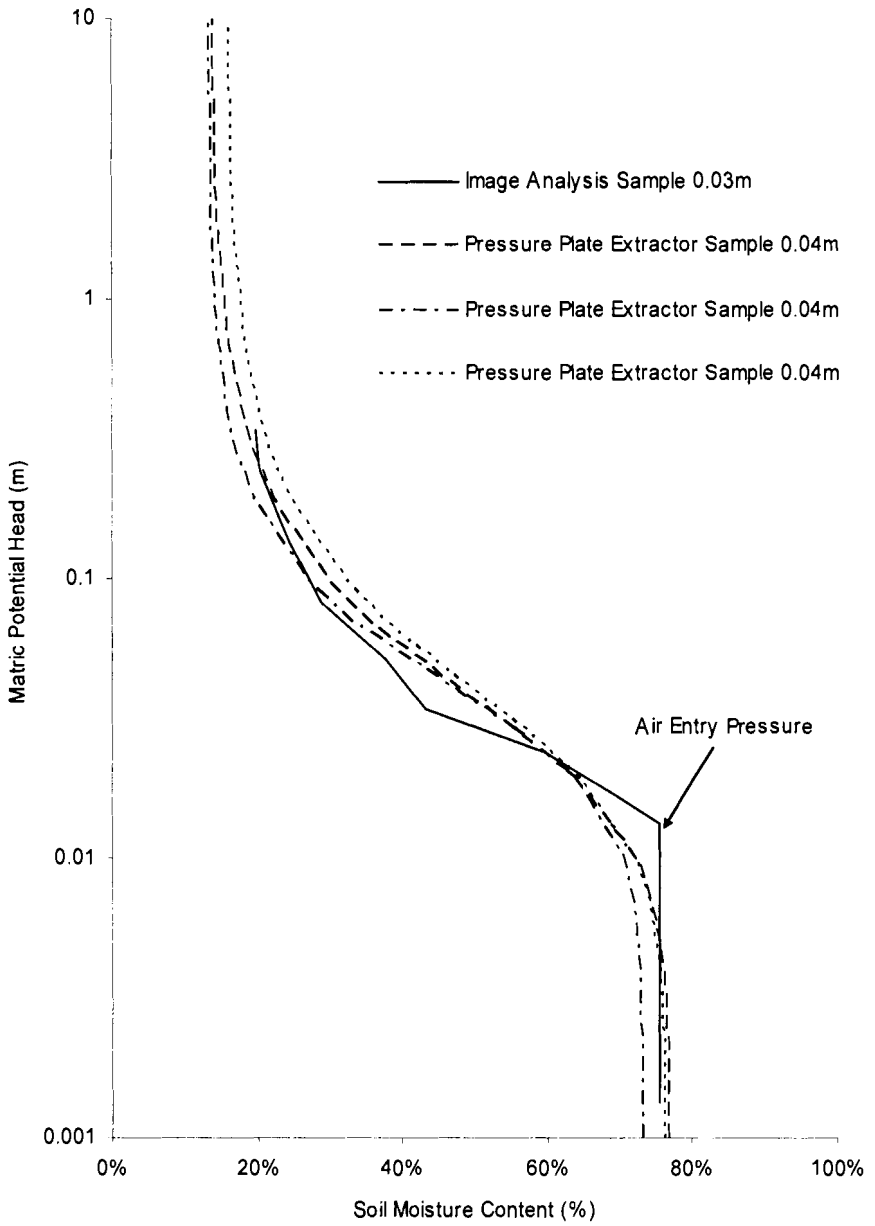

Figure 3-17. Comparison of the water retention characteristic curve generated using image analysis data and experimental curves from pressure plate extractor testing for a shallow sample.

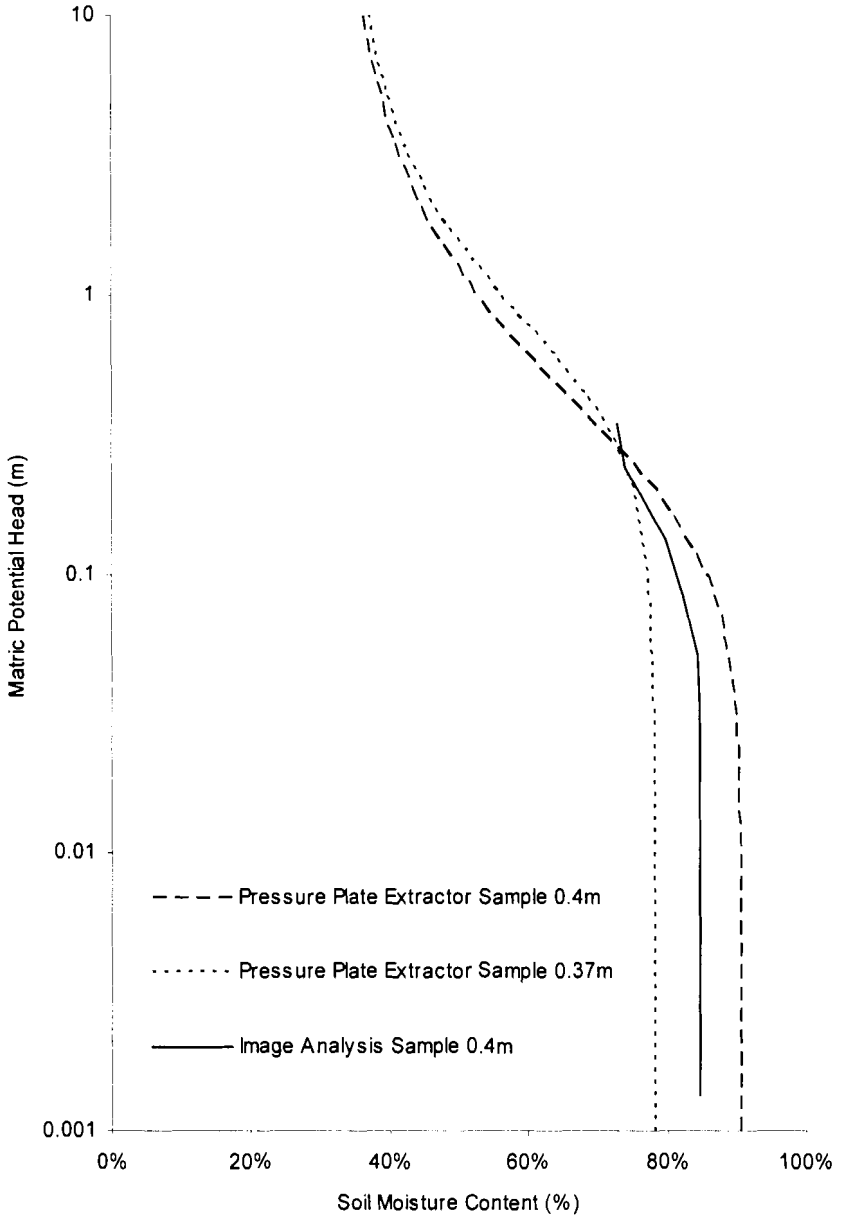

Figure 3-18. Comparison of the water retention characteristic curve generated using image analysis data and experimental curves from pressure plate extractor testing for a deep.

3.14 TABLES

Sample #	Depth (m)	Root Mean Squared Error	
		Water Retention Characteristic Curves	Cumulative PSD Curves
2	0.02	5.6%	9.1%
3	0.38	1.1%	3.7%
4	0.27	1.8%	3.5%
5	0.12	3.9%	8.8%
[illegible]	[illegible]	[illegible]	[illegible]
7	0.04	8.7%	17.3%
9	0.05	3.4%	6.2%
10	0.04	7.2%	14.1%
11	0.15	6.0%	9.8%
13	0.05	1.4%	7.6%
14	0.27	2.7%	5.7%
15	0.07	3.7%	7.0%
16	0.18	3.3%	4.8%
17	0.13	6.9%	10.5%
18	0.10	2.9%	4.4%
	Average	**4.8%**	**8.8%**

Table 3-1. Root mean squared error for water retention characteristic and pore size distribution (PSD) curves calculated using image analysis compared to pressure plate extractor data expressed in percentage volumetric water content and percentage pore area/volume, respectively.

CHAPTER 4 CONCLUDING DISCUSSION

Effective modelling of subsurface flows during the snowmelt period in organic permafrost terrain requires an understanding of two independent factors: the rate of thawing of the active layer and the decline in soil permeability with depth. This study has addressed both of these issues in two distinct, yet related, studies. A thermal algorithm was developed for use in thawing the soil, alongside a method for measuring soil physical properties from image analysis for use in pedo-transfer equations. In both cases, the objectives of each study were met and further areas for research were also identified.

In order to completely close the story described above it is necessary to be in possession of both a soil thaw algorithm, and a relation describing either the decline in permeability with depth or its relation to soil physical properties. Despite the inability of this study to develop such a relation, a significant contribution has been made in its pursuit. Considering the abundance of available pedo-transfer equations in the literature for use with soil structural measurements, the deficiency lies more in the acquisition and reliability of data rather than the equations themselves. Despite the requirement for water retention characteristic data in the thresholding procedure, image analysis still provides a richer source of data for these equations than are provided by indirect methods or by other modes of analysis.

With recent software and imaging equipment, an assessment of the viability of image analysis methods for soil pore measurement is a vital step towards determining its

reliability as a tool in acquiring soil structural data. This study attempted to fill the gap between pedo-transfer functions and data requirements. Although specifically geared towards organic soil and permeability, the approach of this study could be applied to any soil type and desired property, although the successful generation of similar pore size distribution curves from both water retention characteristic curves and image analysis may be unique to organic soil. In theory, soil pore structure is closely related to soil hydraulic properties, however, in reality this has been difficult to demonstrate. Using the water retention characteristic curve as a data source for comparison, this study demonstrates that soil physical properties are related to those of drainage and flow through the capillary equation [3-7]. Finally, the image analysis technique indicated that the derivation of hydraulic radius as 2A/P from the capillary equation is a reasonable representation of pore dimensions.

On the thermal side, it is apparent that an accurate representation of soil thaw in CRHM is not yet possible. However, again this research has shown merit in offering progress in the pursuit of a thermal algorithm for northern peats. It has also illuminated deficiencies in the current representation and method of calculation. Application of these results in hydrologic models should be tempered with the consideration that there are a range of temporal and spatial scales over which these processes can be represented, with the finer details becoming more vital at shorter time steps. In these cases, a linear representation and static energy partitioning of soil thaw is of limited use in predicting the exact detail of such a complex system.

The combination of these two projects form a solid base for a more complete picture of the thermal and hydraulic properties of the active layer during spring thaw.

Although this study was unable to close the book on this story, it is rare for one project to accomplish this. Most scientific research is a series of successive studies or works in progress towards a common goal. Alone, individuals surmount the smaller obstacles in pursuit of the greater goal which is only attainable collectively. In this tradition, I hope, this study has satisfied a small portion of a greater goal.

REFERENCES

Abbey, F. L., D. M. Gray, et al. (1978). Index models for predicting ground heat flux to permafrost during thawing conditions. Proceedings of the Third International Conference on Permafrost,vol. 1,3-9, National Research Council of Canada, Ottawa, Canada.

Ahuja, L. R., D. K. Cassel, et al. (1989). "Evaluation of spatial distribution of hydraulic conductivity using effective porosity data." Soil Science **148**(6): 404-411.

Arya, L. M., F. J. Leij, et al. (1999). "Relationship between the hydraulic conductivity function and the particle-size distribution." Soil Science Society of America Journal **63**: 1063-1070.

Arya, L. M., F. J. Leij, et al. (1999). "Scaling parameter to predict the soil water characteristic from particle-size distribution data." Soil Science Society of America Journal **63**: 510-519.

Bachmann, J., R. Horton, et al. (2002). "Temperature dependence of water retention curves for wettable and water-repellent soils." Soil Science Society of America Journal **66**(1): 44-52.

Bachmann, J., S. K. Woche, et al. (2004). "Extended methodology for determining wetting properties of porous media." Water Resources Research **39**(12).

Berryman, J. G. and S. C. Blair (1987). "Kozeny-Carman relations and image processing methods for estimating Darcy's constant." Journal of Applied Physics **62**(6): 2221-2228.

Bodziony, J., K. Konstankiewicz, et al. (1993). "Assessment of the porosity of soil samples according to the method of stereological analysis." International Agrophysics **7**(1): 35-46.

Boelter, D. H. (1965). "Hydraulic conductivity of peats." Soil Science **100**(4): 227-231.

Bolton, W. R., L. D. Hinzman, et al. (2000). Stream flow studies in a watershed underlain by discontinuous permafrost. AWRA Spring Specialty Conference on Water Resources in Extreme Environments,vol. 31-36.

Bouabid, R., E. A. Nater, et al. (1992). "Measurement of pore size distribution in a lamellar Bt horizon using epifluorescence microscopy and image analysis." Geoderma **53**: 309-328.

Bristow, K. (2002). Thermal Conductivity. Methods of Soil Analysis Part 4. Madison, Wisconsin, USA, Soil Science Society of America. **5:** 1209-1224.

Brooks, R. H. and A. T. Corey (1964). Hydraulic properties of porous media. Fort Collins, Colorado, Colorado State University**:** 27.

Bruand, A., I. Cousin, et al. (1996). "Backscattering electron scanning images of soil porosity for analyzing soil compaction around roots." Soil Science Society of America Journal **60**: 895-901.

Carey, S. K. and M. K. Woo (1998). A case study of active layer thaw and its controlling factors. Seventh International Permafrost Conference,vol. 127-131.

Carey, S. K. and M. K. Woo (1999). "Hydrology of two slopes in subarctic Yukon, Canada." Hydrological Processes **13**: 2549-2562.

Carey, S. K. and M. K. Woo (2000). "Within-slope variability of ground heat flux, subarctic Yukon." Physical Geography **21**(5): 407-417.

Childs, E. C. and C. Collis-George (1950). "The permeability of porous materials." Proc. R. Soc. London: 392-405.

Clymo, R. S. (1983). Peat. Mires: Swamp, bog, fen and moor. A. J. P. Gore. New York, Elsevier Science**:** 159-219.

Coleou, C., E. Xu, et al. (1999). "Capillary rise in snow." Hydrological Processes **13**: 1721-1732.

Crawford, J. W., N. Matsui, et al. (1995). "The relation between the moisture-release curve and the structure of soil." European Journal of Soil Science **46**: 369-375.

De Vries, D. A. and J. R. Philip (1986). "Soil heat flux, thermal conductivity and the null-alignment method." Soil Science Society of America Journal **50**: 12-18.

Dingman, S. L. (1984). Fluvial Hydrology. New York, W.H. Freeman and Company.

Farouki, O. T. (1981). "The thermal properties of soils in cold regions." Cold Regions Science and Technology **5**: 67-75.

Fetter, C. W. (1994). Applied Hydrogeology. Toronto, ON, Prentice-Hall Canada, Inc.

French, H. M. (1996). The Periglacial Environment. Essex, England, Addison Wesley Longman Ltd.

Fuchs, M. (1986). Heat Flux. Methods of soil analysis, Part 1. A. Klute. Madison, Wisconsin, Soil Science Society of America Inc.: 957-968.

Garcia-Bengochea, I. and C. W. Lovell (1981). "Correlative measurements of pore size distribution and permeability in soils." Permeability and Groundwater Contaminant Transport **746**: 137-150.

Giminez, D., R. R. Allmaras, et al. (1997). "Prediction of the saturated hydraulic conductivity-porosity dependence using fractals." Soil Science Society of America Journal **61**(5): 1285-1292.

Giminez, D., W. J. Rawls, et al. (2000). Scaling properties of saturated hydraulic conductivity in soil. Fractals in Soil Science. Y. A. Pachepsky, J. W. Crawford and W. J. Rawls, Elsevier Science.

Granger, R. J. (1999). Partitioning of energy during the snow-free season at the wolf creek research basin. Wolf Creek Research Basin, Hydrology, Ecology, Environment. J. W. Pomeroy, Granger, R.J. Saskatoon, SK, National Water Research Institute: 160.

Haag, R. W. and L. C. Bliss (1974). "Energy budget changes following surface disturbance to upland tundra." Journal of Applied Ecology **11**: 355-374.

Halliwell, D. H. and W. R. Rouse (1987). "Soil heat flux in permafrost: characteristics and accuracy of measurement." Journal of Climatology **7**: 571-584.

Heydorn, C. (2000). Using image analysis techniques to assess the pore structure of peat: Cape Race, Newfoundland. Department of Geography. Waterloo, University of Waterloo: 47.

Hillel, D. (1998). Environmental Soil Physics. San Diego, Academic Press.

Hinkel, K. M. and J. R. J. Nicholas (1995). "Active layer thaw rate at a boreal forest site in central Alaska, U.S.A." Arctic and Alpine Research **27**: 72-80.

Hinkel, K. M., F. Paetzold, et al. (2001). "Patterns of soil temperature and moisture in the active layer and upper permafrost at Barrow, Alaska : 1993-1999." Global and Planetary Change **29**: 293-309.

Hinzman, L. D., D. L. Kane, et al. (1993). Hillslope hydrology in an arctic setting. Sixth International Permafrost Conference,vol. 267-271.

Hinzman, L. D., D. L. Kane, et al. (1991). "Hydrologic and thermal properties of the active layer in the Alaskan arctic." Cold Regions Science and Technology **19**: 95-110.

Hirota, T., J. W. Pomeroy, et al. (2003). "An extension of the force-restore method to estimating soil temperature at depth and evaluation for frozen soils under snow." Journal of Geophysical Research-Atmospheres **107**(24).

Hoag, R. S. and J. S. Price (1997). "The effects of matrix diffusion on solute transport and retardation in undisturbed peat in laboratory columns." Journal of Contaminant Hydrology **28**: 193-205.

Horton, R. and P. J. Wierenga (1983). "Estimating the soil heat flux from observations of soil temperature near the surface." Soil Science Society of America Journal **47**: 14-20.

Ingram, H. A. P. (1978). "Soil layers in mires: function and terminology." Journal of Soil Science **29**: 224-227.

Ingram, H. A. P. (1981). Hydrology. Ecosystems of the World. Mires: Swamp, Bog, Fen and More. A. J. P. Gore. Amsterdam, Elsevier. **4A:** 67-158.

Ingram, H. A. P. (1983). Hydrology. Mires: Swamp, bog, fen and moor. A. J. P. Gore. New York, Elsevier Science: 67-158.

Jackson, J. A. and R. L. Bates (1984). Dictionary of Geological Terms. New York, Doubleday.

Janowicz, J. R. (1999). Wolf Creek research basin - overview. Wolf Creek Research Basin, Hydrology, Ecology, Environment. J. W. Pomeroy, Granger, R.J. Saskatoon, SK, National Water Research Institute: 160.

Jones, H. G. and J. W. Pomeroy (1999). The ecology of snow and snow-covered systems: summary and relevance to Wolf Creek, Yukon. Wolf Creek Research Basin: Hydrology, Ecology, Environment. J. W. Pomeroy and R. J. Granger. Saskatchewan, SK, National Water Research Institute: 160.

Kane, D. L., R. E. Gieck, et al. (1990). "Evapotranspiration from a small Alaskan arctic watershed." Proceedings of the Eighth Northern Research Basins Symposium/Workshop Nordic Hydrology **21**(4-5): 253-272.

Karam, M. A. (2003). "Reforming the force-restore method for predicting ground surface temperature." IEEE Transactions on Geoscience and Remote Sensing **41**(4): 812-816.

Kluitenberg, G. J. (2003). Heat capacity and specific heat. Methods of Soil Analysis Part 4.

Leij, F. J., M. G. Schaap, et al. (2002). The soil solution phase : Indirect methods. Methods of Soil Analysis, Part 4. J. H. Dane and G. C. Topp. Madison, WI, Soil Science Society of America: 1009-1045.

Lettau, H. and B. Davidson (1957). Exploring the atmosphere's first mile. Great Plains Turbulence Field Program,vol. Nebraska, Symposium Publications Division, Permagon Press.

Loxham, M. and W. Burghardt (1986). Saturated and unsaturated permeabilities of north German peats. Peat and Water. C. H. Fuchsman. New York, Elsevier Applied Science Publishers ltd.: 37-59.

Lynch, A. H., F. S. Chapin, et al. (1999). "Surface energy balance on the arctic tundra : measurements and models." American Meteorological Society **12**: 2585-2606.

Marshall, T. J. and J. W. Holmes (1988). Soil Physics. Cambridge, Cambridge University Press.

Mathan, K. K., A. Sundaram, et al. (1995). "Application of Kozeny-Carman equation for the estimation of saturated hydraulic conductivity of soils." Journal of the Indian Society of Soil Science **43**(4): 542-544.

Mbonimpa, M., M. Aubertin, et al. (2002). "Practical pedotransfer functions for estimating the saturated hydraulic conductivity." Geotechnical and Geological Engineering **20**: 235-259.

McGaw, R. W., S. I. Outcalt, et al. (1978). "Thermal properties and regime of wet tundra soils at Barrow, Alaska." Third International Permafrost Conference: 48-53.

McRoberts, E. C. (1975). "Field observations of thawing in soils." Canadian Geotechnical Journal **12**: 126-130.

Minasny, B. (2000). Efficient methods for predicting soil hydraulic properties. Precision Agriculture. Sydney, University of Sydney: 352.

Mishra, S., J. C. Parker, et al. (1989). "Estimation of soil hydraulic properties and their uncertainty from particle size distribution data." Journal of Hydrology **108**: 1-18.

Mooney, S. J., N. M. Holden, et al. (1998). "The rapid preparation of structural images from undisturbed, non-cohesive material (milled peat)." Geoderma **86**(159-168).

Nixon, J. F. (1973). "A study of some factors affecting the thawing of frozen soils." Canadian Geotechnical Journal **10**(3): 439-452.

Pachepsky, Y. A., D. Giminez, et al. (2000). Conventional and fractal geometry in soil science. Fractals in Soil Science. Y. A. Pachepsky, J. W. Crawford and W. J. Rawls, Elsevier Science.

Pare, D. (1984). "The occurrence of permafrost in peatlands." Geoscope **14**(2): 1-18.

Pietroniro, A., T. Prowse, et al. (1996). "Application of a grouped response unit hydrological model to a northern wetland region." Hydrological Processes **10**: 1245-1261.

Pomeroy, J. W., B. Toth, et al. (2003). "Variation in surface energetics during snowmelt in a subarctic mountain catchment." Journal of Hydrometeorology **4**: 702-719.

Price, J. S. (1983). The effect of hydrology on ground freezing in a watershed with organic terrain. Fourth International Permafrost Conference,vol. 1009-1014.

Quinton, W. L., S. K. Carey, et al. (In press). "Controls on soil moisture variability and the development of an impermeable frozen layer in organic-cover permafrost terrains."

Quinton, W. L. and D. M. Gray (2001). Estimating subsurface drainage from organic covered hillslopes underlain by permafrost: toward a combined heat and mass flux model. Soil-Vegetation-Atmosphere Transfer Schemes and Large-Scale Hydrological Models (Proceedings of a Symposium Held During the Sixth IAHS Scientific Assembly),vol. 270,333-341, Maastricht, Netherlands, IAHS.

Quinton, W. L., D. M. Gray, et al. (2000). "Subsurface drainage from hummock-covered hillslopes in the arctic tundra." Journal of Hydrology **237**: 113-125.

Quinton, W. L. and M. Hayashi (2005). The flow and storage of water in the wetland-dominated central Mackenzie river basin: Recent advances and future directions. Prediction in Ungauged Basins: Approaches for Canada's Cold Regions. C. Spence, J. W. Pomeroy and A. Pietroniro, Canadian Water Resources Association: 45-66.

Quinton, W. L., M. Hayashi, et al. (2003). "Connectivity and storage functions of channel fens and flat bogs in northern basins." Hydrological Processes **17**: 3665-3684.

Quinton, W. L. and P. Marsh (1999). "A conceptual framework for runoff generation in a permafrost environment." Hydrological Processes **13**: 2563-2581.

Rajani, B. B. (1988). "A simple model for describing the variation of permeability with porosity for unconsolidated sands." In Situ **12**(3): 209-226.

Ringrose-Voase, A. J. (1991). "Micromorphology of soil structure: description, quantification, application." Australian Journal of Soil Research **29**: 777-813.

Ringrose-Voase, A. J. (1994). "Some principles to be observed in the quantitative analysis of sections of soil." Soil Micromorphology Studies in Management and Genesis **22**: 483-493.

Robinson, S. D. and T. R. Moore (1999). "Carbon and peat accumulation over the past 1200 years in a landscape with discontinuous permafrost, northwestern Canada." Global Biogeochemical Cycles **13**(2): 591-601.

Romanovsky, V. E. and T. E. Osterkamp (2000). "Effects of unfrozen water on heat and mass transport processes in the active layer and permafrost." Permafrost and Periglacial Processes **11**: 219-239.

Roulet, N. T. and M. K. Woo (1986). "Hydrology of a wetland in the continuous permafrost region." Journal of Hydrology **89**: 73-91.

Rouse, W. R., A. K. Eaton, et al. (2003). "Seasonality in the surface energy balance of tundra in the lower Mackenzie River basin." Journal of Hydrometeorology **4**(4): 673-679.

Schaap, M. G. and I. Lebron (2001). "Using microscope observations of thin sections to estimate soil permeability with the Kozeny-Carman equation." Journal of Hydrology **251**: 186-201.

Smith, M. W. (1975). "Microclimatic influences on ground temperatures and permafrost distribution, Mackenzie delta, Northwest Territories." Canadian Journal of Earth Sciences **12**: 1421-1438.

Stoops, G. (2003). Guidelines for analysis and description of soil and regolith thin sections. Madison, WI, Soil Sci. Soc. Am.

Thompson, A. H., A. J. Katz, et al. (1987). "Estimation of absolute permeability from capillary pressure measurements." Society of Petroleum Engineers Annual Technical Conference and Exhibition, Formation Evaluation and Reservoir Geology **62**: 475-481.

Thompson, M. L., P. Singh, et al. (1992). "Cautionary notes for the automated analysis of soil pore-space images." Geoderma **53**: 399-415.

Van Genuchten, M. T. (1980). "A closed form equation for predicting the hydraulic conductivity of unsaturated soils." Soil Science Society of America Journal **44**: 892-898.

Vasilenko, N. and S. Zhuravin (1997). "Experimental study of heat balance and heat exchange in the seasonal melt layer of soils in the permafrost zone (case study in the Stanovoi Range)." Proceedings of Second International Workshop on Energy and Water Cycle in GAME-Siberia **4**: 72-78.

Verry, E. S. and D. H. Boelter (1978). Peatland Hydrology. Wetland functions and values: the state of our understanding. Proceedings of the national symposium on wetlands. P. Greeson. Lake Buena Vista, Florida, American Water Research Association: 389-402.

Vogel, H. J. and U. Babel (1992). Experimental relationship between the morphological pore size distribution and the soil water retention characteristic. Proceedings of the IX International Working Meeting on Soil Micromorphology,vol. 591-600, Townsville, Australia, Elsevier.

Whittow, J. (1984). Dictionary of Physical Geography. Harmondsworth, Middlesex, England, Penguin Books.

Wolfe, L. H. (1963). "Physical and thermal properties of frozen soil and ice." Journal of Petroleum Technology **15**(9).

Woo, M. K. (1983). "Hydrology of a drainage basin in the Canadian high arctic." Annals of the Association of American Aeographers **73**(4): 577-596.

Woo, M. K. (1986). "Permafrost hydrology in North America." Atmosphere-Ocean **24**(3): 201-234.

Woo, M. K. and S. K. Carey (1999). Permafrost, seasonal frost and slope hydrology, central Wolf Creek basin, Yukon. Wolf Creek Research Basin : Hydrology, Ecology, Environment**:** 45-53.

Woo, M. K., P. Marsh, et al. (2000). "Snow, frozen soils and permafrost hydrology in Canada, 1995-1998." Hydrological Processes **14**: 1591-1611.

Woo, M. K. and P. Steer (1983). "Slope hydrology as influenced by thawing of the active layer, Resolute, N.W.T." Canadian Journal of Earth Sciences **20**: 978-986.

Woo, M. K. and Z. Xia (1996). "Effects of hydrology on the thermal conditions of the active layer." Nordic Hydrology **27**: 129-142.

Wright, R. K. (1981). The water balance of a lichen tundra underlain by permafrost. McGill Subarctic Research Paper No. 33, Climatological Research Series No. 13. Montreal**:** 110.